Technical Report Documentation Page

1. Report No.	2. Government Accession No.	3. Recipient's Catalog No.
SWUTC/14/0-6714-1		

4. Title and Subtitle	5. Report Date
EVALUATING THE NEED FOR SURFACE TREATMENTS TO REDUCE CRASH FREQUENCY ON HORIZONTAL CURVES	October 2013 Published: May 2014
	6. Performing Organization Code

7. Author(s)	8. Performing Organization Report No.
Michael P. Pratt, Srinivas R. Geedipally, Adam M. Pike, Paul J. Carlson, Amelia M. Celoza, and Dominique Lord	Report 0-6714-1

9. Performing Organization Name and Address	10. Work Unit No. (TRAIS)
Texas A&M Transportation Institute College Station, Texas 77843-3135	
	11. Contract or Grant No. Project 0-6714

12. Sponsoring Agency Name and Address		13. Type of Report and Period Covered
Texas Department of Transportation Research and Technology Implementation Office 125 E. 11th Street Austin, Texas 78701-2483	Southwest Region University Transportation Center Texas A&M Transportation Institute College Station, Texas 77843-3135	Technical Report: September 2011–August 2013
		14. Sponsoring Agency Code

15. Supplementary Notes

Project performed in cooperation with the Texas Department of Transportation and the Federal Highway Administration.

Project Title: Surface Treatments to Alleviate Crashes on Horizontal Curves

URL: http://tti.tamu.edu/documents/0-6714-1.pdf

16. Abstract

The application of high-friction surface treatments at appropriate horizontal curve locations throughout the state has the potential to improve driver performance and reduce the number of crashes experienced at horizontal curves. These treatments must be implemented judiciously due to their cost, but have the potential to improve safety at lower cost than geometric improvements like curve straightening, and with greater effectiveness than control-device treatments like installing delineators or Chevrons.

An analysis framework has been developed to assess the need for surface treatments at curves based on the concept of margin of safety analysis. Models have been developed to predict vehicle speeds throughout a curve, and calibrated using data from Texas curve sites. Safety prediction models have also been developed to quantify the relationship between skid number and curve crash frequency. This information can be applied to evaluate the safety performance of a curve of interest and estimate the potential safety benefit of installing a high-friction surface treatment.

17. Key Words	18. Distribution Statement
Highway Design, Highway Safety, Rural Highways, Highway Curves, Speed Measurement, Traffic Speed	No restrictions. This document is available to the public through NTIS: National Technical Information Service Alexandria, Virginia 22312 http://www.ntis.gov

19. Security Classif. (of this report)	20. Security Classif. (of this page)	21. No. of Pages	22. Price
Unclassified	Unclassified	118	

EVALUATING THE NEED FOR SURFACE TREATMENTS TO REDUCE CRASH FREQUENCY ON HORIZONTAL CURVES

by

Michael P. Pratt, P.E.
Assistant Research Engineer

Srinivas R. Geedipally, Ph.D., P.E.
Assistant Research Engineer

Adam M. Pike, P.E.
Assistant Research Engineer

Paul J. Carlson, Ph.D., P.E.
Senior Research Engineer

Amelia M. Celoza
Undergraduate Transportation Scholar
Texas A&M Transportation Institute

and

Dominique Lord, Ph.D.
Associate Professor
Texas A&M University

Report 0-6714-1
Project 0-6714
Project Title: Surface Treatments to Alleviate Crashes on Horizontal Curves

Performed in cooperation with the
Texas Department of Transportation
and the
Federal Highway Administration

October 2013
Published: May 2014

TEXAS A&M TRANSPORTATION INSTITUTE
College Station, Texas 77843-3135

DISCLAIMER

The contents of this report reflect the views of the authors, who are responsible for the facts and the accuracy of the data published herein. The contents do not necessarily reflect the official view or policies of the Federal Highway Administration (FHWA) and/or the Texas Department of Transportation (TxDOT). This report does not constitute a standard, specification, or regulation. It is not intended for construction, bidding, or permitting purposes. The engineer in charge of the project was Michael P. Pratt, P.E. #102332.

This document is disseminated under the sponsorship of the Department of Transportation, University Transportation Centers Program, in the interest of information exchange.

NOTICE

The United States Government and the State of Texas do not endorse products or manufacturers. Trade or manufacturers' names appear herein solely because they are considered essential to the object of this report.

ACKNOWLEDGMENTS

The Texas Department of Transportation and the Federal Highway Administration sponsored this research project. Mr. Michael Pratt, Dr. Srinivas Geedipally, Mr. Adam Pike, Dr. Paul Carlson, and Ms. Amelia Celoza with the Texas A&M Transportation Institute, and Dr. Dominique Lord with Texas A&M University prepared this report.

The researchers acknowledge the support and guidance that the Project Monitoring Committee provided:

- Mr. Wade Odell, Research Engineer (TxDOT, Research and Technology Implementation Office).
- Mr. Victor Vargas (TxDOT, Austin District).
- Mr. Bill Orr (TxDOT, Design Division).
- Mr. Darren McDaniel (TxDOT, Traffic Operations Division).
- Ms. Ellen Perry (TxDOT, Paris District).
- Mr. Robert Lee (TxDOT, Construction Division).
- Ms. Sandra Kaderka, Contract Specialist (TxDOT, Research and Technology Implementation Office).

In addition, the researchers acknowledge the valuable contributions of Ms. Brooke Ullman, who was the research supervisor during the first year of the research project, and Mr. Tom Freeman, Mr. Daniel Walker, Mr. Ivan Lorenz, Mr. Raul Avelar, and Mr. Brad Brimley, who assisted with various tasks during the conduct of the project.

The authors recognize that this research was supported by a grant from the U.S. Department of Transportation, University Transportation Centers Program to the Southwest Region University Transportation Center. The Region 6 UTC program continues to provide valuable support to selected TxDOT studies and enhances the research effort.

TABLE OF CONTENTS

LIST OF FIGURES

LIST OF TABLES

CHAPTER 1. OVERVIEW

INTRODUCTION

Roadway safety continues to be a major national concern, with federal, state, and other authorities striving to reduce crashes and their associated costs in terms of fatalities, severe injuries, property damage, and traffic delays. Significant improvements need to be made in a number of critical areas for the United States to catch up with gains that Western European nations have made in the field of safety, where annual fatalities declined by 59 percent between 1970 and 2004 compared to a 19 percent decline in the United States during the same period (*1*). According to the National Highway Traffic Safety Administration (*2*), in 2006 motor vehicle crashes were a leading cause of death in the United States, when the estimated total cost related to highway crashes exceeded $500 billion according to Miller and Zaloshnja (*3*). Of this total, about 43 percent was related to poor road conditions, including inadequate pavement texture/friction.

Additionally, horizontal curves tend to be associated with a disproportionate number of severe crashes. Each year in the United States, about 38,000 fatal crashes occur on the highway system, with 25 percent of the fatalities found to occur on horizontal curves (*4*). Texas accounts for about 3,200 fatal crashes, with about 44 percent of these crashes occurring on horizontal curves. Hence, Texas is over-represented in terms of its proportion of fatal curve-related crashes, relative to the national average. Given this crash information, and to have an impact on overall crash reduction, research needs to be conducted into methods for improving driver performance at horizontal curves. A major component of this effort is evaluating surface treatments that can be used to improve roadway conditions in horizontal curves.

RESEARCH APPROACH

The research team developed an analysis framework to assess the need for surface treatments at curves based on the concept of margin of safety analysis. Margin of safety is defined as side friction demand subtracted from side friction supply (*5*). Vehicle speed, curve geometric characteristics (such as radius and superelevation rate), and curve travel path characteristics all affect friction demand. Meanwhile, pavement characteristics (particularly skid number) and weather conditions affect friction supply.

To assist the practitioner in conducting margin of safety analyses, the researchers developed models to predict vehicle speeds throughout a curve as a function of curve geometric and traffic control characteristics. These models were calibrated using speed data from Texas curve sites. Lane placement data were also collected to yield additional insights about travel path behavior. Previous research has shown that drivers often deviate from the actual path of the curve by cutting or correcting their course, such that they may incur higher side friction demand at a certain point in their travel through the curve, compared to what they would incur if they tracked the marked curve path exactly (*5*, *6*).

Safety prediction models were also developed to quantify the relationship between curve crash frequency and characteristics like radius, lane width, shoulder width, and skid number. Most of these curve characteristics have been the subject of prior research on roadway safety in Texas (*7*, *8*), and the trends in the newly-developed models compared well with those models that were previously developed. The newly-calibrated crash modification factor for skid number allows the practitioner to assess the potential safety benefit of installing a surface treatment that increases pavement friction.

The preceding information was assembled to develop guidelines that can be applied to assess the need and potential benefit of installing a high-friction surface treatment on a rural highway horizontal curve. The guidelines are formulated as an Excel®-based spreadsheet program called Texas Curve Margin of Safety (TCMS). The TCMS program accepts curve geometric and traffic control characteristics as inputs, and provides information about margin of safety, expected crash frequency, and travel path distribution as outputs. The spreadsheet tool is envisioned to be incorporated into TxDOT's pavement design guidance in a similar manner as the existing Form 2088, which is used to select surface aggregates for repaving projects based on a qualitative analysis of friction supply and demand (*9*).

REFERENCES

1. European Conference of Ministers of Transport (ECMT) and Organization for Economic Cooperation and Development (OECD). *Achieving Ambitious Road Safety Targets: Country Reports on Road Safety Performance*. Joint OECD/ECMT Working Group Report. Organization for Economic Cooperation and Development, Paris, France, 2006.
2. National Highway Traffic Safety Administration (NHTSA). *Motor Vehicle Traffic Crashes as a Leading Cause of Death in the United States: Traffic Safety Facts*. DOT HS 811226. Washington, D.C., 2006.
3. Miller, T. R. and E. Zaloshnja. *On a Crash Course: The Dangers and Health Costs of Deficient Roadways*. The Transportation Construction Coalition, Washington, D.C., 2009.
4. Torbic, D., D. Harwood, D. Gilmore, R. Pfefer, T. Neuman, K. Slack, and K. Hardy. *Guidance for Implementation of the AASHTO Strategic Highway Safety Plan. Volume 7: A Guide for Reducing Collisions on Horizontal Curves.* NCHRP Report 500. TRB, National Research Council, Washington, D.C., 2004.
5. Glennon, J., and G. Weaver. *The Relationship of Vehicle Paths to Highway Curve Design.* Research Report 134-5. Texas Transportation Institute, College Station, Texas, 1971.
6. Spacek, P. Track Behavior in Curve Areas: Attempt at Typology. In *Journal of Transportation Engineering*, Vol. 131, No. 9, September 2005, pp. 669–676.
7. Bonneson, J., and M. Pratt. *Roadway Safety Design Workbook.* Report FHWA/TX-09-0-4703-P2, Texas Transportation Institute, College Station, Texas, 2009.
8. Lord, D., M. Brewer, K. Fitzpatrick, S. Geedipally, and Y. Peng. *Analysis of Roadway Departure Crashes on Two-Lane Rural Roads in Texas*. Report FHWA/TX-11/0-6031-1, Texas Transportation Institute, College Station, Texas, 2011.
9. *Pavement Design Guide*. Texas Department of Transportation, Austin, Texas, 2008.

CHAPTER 2. SAFETY TRENDS AND TREATMENTS FOR HORIZONTAL CURVES

INTRODUCTION

Horizontal curves are a necessary part of any highway system, yet they can present significant safety concerns. Research shows that curves are associated with more crashes as their radius decreases or speeds on the roadway increase. These safety concerns arise from:

- The increased driver workload associated with the negotiation of a curve.
- The possibility of failing to detect a curve or judge its sharpness.
- The existence of inadequate side friction supply to keep vehicles on the curve.

Many options to improve curve safety exist, including signs and pavement markings to alert drivers of the presence and sharpness of a curve, surface treatments to increase pavement friction, and geometric improvements like straightening the curve or increasing its superelevation rate. These treatments can decrease side friction demand (by lowering vehicle speeds or providing more generous curve design) or increase side friction supply (by improving the tire-pavement interface). In general, the objective of curve safety treatments is to improve the curve's margin of safety, which is defined as the side friction demand subtracted from the side friction supply.

Pavement surfaces are evaluated in terms of the friction that they can provide to vehicles. Physical characteristics like micro- and macro-texture influence the friction supply, which may degrade with time depending on traffic and weather conditions. Materials that are applied to curves as a high-friction surface treatment must be evaluated to determine whether they provide the required amount of side friction supply, and how often they need to be re-applied due to friction degradation over time.

This chapter consists of two parts. The first part discusses horizontal curve safety, including design and operational issues and methods to quantify curve severity. The second part describes the evaluation of high-friction surface treatments, including the measurement of key physical characteristics and summary of case studies on surface treatments.

HORIZONTAL CURVE SAFETY

This part of the chapter addresses horizontal curve safety trends, focusing on design and operational issues and safety treatments that are commonly used. Geometric attributes like curve radius and superelevation rate affect curve safety, and so do operational issues like driver steering fluctuation, acceleration, and braking. The interaction between these factors results in different margins of safety existing along different portions of the curve.

This part of the chapter consists of three sections. The first section explores curve crash trends and identifies causes for curve crashes. The second section identifies treatments that are used to improve curve safety. The third section discusses methods that are used to quantify curve severity and identify treatments for use at a given curve.

Curve Crash Trends

Statistics have consistently shown that the crash rate on horizontal curves is significantly greater than that on tangent roadway segments of similar character. In an exploration of curve safety trends, Zegeer et al. found that a 1000-ft-radius curve is likely to have 50 percent more crashes than a tangent segment of equivalent length, and a 500-ft-radius curve is likely to have 200 percent more crashes than a tangent segment (*1*). This trend may be caused by drivers failing to detect the presence of a curve or attempting to negotiate the curve at unsafe speeds.

Fitzpatrick et al. analyzed curve safety trends by categorizing curves in terms of speed reduction (*2*). They defined speed reduction as the difference between 85th percentile vehicle speeds on the approach tangent and at the curve midpoint. They found that a curve requiring a 5-mph speed reduction is likely to have 90 percent more crashes than a tangent segment, and a curve requiring a 10-mph speed reduction is likely to have 250 percent more crashes. They calibrated the following crash modification factor (CMF) to estimate a relationship between curve crash frequency and the 85th-percentile curve and tangent speeds:

$$CMF_{sr} = e^{0.126(v_{t,85} - v_{c,85})} \quad (1)$$

where:

CMF_{sr} = crash modification factor for curve speed reduction;
$v_{t,85}$ = 85th percentile approach tangent speed, mph; and
$v_{c,85}$ = 85th percentile curve speed, mph.

The trend in Equation 1 shows that curve crash frequency increases exponentially as the required speed reduction increases. For the purpose of estimating the speed reductions chosen by drivers through curves, Bonneson et al. developed a model to predict the 85th percentile vehicle speed at the midpoint of a curve (*3*). The model was calibrated using a data set of 6677 passenger cars and 1741 trucks at 41 curve sites in Texas. It is described as follows:

$$v_{c,85} = \sqrt{\frac{15.0 R_p (0.1962 - 0.00106 v_{t,85} + 0.000073 {v_{t,85}}^2 - 0.0150 I_{tk} + e/100)}{1 + 0.00109 R_p}} \le v_{t,85} \quad (2)$$

where:

R_p = vehicle path radius, ft; and
I_{tk} = indicator variable for trucks (= 1.0 if model is used to predict truck speed, 0.0 otherwise).

This curve speed model reflects drivers' choice of curve speed as influenced by:

- Their perception of lateral acceleration (which is influenced by speed and curve geometry).
- Comfort limits.
- Desire to maintain speed and minimize travel time (which is more prevalent on higher-speed roadways).

Bonneson and Pratt calibrated a safety prediction model to estimate the effects of geometry and traffic operations on safety (*4*). The model was calibrated for rural highways using Texas data. It includes a CMF to account for the expected increase in crash frequency due to the presence of a horizontal curve. The following equation describes the horizontal curve CMF:

$$CMF_{cr} = 1.0 + 0.97(0.147V)^4 \frac{(1.47V)^2}{32.2R^2}\left(\frac{L_c}{L}\right) \quad (3)$$

where:

CMF_{cr} = crash modification factor for horizontal curve radius;
V = posted speed limit, mph;
R = curve radius, ft;
L_c = horizontal curve length (including spiral transitions), mi; and
L = segment length, mi.

The CMF is illustrated in Figure 1 for a range of curve radii and three posted speed limit values. Two trends are evident. First, crash frequency increases significantly when a curve of any radius is present, but especially if the curve radius is less than about 2000 ft. Second, a curve of a given radius will be associated with a larger increase in crashes if vehicle speeds are higher. For example, a curve with a radius of 2865 ft (i.e., degree of curve = 2.0) would be associated with a crash frequency increase of about 6 percent (CMF_{cr} = 1.06) on a 50-mph roadway and about 44 percent (CMF_{cr} = 1.44) on a 70-mph roadway.

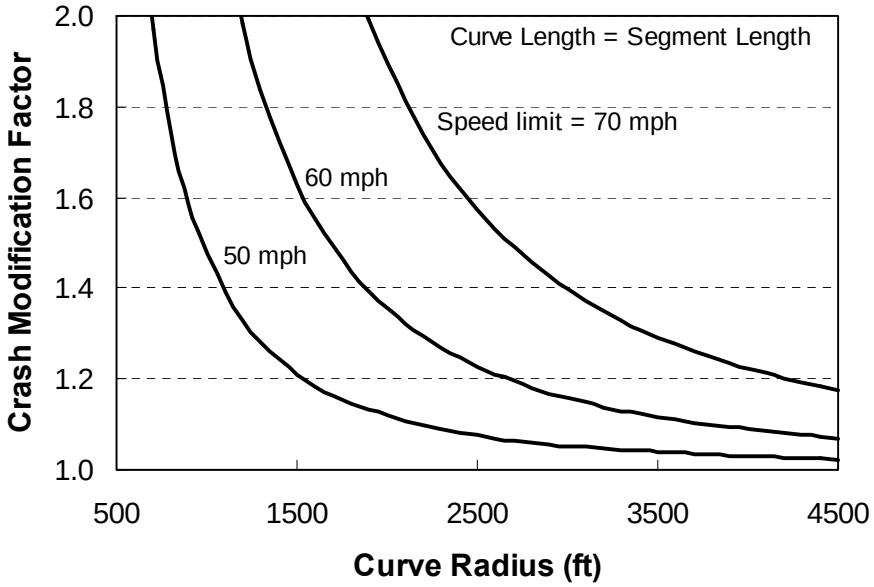

Figure 1. Curve Radius Crash Modification Factor.

Torbic et al. analyzed the distribution of curve-related fatal crashes that were reported in the nationwide Fatality Analysis and Reporting System (FARS) in 2002 (*5*). They found that 76 percent of fatal crashes on curves were single-vehicle crashes, which were primarily run-off-road crashes,

and another 12 percent of the crashes were head-on or sideswipe-opposite direction crashes. Both of these collision types involve lane departure. A head-on or sideswipe-opposite direction crash results if a vehicle crosses into the opposing lane while an opposing vehicle is present. The occurrence of lane departure indicates that the driver either misjudged the curvature or was unable to maintain the curved trajectory.

Lord et al. analyzed roadway departure crash trends in Texas using crash data from 2003 through 2008 (*6*). Their analysis included all roadway departure crashes—on tangents as well as on curves. They calibrated the following model that predicts annual roadway departure crash frequency per mile. The model applies to crashes of all severities and all regions in Texas.

$$\mu = e^{-6.894} \times F^{0.8035} \times e^{(-0.084\,LW - 0.058\,SW - 0.048\,ST2 - 0.285\,ST4 + 0.1118\,C\,Dens - 0.019\,D\,Dens)} \quad (4)$$

where:

μ = estimated annual number of crashes per mile.
F = traffic volume, vehicles per day.
LW = lane width, ft.
SW = shoulder width, ft.
$ST2$ = indicator variable for surface shoulder type presence.
$ST4$ = indicator variable for combination-surface/stabilized shoulder type presence.
$CDens$ = curve density, curves per mile.
$DDens$ = driveway density, driveways per mile.

This model suggests that roadway departure crash frequency per mile will increase exponentially with an increase in curve density. The magnitude of the exponent is 0.1118 multiplied by the curve density, which is measured in curves per mile.

Lord et al. calibrated a second model to predict the annual roadway departure crash frequency per mile on curves. This model suggests that crash frequency per mile increases exponentially with an increase in degree of curve (or a decrease in radius). This model is described as follows:

$$\mu = e^{-6.448} \times F^{0.7657} \times e^{(-0.076\,LW - 0.062\,SW + 0.075\,CD)} \quad (5)$$

where:

μ = estimated annual number of crashes per mile.
F = traffic volume, vehicles per day.
LW = lane width, ft.
SW = shoulder width, ft.
CD = degree of curve.

Lord et al. also conducted an exploratory analysis of single-vehicle roadway departure fatal-and-injury crash rates for horizontal curves, and categorized the 25 TxDOT districts as low-rate, mid-rate, and high-rate. This categorization is illustrated in Figure 2. They were further able to determine that there is a positive correlation between speed limit and curve

density, such that the expected increase in roadway departure crash rate due to curve density is more noteworthy on roadways with higher speed limits.

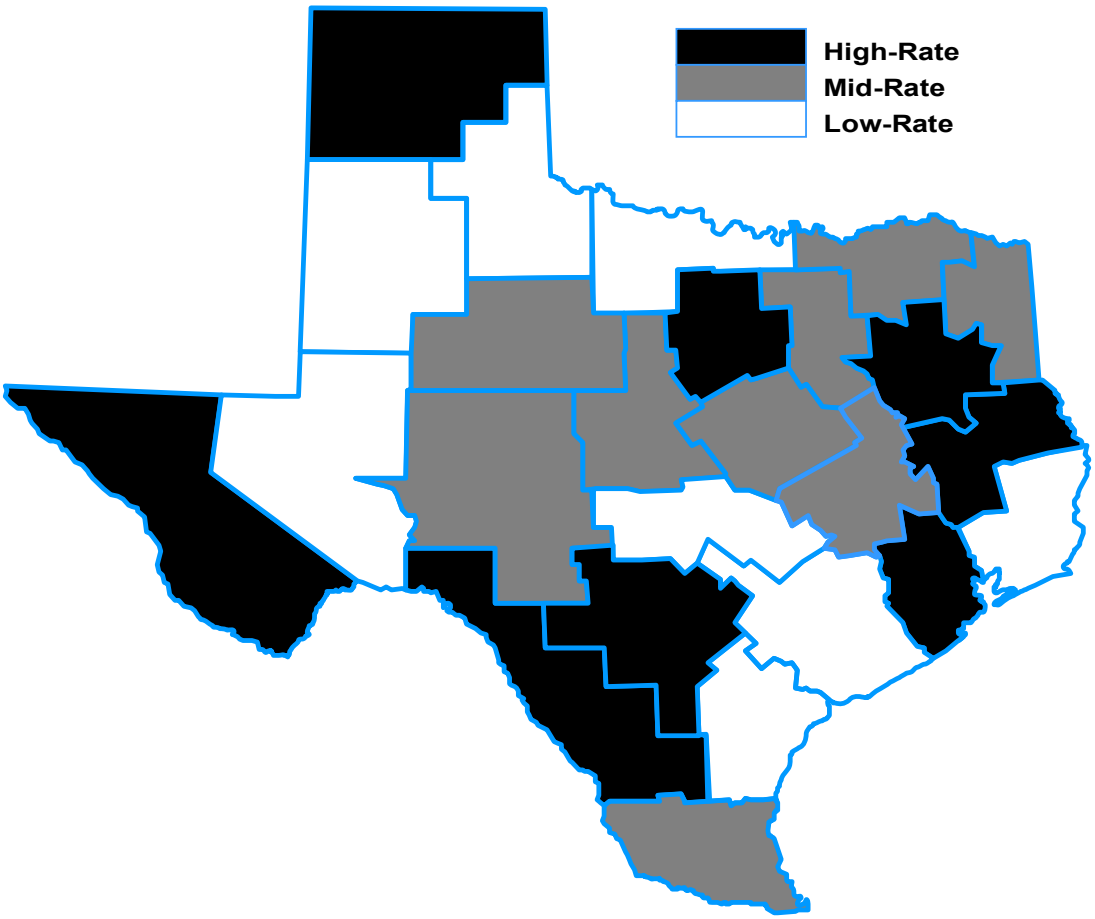

Figure 2. Location of Crash Rate Groups for Single-Vehicle Roadway Departure Fatal-and-Injury Crashes on Horizontal Curves.

Finally, Lord et al. examined the effects of weather and light condition on the severity distribution of roadway departure crashes. They found that a lower percentage of crashes were property-damage-only during clear or cloudy weather than during other weather conditions. For example, 48 percent of roadway departure crashes were property-damage-only during clear or cloudy weather, compared with 63 percent during rain. They opined that this trend may be caused by drivers reducing speed during inclement weather. Their examination of light condition suggested that the percentage of fatal crashes is slightly lower during daylight (2 percent of crashes) than other light conditions (3–5 percent).

The preceding trends show that both presence and sharpness of horizontal curvature influence crash rates on highways, and that curve-related crashes are more frequent on higher-speed roadways.

Design and Operational Factors Affecting Curve Safety

AASHTO's *A Policy on Geometric Design of Highways and Streets* (*Green Book*) states that the design of horizontal curves should be based on a proper relationship between speed, curvature, superelevation rate, and side friction demand (*7*). The *Green Book* offers the following equation to describe the relationship between these variables:

$$f_D = \frac{v^2}{gR} - \frac{e}{100} \quad (6)$$

where:

f_D = side friction demand (lateral acceleration divided by g).
v = vehicle speed, ft/s.
g = gravitational constant (= 32.2 ft/s^2).
R = curve radius, ft.
e = superelevation rate, percent.

This equation is referred to as the "point-mass model" or the "simplified curve formula." It shows that the side friction demand f_D of a vehicle traveling at speed v increases as curve radius R or superelevation rate e decrease. For design purposes, the *Green Book* recommends side friction factors that represent driver comfort limits. These factors are used to determine an appropriate curve radius and superelevation rate for the roadway's design speed.

The design side friction factors in the Green Book are lower than the side friction supply f_S provided in the worst-case combination of worn tires and wet pavement. In other words, vehicles traveling at a speed not exceeding the design speed should be able to traverse the curve safely.

In the design process, curve design safety can be assessed in terms of "margin of safety," which is defined as the difference between side friction demand and side friction supply at a given vehicle speed. If the side friction demand exceeds the side friction supply available to the vehicle, a sliding failure will occur. As Equation 6 shows, vehicle speed and curve geometry affect side friction demand. Tire-pavement interface properties such as tire tread condition, pavement texture, and presence of water or solid contaminants on the pavement surface all affect side friction supply. The concept of margin of safety has been used to evaluate horizontal curve design policies (*8*, *9*, *10*).

As Glennon and Weaver (*10*, *11*) observed, the side friction demand estimate that the point-mass model provides is based on the assumption that drivers traverse the curve "with geometric exactness." Glennon listed several issues that can combine to reduce curve safety at crucial moments during the traversal of the curve (*12*). These issues include:

- Driver steering fluctuations.
- Acceleration or braking within the curve.

- Lack of full superelevation development near the beginning and ending points of the curve.
- Excessive water buildup on the pavement.

These issues are discussed in the following subsections.

Driver Steering Fluctuations

Curve Cutting. In an investigation of curve speed and lane placement, Emmerson observed that drivers tend to "cut" curves by shifting laterally in their lane as they traverse the curve, such that their overall path represents a larger circle than that of the curve itself (*13*). This shifting mitigates side friction demand, but is limited by the curve geometry. Emmerson described the lateral shifting with the following equation:

$$dR = \frac{dS}{1 - \cos\frac{\Delta}{2}} \tag{7}$$

where:

dR = increase in curve radius, ft.
dS = lateral shift (assume 3 ft), ft.
Δ = deflection angle, degrees.

Hence the vehicle's average path radius R_p can be computed as the sum of the curve radius R and the increase in curve radius dR computed with Equation 7. A path described by this average path radius represents the "overall average" path that drivers traverse through the curve.

Steering Corrections and Oscillation. Glennon and Weaver conducted a detailed analysis of curve paths by recording video footage of vehicles as they traversed highway curves (*11*). This study included five curves and about 100 vehicles at each curve. They observed that drivers tend to oscillate about an idealized curved path as they traverse curves, such that their side friction demand varies continuously through the curve. By monitoring the vehicles' speeds and lane placement, and by combining this information with the known superelevation rates for the curves, they were able to identify the portion of the vehicles' paths where maximum side friction demand occurred. They determined that at the location of maximum side friction demand, many vehicles traverse a path with a radius that is smaller than the curve radius.

Glennon and Weaver's data included the path radius at the point of maximum side friction demand ($R_{p,fmax}$) and the minimum vehicle path radius ($R_{p,min}$) along the curve for each of the 484 vehicles in the data set. A reexamination of these data was conducted by computing the ratio of $R_{p,fmax}$ to $R_{p,min}$ for each vehicle, and then computing summary statistics for these ratios. Table 1 shows the results of this reanalysis. As shown, the overall 95th percentile ratio of $R_{p,fmax}$ to $R_{p,min}$ was 1.13, indicating that driver steering fluctuations caused as much as 13 percent change in vehicle path radius.

Table 1. Driver Steering Fluctuation Data (*11*).

Curve Number	Number of Vehicles	Degree of Curve	Ratio of $R_{p,fmax}$ to $R_{p,min}$		
			Average	85th percentile	95th percentile
1	99	7	1.02	1.05	1.09
2	104	4	1.01	1.03	1.07
3	93	5	1.05	1.13	1.16
4	92	2	1.03	1.10	1.13
5	96	2.5	1.01	1.03	1.05
All Observations	484	--	1.03	1.07	1.13

Winsum and Godthelp conducted a simulator study of steering behavior in curves to gain insight into drivers' decision processes and cues (*14*). This study included 16 drivers and a road course with four curves. The curves had radii of 130 ft, 260 ft, 394 ft, and 525 ft, respectively. They found that driver steering behavior can be described as a closed-loop feedback process while the driver is within the curve and an open-loop process while the driver is entering or exiting the curve. During the closed-loop portion of the curve maneuver, drivers used time to lane crossing as a visual cue for course corrections, using values of 2.5–3.0 s. That is, drivers made steering corrections when they perceived that they were fewer than 2.5–3.0 s from departing their travel lane. This trend was consistent across the four curves, so it did not correlate with radius.

Winsum and Godthelp defined "steering error" as the required steering angle for perfect curve traversal subtracted from the actual steering angle. With this definition, an error of positive magnitude indicates oversteering, when the vehicle's path radius is sharper than the curve radius. The results of the study indicated that drivers' steering errors tended to oscillate around 0 during closed-loop steering, and the magnitudes of error were similar between the closed-loop and open-loop portions of the curve maneuver.

Winsum and Godthelp found that while steering error magnitude varied by curve radius, the steering error ratio was roughly constant across the four curves on their simulated course, and ranged from 0.10 to 0.12. They defined steering error ratio as follows:

$$\frac{\delta_{se}}{\delta_{sr}} = \frac{\delta_s - \delta_{sr}}{\delta_{sr}} \tag{8}$$

where:

δ_{se} = steering error, degrees.
δ_{sr} = required steering angle, degrees.
δ_s = actual steering angle, degrees.

Steering error ratios can be converted to steering fluctuation factors using an equation that Bonneson reported (*15*):

$$c_r = 1000 \frac{\delta_s}{r_s L\left(1 + bv^2\right)} \tag{9}$$

where:

c_r = vehicle path curvature (=1000/R_p), ft^{-1}.
r_s = steering-wheel to front-wheel angle ratio.
L = vehicle wheelbase, ft.
b = constant representing the relationship between tire slip angle and vehicle speed.

For a given combination of vehicle speed v and vehicle characteristics r_s, L, and b, Equation 9 can be rewritten as follows:

$$\delta_s = \frac{k}{R_p} \tag{10}$$

where:

k = constant representing a combination of vehicle properties and speed.

The combination of path radius R_p and steering angle δ_s represents actual steering behavior. In the case of perfect steering, $R_p = R$ and $\delta_s = \delta_{sr}$. Substituting Equation 10 into Equation 8 yields the following result:

$$\frac{\delta_{se}}{\delta_{sr}} + 1 = \frac{R}{R_p} \tag{11}$$

Using Equation 10, the steering error ratios of 0.10–0.12 that Winsum and Godthelp had reported correspond to ratios R/R_p of 1.10–1.12.

Bonneson (*15*) defined a "steering fluctuation factor" b_s as the ratio of the curve radius R to the minimum path radius $R_{p,min}$. He recommended using the minimum path radius (or R/b_s) for the purpose of quantifying maximum side friction demand. He further recommended using a steering fluctuation factor of 1.15, which is slightly higher than the values that Glennon and Weaver (*11*) and Winsum and Godthelp (*14*) both reported. A steering fluctuation factor of 1.15 represents the 97th percentile steering fluctuation in the data that Glennon and Weaver reported.

Characterization of Curve Travel Paths. Spacek conducted a curve travel path evaluation that involved tracking about 2000 vehicles as they traversed curves (*16*). Ten curves were included in his evaluation. He identified the six common curve path types that are illustrated in Figure 3.

Spacek found that less than 1 percent of drivers adopted paths that can be characterized as the "ideal" path that is assumed in geometric design. Roughly half of drivers adopted paths that can be characterized as "normal" (which involves some curve cutting, but staying within the travel lane) or "cutting" (which involves a greater amount of curve cutting that results in encroachment on the centerline). A path radius that is somewhat greater than the curve radius describes the normal and cutting paths. As a result, these paths are associated with somewhat less side friction demand than assumed in the design of the curve. The normal and cutting paths are similar to those that Emmerson observed (*13*).

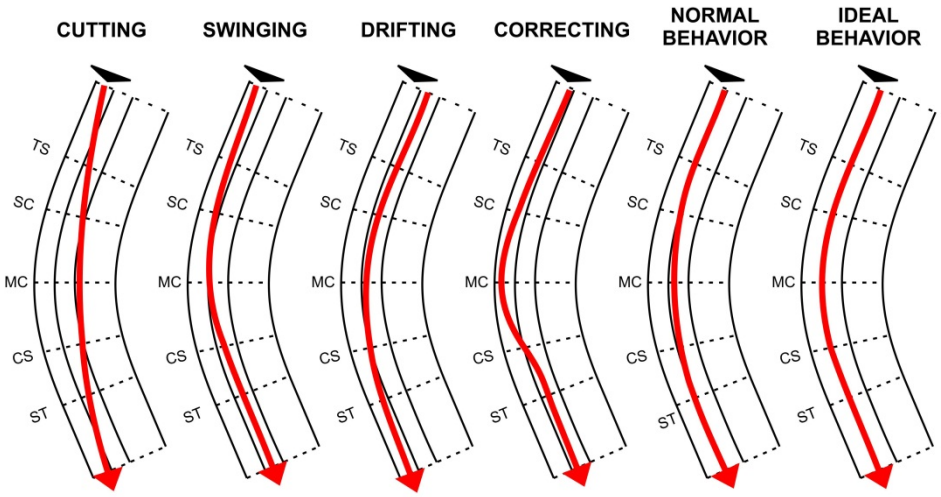

Figure 3. Curve Travel Path Types (*16*).

In Spacek's data set, the number of drivers exhibiting the correcting travel path type varied by site; the site with the highest crash frequency had the highest frequency of correcting paths, at 11.5 percent of vehicles. A more severe correcting maneuver results in a greater increase in side friction demand.

Hence, for the purpose of determining maximum side friction demand, the minimum path radius for a typical correcting path should be considered. This radius accounts for the elevated side friction demand associated with a correcting path. The minimum path radius can be computed using the steering fluctuation factor of 1.15 that Bonneson recommended (*15*), as follows:

$$R_{p,\min} = \frac{R}{1.15} \tag{12}$$

Acceleration or Braking within the Curve

When a vehicle traverses a curve, its tires must provide side friction force to prevent the vehicle from sliding off the curve in a direction tangent to the direction of travel. The tire-pavement interface must provide this force in addition to friction forces associated with braking friction, tractive effort, and rolling resistance. When a driver applies the accelerator or brakes on a curved path, the side friction supply decreases. The change in friction supply can be quantified using the friction ellipse equation (*15*):

$$f_s = f_{s,max}\sqrt{1-\frac{f_{x,D}}{f_{x,max}}} \tag{13}$$

where:

f_s = available side friction supply.
$f_{s,max}$ = maximum side friction supply.
$f_{x,D}$ = tractive or braking friction demand factor.
$f_{x,max}$ = maximum forward friction supply (approximately equal to $f_{s,max}$).

Equation 13 shows that when the brakes or accelerator are not applied, side friction supply is maximized. However, research has shown that drivers often continue to brake after they enter a curve, adopt a reduced speed along the middle portions of the curve, and begin to accelerate shortly before exiting the curve (*17*, *2*). Fitzpatrick et al. developed models that predict deceleration rate at the curve PC and acceleration rate at the curve PT as a function of radius (*2*). These models can be used to predict acceleration or deceleration rates, which represent the term $f_{x,D}$ in Equation 13 when converted to units of *g*. Equation 13 can then be applied to compute the reduced side friction supply f_s that is available during braking or acceleration.

Braking frequently occurs near the curve PC, as drivers begin to enter the curve but have not yet slowed to their desired curve speed. In addition, braking occasionally occurs in the middle portions of the curve, such as when an object or stopped vehicle is encountered on the curve. Hence, it is desirable to compute a reduced friction supply due to braking at the middle of the curve in addition to its beginning and ending points.

Lack of Full Superelevation

In Glennon and Weaver's data set (*11*), each vehicle's point of maximum side friction demand did not necessarily coincide with the point of minimum path radius. The point of maximum side friction demand is influenced by the combination of path radius, vehicle speed, and superelevation rate, all of which vary along the curve. In their data set, Glennon and Weaver reported the approximate location where maximum side friction demand occurred for each of the 484 vehicles. They reported this location in terms of quarters of the curve's length. Figure 4 provides this distribution. The figure shows that in about 75 percent of cases, the point of maximum side friction demand occurs in the first or last quarters of the curves' length.

Glennon identified the first and last portions of a curve as problem areas due to the lack of full superelevation (*12*). The beginning portion of a curve is labeled as "problem area 3" in Figure 5.

Water Buildup

The *Green Book* recommends a cross slope of no less than 1 percent to minimize water buildup on roadways. However, in the case of a curve deflecting to the left, it is necessary to transition from a normal-crown cross slope to a superelevated pavement surface. As a result, the approach to the curve will have a portion of pavement where the cross slope is less than 1 percent, and this portion of the curve approach may be associated with elevated potential of hydroplaning. This area is labeled as "Problem Area 1" in Figure 5.

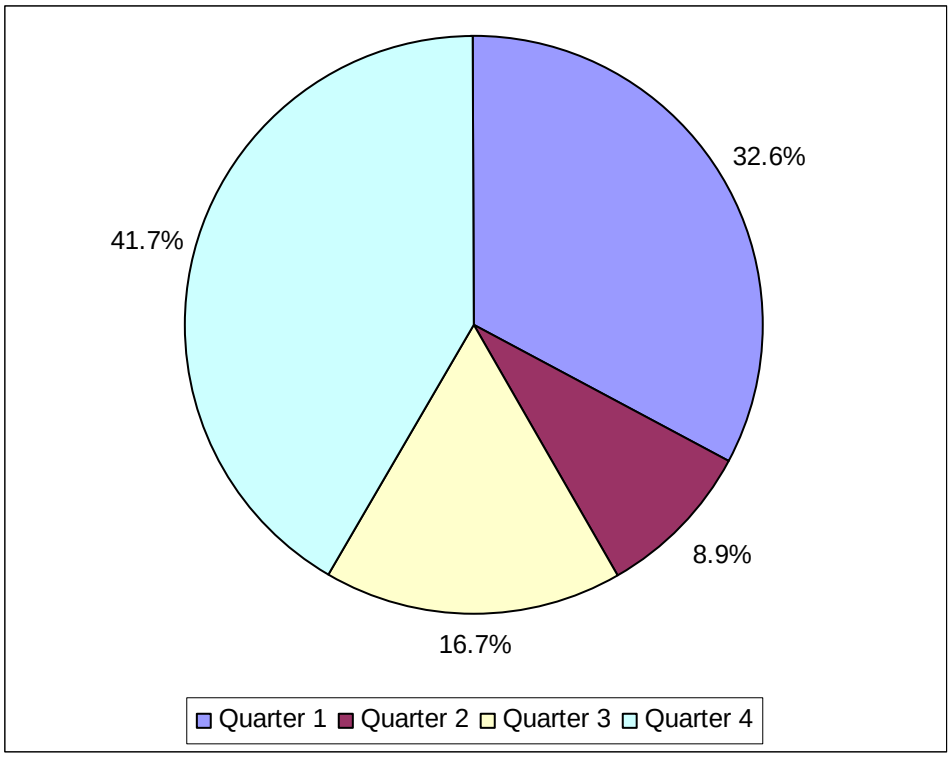

Figure 4. Locations of Maximum Side Friction Demand for 484 Vehicles in Curves.

Summary

To determine the margin of safety at a specific curve, follow these steps:

1. Given the curve's radius and deflection angle, and assuming a steering fluctuation factor to reflect steering error, determine the minimum path radius. These calculations are made using Equations 7 and 12.
2. Given the minimum path radius, approach tangent speed, and superelevation rate, determine the 85th-percentile speed at the midpoint of the curve. This estimation is done using Equation 2.
3. Given the 85th-percentile tangent and curve speeds, use speed profile models (*2*) to estimate vehicle speeds, acceleration rates, and deceleration rates at the beginning and ending points of the curve.
4. Use the vehicle speeds, acceleration and deceleration rates, and the friction ellipse (Equation 13), and superelevation rates to compute side friction demand at the following three points along the curve: beginning, midpoint, and ending.
5. Compare these side friction demands to the side friction supply that the tire-pavement interface provided. Subtract the latter from the smallest of the former to obtain the margin of safety.

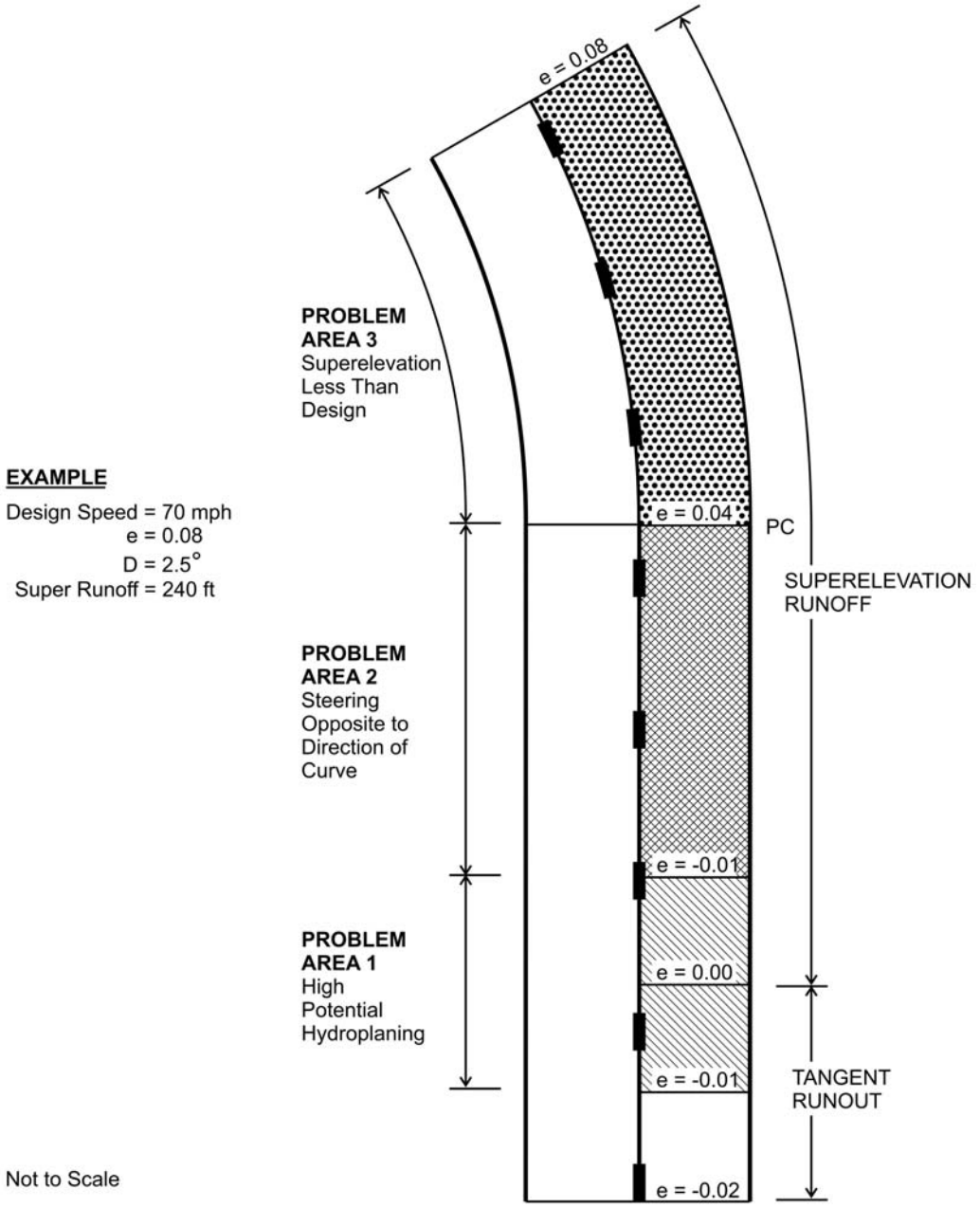

Figure 5. Problem Areas on Horizontal Curves (*12*).

This type of analysis allows the margin of safety of a curve to be estimated for several combinations of vehicle speed, acceleration or deceleration, steering error, and varying superelevation rate. The first four steps were described in the preceding section. The fifth step will be addressed in the next part of this chapter.

Safety Treatments

Various treatments are available to improve safety on horizontal curves. The treatments are generally designed to improve driver alertness and ability to judge the curve's sharpness, or to reduce the curve's sharpness through geometric improvement. Torbic et al. listed the following curve safety treatment strategies (*5*):

- Provide advance warning of unexpected changes in horizontal alignment.
- Enhance delineation along the curve.
- Provide dynamic curve warning system.
- Install rumble strips (shoulder and/or centerline).
- Prevent edge dropoffs.
- Provide skid-resistant pavement surfaces.
- Improve design and application of barrier and attenuation systems.
- Widen the roadway.
- Improve or restore superelevation.
- Modify horizontal alignment.

The first two of these treatment strategies typically involve installing traffic control devices like curve warning signs or advisory speed plaques, or delineation devices like delineator posts, Chevrons, or the Large Arrow sign. The third treatment strategy often involves installing a combination of traditional traffic control devices and flashers that activate when drivers approach a curve at unsafe speeds. The fourth treatment strategy is designed to warn drivers who are close to departing their lane on a curve.

The last six treatment strategies involve more significant changes to the curve, ranging from repaving with skid-resistant material to realigning and straightening the curve. These strategies are designed to:

- Make the curve more "forgiving" to driver steering errors.
- Reduce driver efforts required to traverse the curve.
- Mitigate the consequences of running off the road.

In particular, the provision of skid-resistant surfaces, increasing superelevation, and increasing curve radius through realignment are designed to increase the curve's margin of safety, either by increasing side friction supply or by reducing side friction demand.

Curve Severity Assessment

Curve safety treatments are typically selected based on observed safety performance (i.e., crash frequency) or quantitative measures of curve severity. One measure of curve severity is "speed differential," defined as the difference between the posted regulatory speed limit and curve advisory speed. The *Manual on Uniform Traffic Control Devices* (MUTCD) contains guidelines on the selection of curve safety treatments based on speed differential (see Table 2).

Table 2. Curve Traffic Control Devices.

Type of Horizontal Alignment Sign	Difference Between Speed Limit and Advisory Speed				
	5 mph	10 mph	15 mph	20 mph	25 mph or more
Turn, Curve, Reverse Turn, Reverse Curve, Winding Road, Combination Horizontal Alignment/ Intersection	Recommended	Required	Required	Required	Required
Advisory Speed Plaque	Recommended	Required	Required	Required	Required
Chevrons and/or One Direction Large Arrow	Optional	Recommended	Required	Required	Required
Exit Speed and Ramp Speed on Exit Ramp	Optional	Optional	Recommended	Required	Required

Similar guidelines have been provided in other references, but with "speed differential" defined as the difference between the 85th percentile tangent speed and the advisory speed. Two such references include policy documents from Australia (*18*) and New Zealand (*19*). By referencing actual vehicle speeds, the guidelines in these documents are more sensitive to driver behavior.

Bonneson et al. suggested another method of assessing curve severity based on side friction demand households (*3*). This method is applied by estimating the 85th-percentile tangent and curve speeds and locating their intersection in the contour plot shown in Figure 6. Note that the latter of these two speeds can be estimated using Equation 2.

The contour lines in Figure 6 represent thresholds of side friction demand differentials (i.e., increases over the base or "comfort" level) that drivers experience as they traverse curves. These quantities are also proportional to kinetic energy reductions that occur when drivers decelerate from tangent speed to curve speed. This type of curve severity assessment more closely matches driver behavior than the use of posted speeds (either regulatory speed limits or advisory speeds).

Table 3 provides the guidelines that accompany the contour plot. As was the case with the guidelines in Table 2, the general trend is for more devices to be recommended for curves that are more severe.

The guidelines in Table 3 refer only to curve safety treatments involving signs or pavement markings. Note, however, that for curves of severity category "E," special treatments such as oversize signs, flashers, wider edgelines, and profiled pavement markings are recommended. These guidelines could be expanded to include geometry-based treatments like straightening, superelevation improvement, or the provision of a surface treatment to increase side friction supply. Glennon provided friction-based guidelines (*20*) that include such treatments for curves of the greatest severity category. The concept of margin of safety analysis could also be combined with these guidelines.

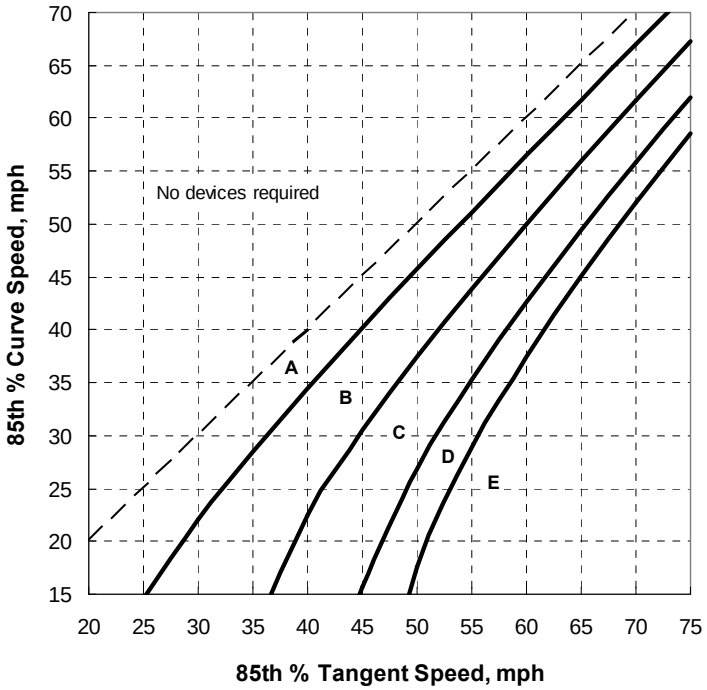

Figure 6. Friction-Based Guidelines for the Selection of Curve Traffic Control Devices.

Table 3. Friction-Based Guidelines for the Selection of Curve Traffic Control Devices.

Advisory Speed, mph	Device Type	Device Name	Device Number	Severity Category (Friction Differential, *g*) [e]				
				A (0.00)	B (0.03)	C (0.08)	D (0.13)	E (0.16)
35 mph or more	Warning Signs	Curve, Reverse Curve, Winding Road, Hairpin Curve [a]	W1-2, W1-4, W1-5, W1-11	✓	✓	✓	✓	✓
		Advisory Speed plaque	W13-1		✓	✓	✓	✓
		Combination Curve/ Advisory Speed	W1-2a			✓	✓	✓
		Chevrons [b]	W1-8				✓	✓
30 mph or less	Warning Signs	Turn, Reverse Turn, Winding Road, Hairpin Curve [a]	W1-1, W1-3, W1-5, W1-11	✓	✓	✓	✓	✓
		Advisory Speed plaque	W13-1		✓	✓	✓	✓
		Combination Turn/ Advisory Speed	W1-1a			✓	✓	✓
		Large Arrow sign	W1-6				✓	✓
Any	Delineation Devices	Raised pavement markers		✓	✓	✓	✓	✓
		Delineators [c]				✓	✓	✓
	Special Treatments [d]							✓

Notes:
a–Use the Curve, Reverse Curve, Turn, Reverse Turn, or Winding Road sign if the deflection angle is less than 135 degrees. Use the Hairpin Curve sign if the deflection angle is 135 degrees or more.
b–A Large Arrow sign may be used on curves where roadside obstacles prevent the installation of Chevrons.
c–Delineators do not need to be used if Chevrons are used.
d–Special treatments could include oversize advance warning signs, flashers added to advance warning signs, wider edgelines, and profiled pavement markings.
e–✓: optional; ✓: recommended. Severity category is determined using Figure 6.

HIGH-FRICTION SURFACE TREATMENT EVALUATION

The primary objective of evaluating high-friction surface treatments is to determine how much these treatments may improve pavement characteristics and thereby reduce crashes at the installation sites. Another important objective is to determine how the treatments' friction-increasing characteristics may degrade over time, and thus how often they may need to be replaced. These objectives are met through analysis of a surface treatment's characteristics and field-monitoring of the treatment over time.

This part of the chapter is divided into two sections. The first section reviews methods of quantifying the key physical characteristics of high-friction surface treatments and explains how the characteristics relate to safety. The second section presents the results of case studies that have been conducted on surface treatments.

Characterization of High-Friction Surface Treatments

Larson (*21*) identified poor roadway conditions as a contributing factor in about 30 percent of annual highway fatalities in the United States. These poor conditions include low pavement friction or issues with pavement macro-texture and roughness. Friction (the factor most affected by surface treatments) is the retarding force developed at the tire-pavement interface that helps to counteract longitudinal sliding during braking or sideways sliding when a vehicle traverses a curve. This variable is usually measured in terms of the coefficient of friction, which is the ratio of the drag force underneath the tire to the vertical tire load.

Physical Characteristics of Surface Treatments

Pavement micro-texture and macro-texture, and road surface conditions all affect friction. For example, the presence of water on the surface reduces the direct contact between the pavement and tire. Water films on the surface combined with vehicle speed can lead to loss of directional control or hydroplaning. The longitudinal and transverse road profile and surface macro-texture influence water film thickness. This is an issue particularly at the region labeled as "Problem Area 1" on Figure 5.

The deviations of a pavement surface from a true planar surface define texture (*22*). This pavement surface characteristic is differentiated into the following three distinct levels:

- Micro-texture covers wavelengths in the 1 μm to 0.5 mm range, with amplitudes less than 0.2 mm. It is related to the relative roughness of aggregate particles that make up the major volume of asphalt and Portland cement concrete (PCC) mixtures placed on road surfaces.
- Macro-texture covers wavelengths in the 0.5 mm to 51 mm range, with vertical amplitudes between 0.1 and 20 mm (*23*). In asphalt concrete pavements, macro-texture is related to the mix gradation; in PCC pavements, macro-texture is provided by the grooves that are intentionally formed while the concrete is still plastic or cut when the concrete has hardened. These grooves provide channels for water to flow from under the vehicle's

tire. Other texturing methods such as grinding or skid-abrading in concrete pavements also provide macro-texture.

- Mega-texture covers wavelengths in the same order of size as the tire-pavement interface (*22*). It is manifested in the distress, defects or waviness of the pavement surface, and primarily influences pavement smoothness or roughness.

The AASHTO *Guide for Pavement Friction* (*22*) identifies available methods for measuring pavement texture and friction (see Table 4). They are generally grouped as tests that can be conducted at highway speed versus static tests requiring traffic control. The specifications in the last column of Table 4 provide more detailed descriptions of the methods.

Table 4. Methods for Measuring Pavement Texture and Friction.

Pavement Surface Characteristic	Test Method or Equipment	Test Category	Related Specifications
Macro-texture	Non-contact lasers	Highway-speed	ASTM E1845, ISO 13473-1, ISO 13473-2, ISO 13473-3
	Sand-patch	Requires traffic control	ASTM E965, ISO 10844
	Outflow meter	Requires traffic control	ASTM E2380
	Circular texture meter	Requires traffic control	ASTM E2157
Micro-texture	British pendulum tester (BPT)[1]	Requires traffic control	ASTM E303
	Dynamic friction tester (DFT)[1]	Requires traffic control	ASTM E1911
	Sideways force coefficient routine investigation machine (SCRIM)[1]	Highway-speed	ASTM E670
Friction	Locked-wheel[2]	Highway-speed	ASTM E274
	Side-force[3]	Highway-speed	ASTM E670
	Fixed-slip[4]	Highway-speed	Various agency specifications
	Variable-slip[4]	Highway-speed	ASTM E1859
	Portable testers (such as BPT and DFT)	Requires traffic control	ASTM E303, ASTM E1911
	Deceleration rate measurement	Requires traffic control	ASTM E2101
	Stopping distance measurement	Requires traffic control	ASTM E2101

Notes:
1–Not a direct measurement of micro-texture. However, micro-texture can be evaluated from test data.
2–Simulates emergency braking without anti-lock system.
3–Measures ability to maintain control on curves.
4–Permits assessment of anti-lock brake systems in pavement friction measurements.

Aggregate type largely determines the durability of the surface material, in terms of susceptibility to polishing under traffic (*22*). The aggregate size and gradation of the asphalt concrete mix and the texturing method used on PCC surfaces largely determine the initial macro-texture of the pavement surface. Because of the influence of micro-texture and macro-texture, pavement friction is expected to decrease with pavement age due to aggregate polishing under traffic (which reduces micro-texture) and wearing of the aggregate under traffic and weather conditions (which diminishes macro-texture).

For the purpose of characterizing aggregate geometry, Masad (*24*) developed an aggregate imaging system (AIMS) to measure the shape, angularity, and texture properties of coarse and fine aggregates. AIMS permits contractors to control the quality of aggregates during production and provides measured aggregate characteristics that have been related to the performance of various hot-mix layers.

In a recent project that Masad et al. conducted for TxDOT (*25*), TTI researchers used AIMS to develop a model that relates the friction number at 60 km/h (F60) to aggregate characteristics, gradation, and traffic level. Their research showed that aggregate gradation and AIMS texture indices have a statistically significant correlation with the rate of change and terminal values of F60. To consider aggregate gradation in developing the friction model, researchers fitted the cumulative Weibull function to the aggregate size distribution data for the different aggregate types and asphalt concrete mixtures characterized during the research project.

Table 5 summarizes the parameters of the friction model that Masad et al. developed (*25*). The relationships for predicting the initial, terminal, and rate of change of F60 values were all found to be statistically significant. The friction model summarized in Table 5 can help predict the friction that can be expected of a given mix based on the aggregate gradation and resistance to polishing. This model can also be used to select the appropriate aggregate type commensurate to the friction demand of a given horizontal curve.

Table 5. Equations for Predicting Parameters of the Friction Model (*25*).

Parameter	Prediction Equation	R^2
Terminal F60	$\frac{18.422 + \lambda}{118.936 - 0.0013\ AMD^2}$	0.96
Initial F60	$0.4984 \ln\left[5.656\times10^{-4}\ (a_{agg} + b_{agg}) + 5.846\times10^{-2}\ \lambda - 4.985\times10^{-2}\ \kappa) + 0.8\right]$	0.82
Rate of change of F60	$0.765\ \exp\left(\frac{-7.297\times10^{-2}}{c_{agg}}\right)$	0.90
where:		
AMD = aggregate texture after Micro-Deval test $a_{agg} + b_{agg}$ = aggregate initial texture using texture model c_{agg} = aggregate texture rate of change using texture model λ, κ = Weibull scale and shape factors, respectively		

Identification and Assessment of Effective Surface Treatments

The methods listed in Table 4 can be used to measure surface friction at horizontal curve sites where side friction supply is believed to be inadequate. The side friction supply can then be subtracted from the side friction demand to obtain the curve's margin of safety. This represents the fifth step in the margin of safety analysis process described in the first part of this chapter. An inadequate margin of safety can indicate the need to increase side friction supply through the provision of a surface treatment, and also indicate the amount of side friction supply increase that would be needed. It would then be necessary to identify a surface treatment that could provide the needed increase in side friction supply. Additionally, the methods listed in Table 4 can be used periodically to monitor the effectiveness of a surface treatment as it degrades with time.

The model summarized in Table 5 can be used to estimate both the initial effectiveness of a proposed surface treatment and its decrease in effectiveness over time. This type of analysis is important for two reasons:

- A proposed surface treatment must be determined to be sufficient to meet the margin of safety requirements for a given curve before it is installed.
- It must be determined whether, or how often, the surface treatment will need to be replaced so the needed margin of safety will continue to be available.

Current Installation Results and Lessons Learned

The AASHTO *Guide for Pavement Friction* provides guidance on aggregates, mixtures, and surface types that provide long-lasting, high-quality friction surfaces, with due consideration to other issues related to noise, cost, splash-spray, hydroplaning potential, and tire wear. Surface treatment design requires proper selection of aggregates, hot-mix asphalt/Portland cement concrete (PCC) mixtures, and PCC texturing techniques to provide the needed side friction supply at a particular site.

The Federal Highway Administration (*26*) recommends using dense-graded asphalt mixtures with a high-quality, polish resistant aggregate to provide adequate surface texture. According to the FHWA, the following aggregate characteristics affect surface friction:

- Aggregate angularity–frictional resistance is expected to be higher with wearing courses that utilized angular aggregates. In addition, aggregates with a high number of fractured faces improve asphalt concrete mix stability.
- Aggregate soundness–indicates the aggregate's resistance to weathering.
- Aggregate toughness–indicates the aggregate's resistance to abrasion and degradation during handling and construction and while in service.
- Polish resistance–use of high-quality, polish-resistant aggregate is recommended.

Because of the expense associated with placing dense-graded mixtures having high-quality, polish-resistant aggregates, highway agencies have applied less expensive surface treatments on existing hot-mix asphalt concrete pavements to improve skid resistance. Chip

seals and micro-surfacings are among the most common treatments. Chip seals consist of applying asphalt directly to the pavement surface, followed by an application of aggregate chips (9.5 to 15mm in size), which are then rolled to achieve 50 to 70 percent embedment. When properly placed, this surface treatment provides good frictional characteristics at both high and low speeds.

Micro-surfacing is an advanced form of slurry seal that uses a combination of emulsified asphalt, water, fine aggregate, mineral filler, and polymer additives. The New York Department of Transportation has successfully used this form of surface treatment in its Skid Accident Reduction Program (SKARP). Between 1990 and 2000, Bray (*27*) reported a 34 percent reduction in annual roadway fatalities in New York. Bray attributes this reduction to the state's pavement preservation program (which features the application of thin non-carbonate overlays or micro-surfacing treatments on high-crash frequency, low friction pavements) combined with the state's SKARP and Safety Appurtenance Program.

A surface treatment called Typegrip® was installed on a loop entrance ramp in Florida, and before-after analyses were conducted on crashes and safety surrogate measures (*28*). The Typegrip® treatment consists of an epoxy resin topped with calcined bauxite. A small reduction in crashes was observed following the installation of the treatment, but it was not found to be statistically significant. Speeds were found to decrease by an average of 3.72 mi/h in dry conditions and 2.62 mi/h in wet conditions, and the proportion of vehicles encroaching on the shoulder in wet conditions decreased substantially.

Surface treatments consisting of calcined bauxite were evaluated at five sites in New Zealand (*29*). Two of the sites were highway entrance ramps, two were exit ramps, and one was a traffic circle at an interchange. Crash counts were conducted before and after the treatments were installed. Though the findings are limited due to a paucity of time included in the "after" periods, the authors suggested that the exit ramp sites experienced notable reductions in crashes, which were frequent in the "before" period due to loss of control while cornering.

Izeppi et al. conducted a benefit-cost analysis of several types of surface treatments (*30*). They reported crash counts for a steel-slag-based treatment called Italgrip® that was installed at four sites in Wisconsin. Table 6 provides the crash counts.

Table 6. Before-After Crash Counts at Four Surface Treatment Sites.

Site Number	Before Period (3 years)				After Period (3 years)			
	Incidents	Vehicles Involved	Injuries	Fatalities	Incidents	Vehicles Involved	Injuries	Fatalities
1	5	7	2	0	0	0	0	0
2	11	30	6	0	1	4	0	0
3	3	16	3	0	0	0	0	0
4	9	10	3	0	1	3	2	0

Along with these crash counts, the authors considered the installation costs of the surface treatments. They reported benefit-cost ratios of 0.47, 3.41, 8.45, and 2.23, respectively, for the four sites.

In summary, various case studies like the aforementioned ones have been conducted on surface treatments that have been installed to increase pavement friction. Some of these case studies were conducted at curve sites, where side friction is of concern, while others were conducted at tangent sites where increased pavement friction is needed because of frequent stopping, such as at toll plazas. The studies generally report positive results in terms of reduced crashes or improvements in safety surrogate measures like shoulder encroachments. However, benefit-cost analysis does not always show that the treatments were cost-justified.

REFERENCES

1. Zegeer, C., R. Stewart, D. Reinfurt, F. Council, T. Neuman, E. Hamilton, T. Miller, and W. Hunter. *Cost-Effective Geometric Improvements for Safety Upgrading of Horizontal Curves.* FHWA-RD-90-021. Federal Highway Administration, U.S. Department of Transportation, Washington, D.C., 1991.
2. Fitzpatrick, K., L. Elefteriadou, D.W. Harwood, J.M. Collins, J. McFadden, I.B. Anderson, R.A. Krammes, N. Irizarry, K.D. Parma, K.M. Bauer, and K. Passetti. *Speed Prediction for Two-Lane Rural Highways.* FHWA-RD-99-171. Federal Highway Administration, U.S. Department of Transportation, Washington, D.C., 2000.
3. Bonneson, J., M. Pratt, J. Miles, and P. Carlson. *Development of Guidelines for Establishing Effective Curve Advisory Speeds*. Report FHWA/TX-07/0-5439-1, Texas Transportation Institute, College Station, Texas, 2007.
4. Bonneson, J., and M. Pratt. *Roadway Safety Design Workbook*. Report FHWA/TX-09-0-4703-P2, Texas Transportation Institute, College Station, Texas, 2009.
5. Torbic, D., D. Harwood, D. Gilmore, R. Pfefer, T. Neuman, K. Slack, and K. Hardy. *Guidance for Implementation of the AASHTO Strategic Highway Safety Plan. Volume 7: A Guide for Reducing Collisions on Horizontal Curves.* NCHRP Report 500. TRB, National Research Council, Washington, D.C., 2004.
6. Lord, D., M. Brewer, K. Fitzpatrick, S. Geedipally, and Y. Peng. *Analysis of Roadway Departure Crashes on Two-Lane Rural Roads in Texas*. Report FHWA/TX-11/0-6031-1, Texas Transportation Institute, College Station, Texas, 2011.
7. *A Policy on Geometric Design of Highways and Streets.* 5th Edition. American Association of State Highway and Transportation Officials, Washington, D.C., 2004.
8. Morrall, J., and R. Talarico. Side Friction Demanded and Margins of Safety on Horizontal Curves. In *Transportation Research Record: Journal of the Transportation Research Board, No. 1435*, TRB, National Research Council, Washington, D.C., 1994, pp. 145–152.
9. Harwood, D., and J. Mason. Horizontal Curve Design for Passenger Cars and Trucks. In *Transportation Research Record: Journal of the Transportation Research Board, No. 1445*, TRB, National Research Council, Washington, D.C., 1994, pp. 22–33.
10. Glennon, J., and G. Weaver. Highway Curve Design for Safe Vehicle Operations. In *Highway Research Record, No. 390*, Highway Research Board, National Research Council, Washington, D.C., 1972, pp. 15–26.
11. Glennon, J., and G. Weaver. *The Relationship of Vehicle Paths to Highway Curve Design.* Research Report 134-5. Texas Transportation Institute, College Station, Texas, 1971.
12. Glennon, J. *State of the Art Related to Safety Criteria for Highway Curve Design.* Research Report 134-4. Texas Transportation Institute, College Station, Texas, 1969.

13. Emmerson, J. Speeds of Cars on Sharp Horizontal Curves. In *Traffic Engineering & Control*, Vol. 11, No. 3, July 1969, pp. 135–137.
14. Winsum, W., and H. Godthelp. Speed Choice and Steering Behavior in Curve Driving. In *Human Factors*, Vol. 38, No. 3, 1996, pp. 434–441.
15. Bonneson, J. *Superelevation Distribution Methods and Transition Designs*. NCHRP Report 439. TRB, National Research Council, Washington, D.C., 2000.
16. Spacek, P. Track Behavior in Curve Areas: Attempt at Typology. In *Journal of Transportation Engineering*, Vol. 131, No. 9, September 2005, pp. 669–676.
17. Koorey, G., S. Page, P. Stewart, J. Gu, A. Ellis, R. Henderson, and P. Cenek. *Curve Advisory Speeds in New Zealand.* Transfund New Zealand Research Report No. 226. Transfund New Zealand, Wellington, New Zealand, 2002.
18. *Manual of Uniform Traffic Control Devices.* Queensland Government, Department of Main Roads, Brisbane, Australia, 2003.
19. *Manual of Traffic Signs and Markings.* Transit New Zealand, Wellington, New Zealand, 2001.
20. Glennon, J.C. *Thoughts on a New Approach for Signing Roadway Curves*. http://www.johncglennon.com/papers.cfm?PaperID=18 . Accessed December 7, 2006.
21. Larson, R. M. *Using Friction and Texture Data to Reduce Traffic Fatalities, Serious Injuries, and Traffic Delays*. International Conference for Surface Friction for Roads and Runways, Christchurch, New Zealand, 2005.
22. American Association of State Highway and Transportation Officials (AASHTO). *Guide for Pavement Friction*. Washington, D.C., 2008.
23. Henry, J. J. *Evaluation of Pavement Friction Characteristics*. National Cooperative Highway Research Program Synthesis of Highway Practice 291. TRB, Washington, D.C., 2000.
24. Masad, E. *Aggregate Imaging System (AIMS): Basics and Applications*. Report 5-1707-01-1, Texas Transportation Institute, Texas A&M University System, College Station, Texas, 2005.
25. Masad, E., A. Rezaei, A. Chowdhury and P. Harris. *Predicting Asphalt Mixture Skid Resistance Based on Aggregate Characteristics*. Research Report 0-5627-1, Texas Transportation Institute. The Texas A&M University System, College Station, Texas, 2009.
26. Federal Highway Administration (FHWA). *Surface Texture for Asphalt and Concrete Pavements*. Technical Advisory T 5040.36, Washington, D.C., 2005.
27. Bray, J. S. *Skid Accident Reduction Program (SKARP): Targeted Crash Reductions*. Institute of Transportation Engineers Technical Conference and Exhibit, Fort Lauderdale, Florida, 2003.
28. Reddy, V., T. Datta, P. Savolainen, and S. Pinapaka. *Evaluation of Innovative Safety Treatments: A Study of the Effectiveness of Typegrip High Friction Surface Treatment*. HNTB Corporation, Fort Lauderdale, Florida, 2008.
29. Iskander, R., and A. Stevens. *The Effectiveness of the Application of High Friction Surfacing on Crash Reduction*. Beca Infrastructure Limited, Auckland, New Zealand, 2005.
30. Izeppi, E., G. Flintsch, and K. McGhee. *Field Performance of High Friction Surfaces*. Report FHWA/VTRC 10-CR6, Virginia Tech Transportation Institute, Blacksburg, Virginia, 2010.

CHAPTER 3. CRASH DATA ANALYSIS

INTRODUCTION

Current research efforts focus on run-off-road (ROR) crashes on horizontal curves because of the disproportionate number of fatal crashes occurring in these locations. According to the Fatality Analysis Reporting System of the 38,000 fatal crashes on the U.S. highway system in 2002, approximately 25 percent of them occurred along horizontal curves (*1*). Additionally, approximately half of all fatal crashes were roadway departure, or run-off road crashes (*2*).

Previous research has indicated that many ROR crashes resulted from vehicles traveling too fast for the weather or roadway conditions of the curve (*1*). Available safety tools attempt to alleviate these challenges. Geometric improvements, such as curve straightening to increase the radius, reduce the severity of curves. This type of improvement is expensive and may necessitate the acquisition of right-of-way. Other improvements include traffic control improvements or surface treatments. Traffic control improvements alert drivers to the presence of a curve. These improvements include curve advisory speed signs, which communicate to drivers the importance of reducing speeds to safely negotiate a curve, and supplemental devices like delineators or Chevrons. Treatments such as rumble strips or profiled markings provide drivers with an auditory and vibratory warning that their vehicle is departing the travel lane. Additionally, wider edgelines have been proposed as low-cost enhancements to improve safety. Edgelines serve as a pavement marking to "define or delineate the edge of a roadway" and act as a visual reference to prevent motorists from drifting their travel lane (*3*).

Surface treatments increase the amount of side friction present on a curve, increasing the margin of safety for drivers traversing the curve. Surface treatments can include the use of:

- Conventional materials like seal coat or hot-mix asphalt.
- Special materials like permeable friction course (PFC) or calcined bauxite.
- Texture alteration through methods like pavement grooving with a milling machine.

The costs associated with these treatments dictate that the treatments be implemented only where a safety analysis indicates a potential benefit that could not be obtained with lower-cost treatments. Hence, an exploration of safety trends on Texas highway curves is needed as a step toward developing guidelines for the use of surface treatments on curves.

This chapter consists of three parts. The first part describes the development of a horizontal curve safety database. The second part documents an exploratory analysis that was conducted on the trends observed in the safety data. The third part summarizes the analysis findings.

EXPLORATORY ANALYSIS

Two sets of horizontal curves were assembled for analysis. The first set consisted of the top 101 curve ROR crash locations in Texas, and the second set consisted of 400 randomly chosen ("control") horizontal curves.

Curve Identification

The top 101 ROR crash curves were identified using a combination of the following four crash risk criteria:

- Total crash count.
- ROR crash count.
- Total crash rate.
- ROR crash rate.

These criteria were computed for all horizontal curves on state-maintained roads in Texas, using a database that was generated by merging the Texas Reference Marker (TRM) database and the Crash Records Information System (CRIS) database. Fatal and injury crashes were included in the merged database.

The top 101 ROR crash curves and the 400 control curves were located on maps using their control section, milepoint, and distance from origin (DFO) linear referencing data from the TRM database, then comparing these data to similar data from reference locations like highway intersections. Using Google Earth®'s "path measure" tool, the curve was located by starting at a known milepoint at an intersection and measuring to the curve. A placemark was then positioned on the curve with the curve identification number.

Figure 7 illustrates the top 101 ROR crash locations in Texas. Figure 8 illustrates the 400 control curves. As shown, the distributions of both sets of curves generally reflect the distribution of roadway mileage in the state.

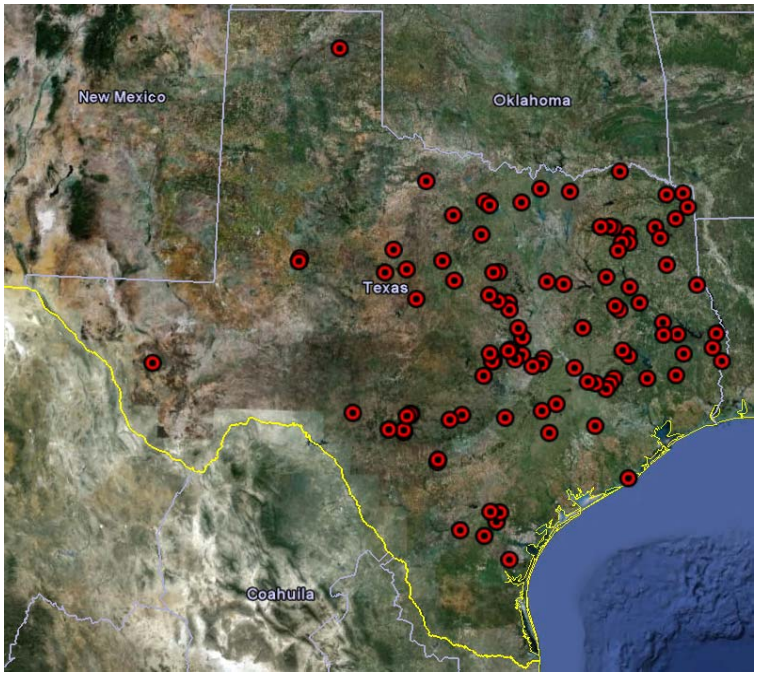

Figure 7. Top 101 ROR Crash Curves.

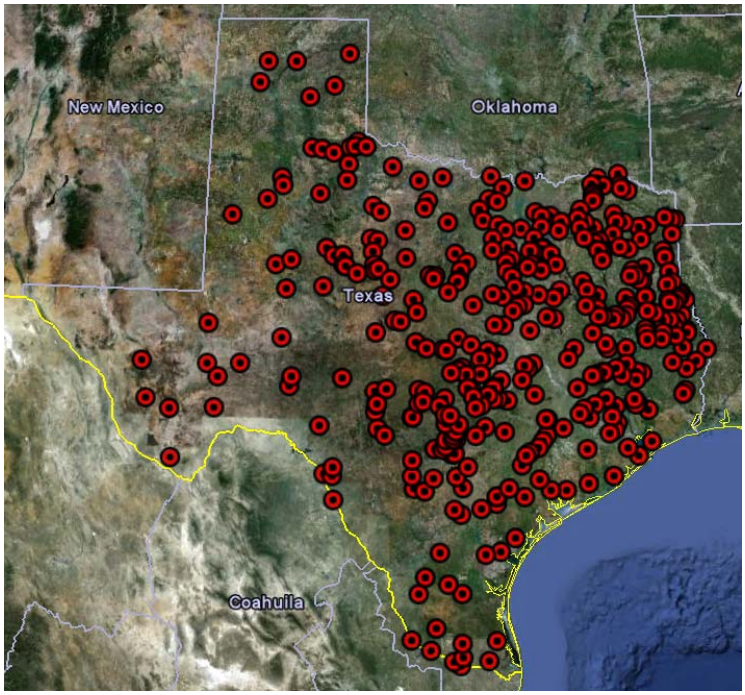

Figure 8. Additional 400 Locations.

Geometric Characteristics

The researchers conducted a query of the merged TRM-CRIS database to obtain a preliminary comparison of the top 101 curves and the entire population of curves in Texas. Table 7 shows the results of this comparison. Matched against the statewide population of curves, the top 101 curves tend to have smaller radii, larger deflection angles, and narrower cross sections.

Detailed geometric data were collected for the top 101 curves and the 400 control curves using aerial photography. In Google Earth, placemarks were put on specific locations of the curve, starting before the point of curvature and ending after the point of tangency (see Figure 9). The locations of the placemarks were then saved in a keyhole markup language (kml) file with the curve identification number as the file name. A Microsoft Excel® spreadsheet program was used to extract the placemarks' latitude and longitude coordinates from the kml files to calculate the radius, length, and deflection angle for each curve.

Aerial and street view images in Google Earth were used to compile cross sectional data. These data included number of lanes, lane width, and shoulder width. The widths were obtained with Google Earth's measuring tool.

Traffic control characteristics were found using street view images on Google Earth. These characteristics included the regulatory speed limit and curve advisory speed, as well as the presence of treatments including:

- Delineators.
- Chevrons (W1-8).
- The Large Arrow sign (W1-6).
- Shoulder rumble strips.
- Centerline rumble strips.

Crash data were retrieved from the CRIS database for the years 2007–2011. These data consisted of information describing date and location of the crash, severity, and weather conditions. For this analysis, the following four crash severity levels were used:

- Fatal (K).
- Incapacitating injury (A).
- Non-incapacitating injury (B).
- Minor injury (C).

Contributing factors associated with the curve crashes were queried, and are shown in Figure 10. Compared to the statewide population of curves, the top 101 curves experienced more speed-related crashes and fewer crashes with unknown or unspecified contributing factors. The distribution of crashes related to animals, driver inattention, lane-keeping failure, and faulty evasive action were similar between the top 101 curves and the statewide population of curves.

Table 7. Geometric Characteristics of Curves.

Variable	Value	All Texas Curves		Top 101 Curves	
		Frequency	Percent	Frequency	Percent
Radius (ft)	Tangent-3820	10765	31.2	12	11.9
	3820–1270	15573	45.2	29	28.7
	1270–600	6512	18.9	33	32.7
	≤ 600	1611	4.7	27	26.7
Deflection Angle (°)	0–20	17498	50.8	38	37.6
	20–40	9596	27.8	21	20.8
	40–60	4057	11.8	19	18.8
	≥ 60	3310	9.6	23	22.8
AADT (veh/d)	<100	2181	6.3	1	1.0
	100–500	11864	34.4	43	42.6
	500–1000	7097	20.6	47	46.5
	≥ 1000	13319	38.6	10	9.9
Surface Type	Low Type Bituminous Surface-Treated	23497	68.2	79	78.2
	Intermediate Type Mixed	639	1.9	5	5.0
	High Type Flexible	9318	27.0	15	14.9
	High Type Rigid	68	0.2	0	0.0
	High Type Composite	939	2.7	2	2.0
Surface Width (ft)	≤ 18	2296	6.7	10	9.9
	20	13664	39.7	45	44.6
	22	4842	14.1	22	21.8
	24	11167	32.4	23	22.8
	≥ 26	2492	7.2	1	1.0
Shoulder Width (ft)	0	4914	14.3	12	11.9
	1–3	11951	34.7	56	55.4
	4–6	10682	31.1	33	32.7
	> 6	6851	19.9	0	0
	missing	63		0	

Figure 9. Google Earth Placemarks.

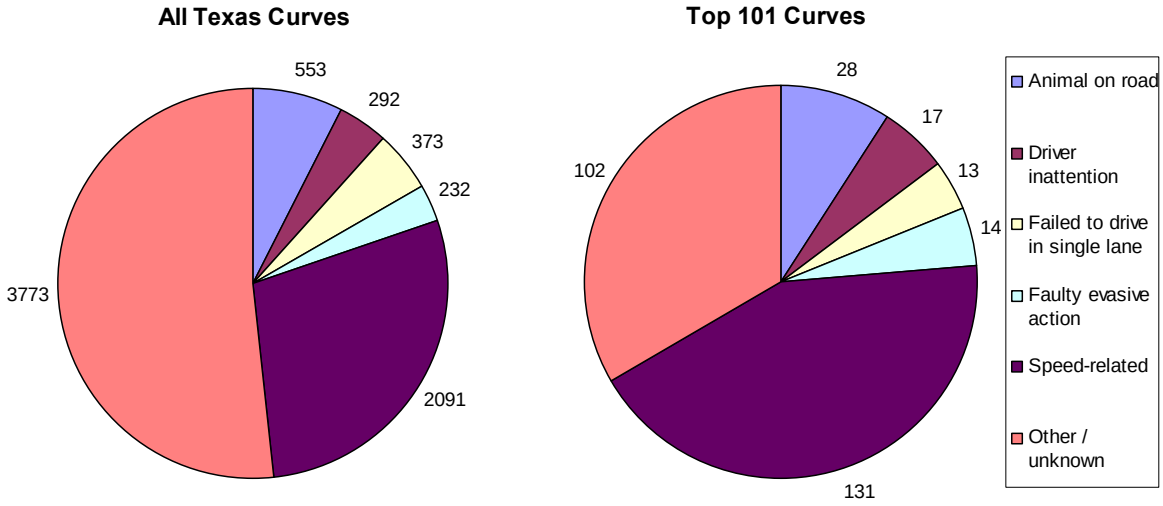

Figure 10. Crash Contributing Factors.

Analysis

Researchers attempted to collect data for all 501 curve sites (top 101 + 400 control) including geometric, cross section, and traffic control characteristics. However, some of the curves had to be discarded because of low-quality aerial or street view images. Additionally, curves that had a less than 5-degree deflection angle were omitted from analysis. When curve alignment characteristics where analyzed, 458 sites had the appropriate data available (curve

radius, length, and deflection angle). These sites were associated with a total of 511 crashes, including 306 ROR crashes. For the rest of the analysis tasks (cross section, traffic control, etc.), complete data were required. A total of 386 sites were available for these efforts. These sites were associated with a total of 470 crashes, including 272 ROR crashes. Table 8 through Table 16 summarize the database utilized in subsequent analyses.

Table 8. Sample Size.

	High ROR Crash Locations			Control			Total Curve Count
	Curve Count	Total Crash Count	ROR Crash Count	Curve Count	Total Crash Count	ROR Crash Count	
Complete Data	88	183	158	298	287	113	386
Partial Data	12	34	29	60	7	6	72
Grand Total	100	217	187	358	294	119	458

Table 9. Data Range of Curve Geometric Characteristics.

	Min.	Average	Max.	Min.	Average	Max.
Radius (feet)	224	1263	5986	486	3797	40807
Length (miles)	0.10	0.17	0.96	0.10	0.20	0.47
Deflection Angle (degrees)	5.25	52.15	143.90	0.67	27.82	95.56
Lane Width (feet)	8.40	10.97	13.40	8.30	11.54	22.95
Shoulder Width (feet)	0	2	6.95	0	5	14.10

Table 10. Traffic Control Device Presence.

Device	Curve Count			
	High ROR Crash Locations		Control	
	Present	Not Present	Present	Not Present
Chevrons	24	64	13	285
Delineators	8	80	1	297
Large Arrow	0	88	1	297

Table 11. Rumble Strip Presence.

Rumble Strip Location	Undivided Cross Sections		Divided Cross Sections	
	High ROR Crash Locations	Control	High ROR Crash Locations	Control
None	88	249	0	20
Shoulder	0	2	0	27
Centerline	0	3		

The exploratory analysis was conducted using two methods. The first method involved analyzing the combined database that included the high ROR crash locations and the control locations. The second method involved analyzing the high ROR crash locations and the control locations separately to identify notable differences between the two groups. The highlights of these analyses are described in the following sections.

Combined Data Set Analysis

Alignment characteristics of horizontal curves were compared with crash rates. Two rates were analyzed: total crash rate and run-off road crash rate, measured in crashes per million vehicle-miles (cr/mvm). Figure 11 illustrates that as radius increases, crash rate decreases. This trend is consistent with the findings of previous research (*4*, *5*).

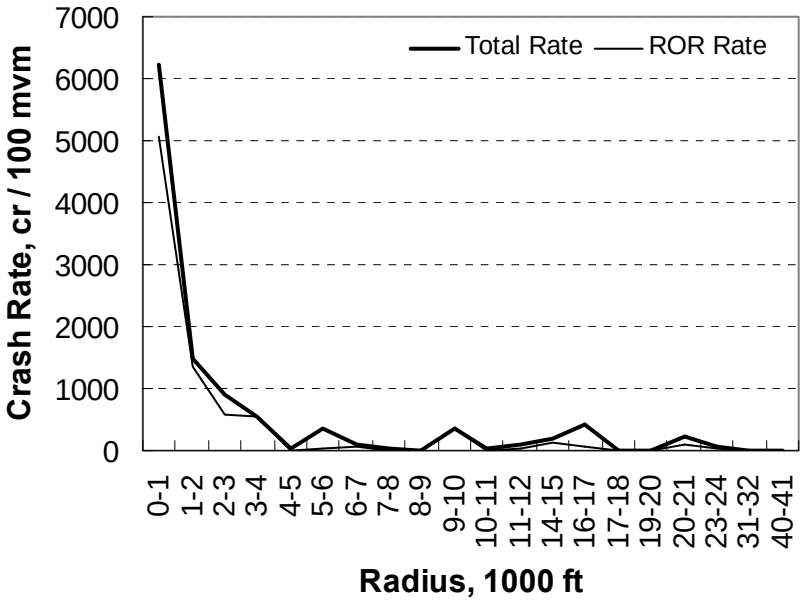

Figure 11. Crash Rate versus Radius.

Figure 12 summarizes the number of ROR crashes by crash rate and average shoulder width. Overall, as the average shoulder width decreases, the crash rate increases. The trends in Figure 12 partially reflect the distribution of the sites within the binned average shoulder width ranges. The most notable observation is that all curves within the higher crash rate ranges have average shoulder widths of 4 ft or less.

Figure 13 illustrates the relationship between ROR crash rates and shoulder rumble strips on divided highway curves. The presence of shoulder rumble strips appears to have a mixed effect on the rates of ROR crashes of different severities. This comparison could not be repeated for undivided highway curves because none of these curves had shoulder rumble strips.

Figure 14 illustrates the relationship between ROR crash rate and speed reduction, which is defined as the difference between the regulatory speed and the curve advisory speed. For curves that have no posted advisory speed, the speed reduction is defined as 0 mph. There is a general trend toward increasing crash rate as the speed reduction increases. It can also be seen that fatal crashes are rare on curves with speed reductions of 25 mph or less.

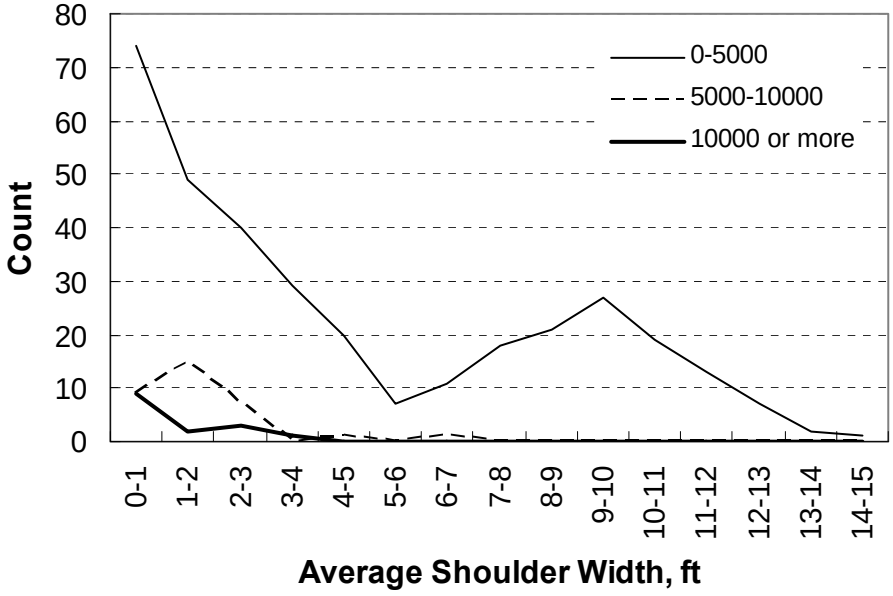

Figure 12. ROR Crash Rate and Average Shoulder Width.

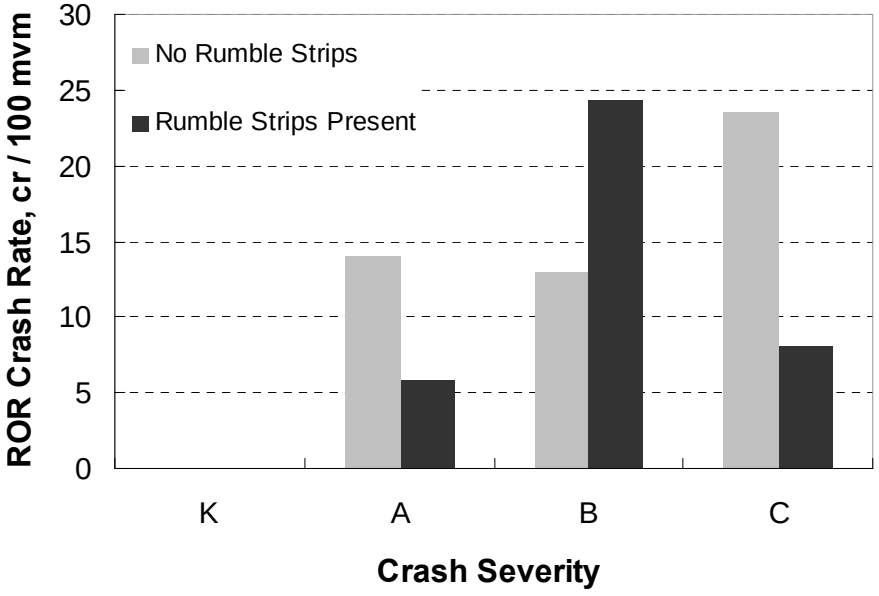

Figure 13. ROR Crash Rates and Shoulder Rumble Strips on Divided Highways.

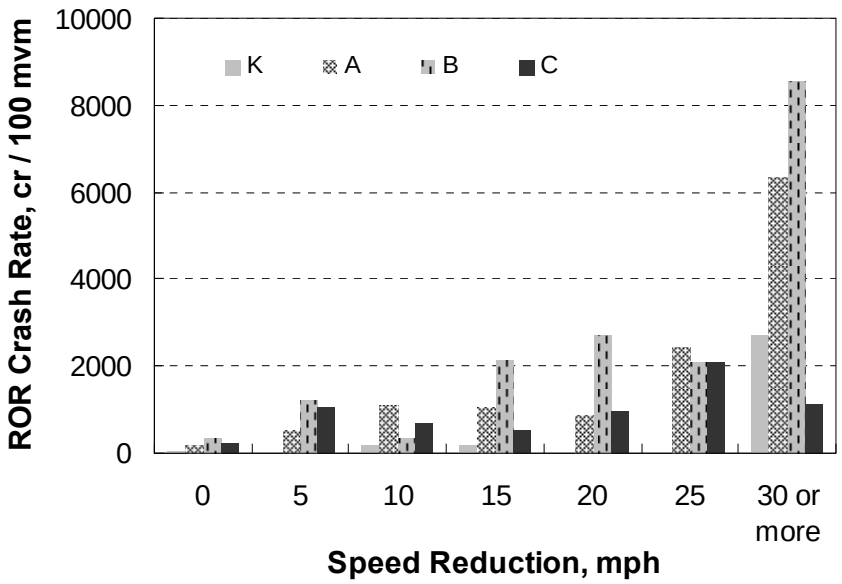

Figure 14. ROR Crash Rate and Speed Reduction.

Separate Analysis of High ROR Crash Locations and Control Locations

Figure 15 compares the distributions of radii that were measured at the high ROR crash locations and the control locations. It can be seen that high ROR crash locations have a higher percentage of curves with smaller radii. Additionally, very few of the high ROR crash locations have curve radii in excess of 2000 ft.

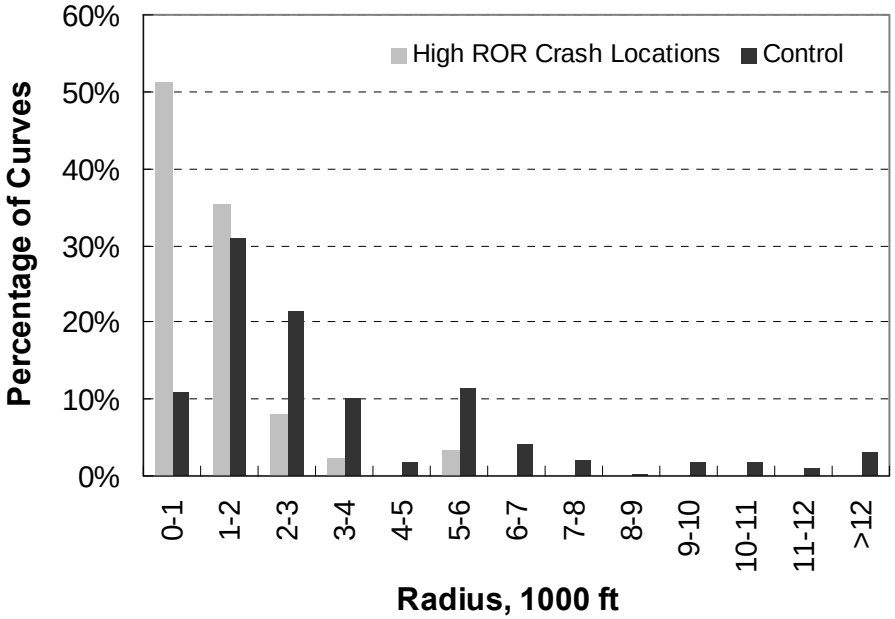

Figure 15. Distribution of Curves by Radius.

Figure 16 compares high ROR crash locations and control locations by deflection angle. The control locations have a higher percentage of curves with small deflection angles. The high ROR crash locations have more curves with a large deflection angle, suggesting a more severe curve.

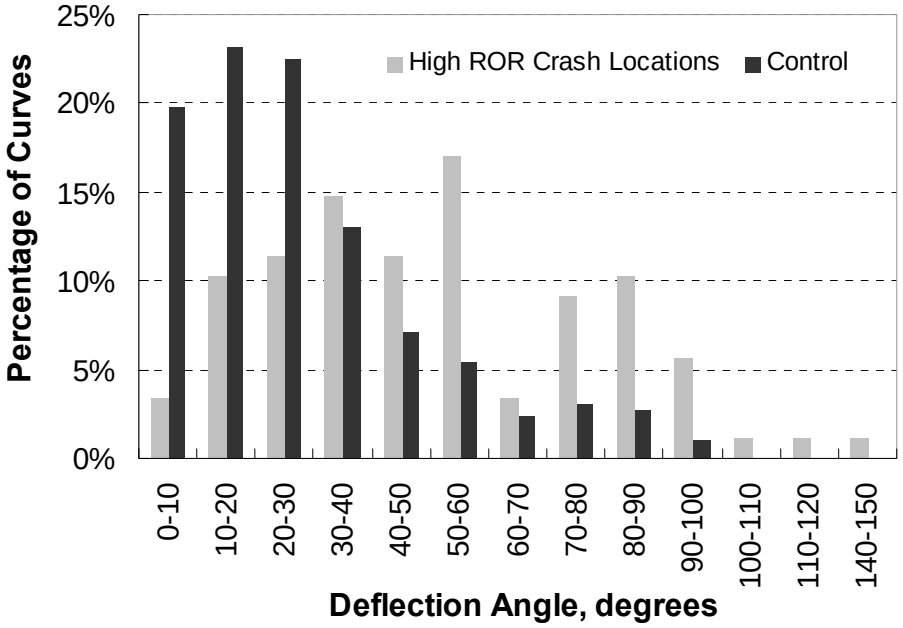

Figure 16. Distribution of Curves by Deflection Angle.

Figure 17 compares high ROR crash locations and control locations by lane width. Both sets follow a similar trend with the control set having slightly wider lanes, as seen in the 12- to 13-foot lane widths. More generous lane widths allow drivers to "cut" the curve to a greater extent, and increase the amount of lane-drifting that can occur before a correcting maneuver becomes necessary. Additionally, on undivided roadways, wider lanes increase the separation between vehicles traveling in opposing directions.

Figure 18 compares high ROR crash locations and control locations by average shoulder width. The control set has a higher percentage of curves with larger shoulder widths. The wider shoulders allow errant drivers more time to return to the lane before departing the pavement surface. Additionally, on divided highways, wider shoulders allow for more distance between opposing traffic.

Figure 19 illustrates the difference between regulatory and curve advisory speeds on high ROR crash locations and control locations. A difference of 0 mph indicates that a curve advisory speed was not posted. More curve advisory speed signs are posted at high ROR crash locations.

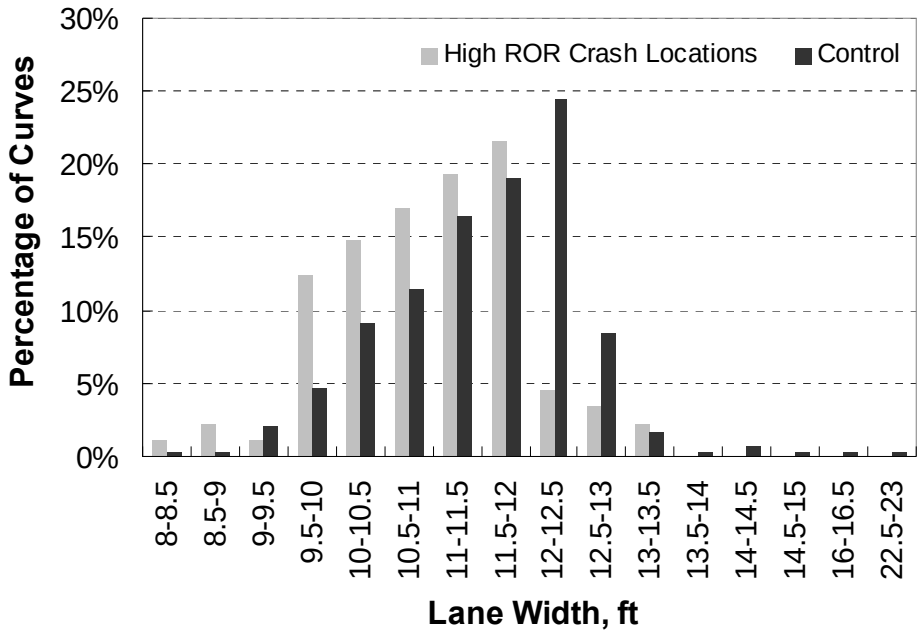

Figure 17. Distribution of Curves by Lane Width.

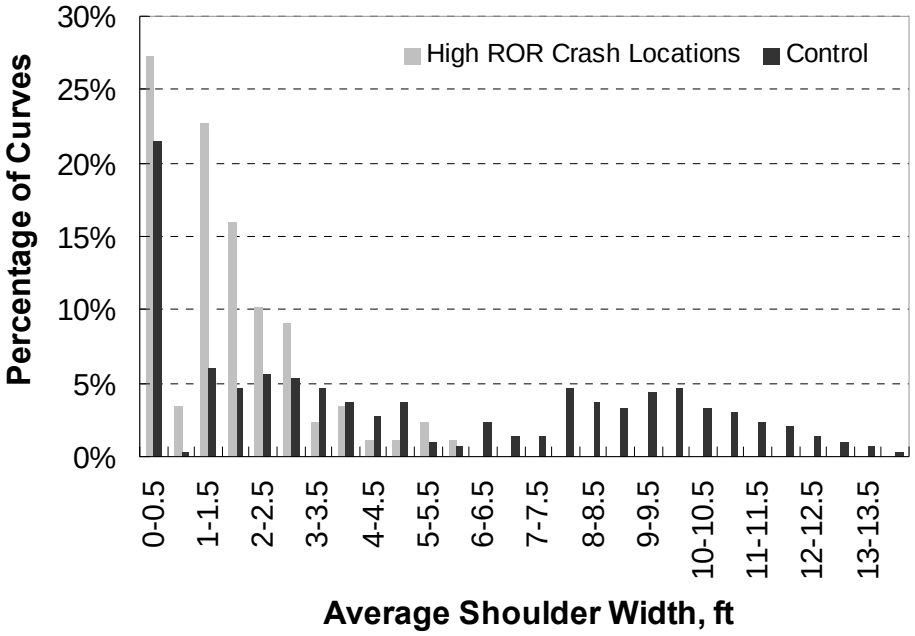

Figure 18. Distribution of Curves by Average Shoulder Width.

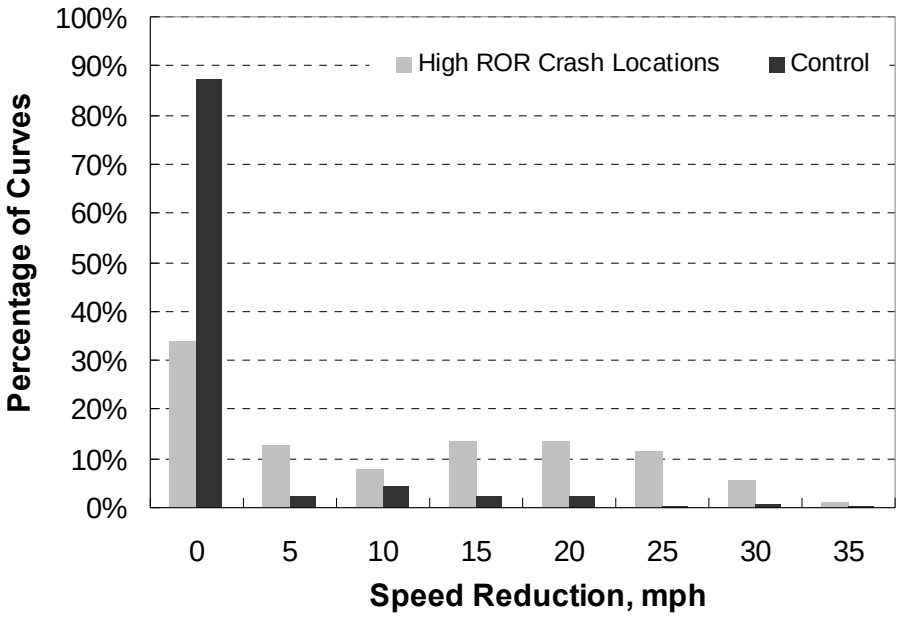

Figure 19. Distribution of Curves by Speed Reduction.

Findings

The exploratory analysis identified important variables when comparing ROR crash rates on high ROR crash locations and control locations. Radius, deflection angle, lane width, and shoulder width have been identified as key geometric variables. The presence of rumble strips has also been found to be relevant to the safety performance of a curve, as has the reduction between the regulatory speed limit and the advisory speed, which can function as a qualitative measure of curve severity.

The findings from this exploratory analysis are preliminary, as they may be influenced by correlation between variables and the distribution of site characteristics within the databases. Additional investigation is needed to fully quantify the effects of the key variables on curve safety performance. The findings of this exploratory analysis will be used to direct the development of cross-sectional safety prediction models. Model development offers the advantage of quantifying the effects of a range of variables even if some of the variables are correlated, and yielding insight that is more applicable to a range of sites.

CROSS-SECTIONAL MODEL DEVELOPMENT

This part of the chapter presents the results of the cross-sectional statistical analysis. The primary objective of this task was to develop safety performance functions (SPFs) to describe the relationship between crash frequency and traffic and geometric variables for horizontal curves in Texas. The development of cross-sectional safety prediction models offer the advantage of quantifying the effects of a range of variables even if some of the variables are correlated, and yielding insight that is more applicable to a range of sites. In general, a robust safety prediction methodology would require the use of a cross-sectional study approach.

Cross-sectional data each have an independent variable value averaged for each site over a particular period of time. In contrast, with panel data, each independent variable value is measured for each site for each year. The cross-sectional data approach has the following advantages:

- It provides a more robust predictive model than panel data when the year-to-year variability in the independent variables is largely random.
- Using cross-sectional data for model calibration will minimize the problems associated with over-representation of segments or intersections with zero crash.

This chapter consists of three parts. The first part describes the development of a horizontal curve safety database. The second part documents the regression analysis. The third part summarizes the analysis findings.

Database Development

The database assembled for developing the cross-sectional models consisted of a set of similar horizontal curves. The horizontal curve information was extracted from the Texas Reference Marker System (TRM) Geometrics (Geo-Hini) database. The Geo-Hini database contains geometrics for all curves on all highways in the state. Each curve is given a unique curve identifier number, and the beginning and end milepoints of each curve are located through a given reference marker and curve length from that marker. Only normal curves (i.e., curves that deflect at a constant rate) that are ≥ 0.1 miles in length were considered in this analysis.

The horizontal curve database was combined with the TxDOT's Road-Highway Inventory Network (RHiNo) database using the control section number and milepoints. Variables that extracted from the Rhino database included Annual Daily Traffic (ADT) and truck percentage.

Pavement data were obtained from the Pavement Management Information System (PMIS) database. Specifically, the following quantities were extracted:

- Skid score (or skid number).
- Condition score.
- Distress score.
- Ride score.
- International roughness index (IRI).

These quantities provide insight into friction supply and general pavement condition. The curves of interest were located in the PMIS database using reference markers and displacements.

Researchers retrieved crash data for the years 2007–2011 from TxDOT's Crash Records Information System (CRIS) database. These data consisted of information describing date and location of the crash, severity, and weather conditions. Since it is widely recognized that property damage only (PDO) crash counts vary widely on a regional basis due to significant

variation in reporting threshold, only those crashes that are associated with injury or fatality were considered in this study. The following four crash severity levels were used:

- Fatal (K).
- Incapacitating injury (A).
- Non-incapacitating injury (B).
- Minor injury (C).

Once the crash and road-related data were collected for each horizontal curve, the data were combined using control section number and milepoints. Three separate databases were built:

- One for horizontal curves on two-lane segments.
- Another for horizontal curves on four-lane undivided segments.
- A third for horizontal curves on four-lane divided segments.

Table 12 presents the summary statistics of the variables used for SPF development. The database assembled for calibration included crash frequency as the dependent variable. The crash data were separated into four categories:

- All crashes.
- All wet-weather-related crashes.
- Run-of-the-road (ROR) crashes.
- ROR wet-weather-related crashes.

Geometric design features, traffic control features, and traffic characteristics were included as independent variables.

Table 12. Summary Statistics for Horizontal Curve SPF Development.

Variable	Two-Lane			Four-Lane Undivided			Four-Lane Divided		
	Range	Mean (SD)*	Total	Range	Mean (SD)*	Total	Range	Mean (SD)*	Total
Curve Length (Miles)	0.1–0.99	0.19 (0.09)	4051	0.1–0.86	0.21 (0.1)	154	0.1–0.99	0.29 (0.16)	381
ADT (Vehicles/day)	14–40,200	1443 (1990)	--	412–34,400	9045 (6558)	--	972–70368	15633 (11333)	--
Average Lane Width (ft)	8–16	10.96 (1.1)	--	10–16	12.5 (1.5)	--	10–15	12.0 (0.4)	--
Average Inside Shoulder Width (ft)	--	--	--	--	--	--	0–14	4.63 (1.69)	--
Average Outside Shoulder Width (ft)	0–17	3.7 (2.9)	--	0–12	4.4 (3.7)	--	0–16	9.63 (1.94)	--
Radius (ft)	355–28662	2705 (2032)	--	520–28250	3886 (2580)	--	755–40866	5740 (3437)	--
Maximum Speed (Miles/hour)	30–75	60.0 (7.1)	--	35–75	60.0 (9.6)	--	45–80	68.3 (7.1)	--
Skid Number	1–99	44.2 (14.6)	--	8–69	38.1 (13.4)	--	4–78	35.0 (12.4)	--
All Crashes	0–13	0.69 (1.26)	3772	0–34	0.67 (1.66)	486	0–31	1.35 (2.24)	1807
All Wet-Weather Crashes	0–4	0.12 (0.45)	495	0–3	0.09 (0.35)	65	0–20	0.31 (0.95)	411
ROR Crashes	0–10	0.59 (1.14)	2956	0–12	0.37 (0.85)	270	0–14	0.85 (1.38)	1128
ROR Wet-Weather Crashes	0–4	0.10 (0.42)	430	0–3	0.06 (0.30)	46	0–8	0.21 (0.65)	286

*SD: standard deviation

Modeling Approach

The probabilistic structure used for developing the models or Safety Performance Functions (SPFs) was the following: the number of crashes at the i^{th} segment, Y_i, when conditional on its mean μ_i, is assumed to be Poisson distributed and independent over all segments as (*6*):

$$Y_i \mid \mu_i \sim Po(\mu_i) \tag{14}$$

where:

i = 1, 2, …, I.

The mean of the Poisson distribution is structured as:

$$\mu_i = f(X;\beta)e^{e_i} \tag{15}$$

where:

$f(.)$ = function of the covariates (X).
β = vector of unknown coefficients.
e_i = model error independent of the covariates.

It is usually assumed that e^{e_i} is independent and Gamma distributed with a mean equal to 1 and a variance $1/\phi$ for all i (with $\phi > 0$). With this characteristic, it can be shown that Y_i, conditional on $f(.)$ and ϕ, is distributed as a negative binomial (or Poisson-gamma) random variable with a mean $f(.)$ and a variance $f(.)(1+f(.)/\phi)$ respectively. The term ϕ is usually defined as the "inverse dispersion parameter" for the negative binomial distribution.

Although the dispersion parameter ($\alpha = 1/\phi$) or its inverse (ϕ) is now often modeled as a function of the covariates in the data (*6*, *7*, *8*, *9*), the models were estimated using a fixed dispersion parameter to simplify the model development.

An important characteristic associated with the development of statistical relationships is the choice of the functional form linking crashes to the covariates. For this work, the functional form is as follows:

$$\mu_i = L \times y \times e^{\beta_0} \times F^{\beta_1} \times CMF_1 \times \ldots \times CMF_k \quad (16)$$

where:

μ_i = estimated annual number of crashes per mile.
L = segment length, mi.
y = number of years of crash data, years.
F = traffic volume, vehicles per day.

The coefficients of the regression models were estimated using the Statistical Analysis Software (SAS) program (*10*). The log-likelihood and Akaike Information Criterion (AIC) statistics were used to assess the model goodness-of-fit. Only variables that had a large influence on the predicted values were included in the models.

Modeling Results

Two-Lane Horizontal Curves

Table 13 summarizes the parameter estimates associated with the calibrated SPFs for horizontal curves on two-lane highways. The predictive models were developed separately for the four categories described above. The variables that are significant for all type of crashes were also significant for ROR crashes. An examination of the coefficient values and their implication on the corresponding SPF predictions are documented further below. In general, the sign and magnitude of the regression coefficients in Table 13 are logical and consistent with previous research findings. The list of variables presented in Table 13 reflects the findings from several preliminary regression analyses where different combinations of variables were examined. The list that is presented represents the variables that are significant in the model, while also having coefficient values that are logical and constructs that are theoretically defensible and properly bounded.

Table 13. Parameter Estimation for Horizontal Curves on Two-Lane Highways.

Variable	All Crashes		Wet Weather Crashes		Run-off-the-Road Crashes		Wet Weather Run-off-the-Road Crashes	
	Estimate	**Std. err.**	**Estimate**	**Std. err.**	**Estimate**	**Std. err.**	**Estimate**	**Std. err.**
Intercept	−8.0034	0.194	−9.9089	0.507	−8.186	0.219	−9.8329	0.539
LN (ADT)	0.8225	0.021	0.8462	0.057	0.8018	0.024	0.8152	0.061
Curve Radius	0.5796	0.036	--	--	0.8129	0.093	--	--
Lane Width	−0.0642	0.020	−0.0903	0.053	−0.0625	0.023	−0.0962	0.056
Shoulder Width	−0.0421	0.007	--	--	−0.0473	0.008	--	--
Skid Number	−0.0032	0.001	−0.0189	0.003	−0.0047	0.001	−0.0233	0.004
Dispersion	1.4036	0.126	0.2577	0.046	1.0761	0.101	0.2467	0.048
AIC	18497		4103		15927		3683	

The annual crash frequency for horizontal curves on two-lane highways is obtained by combining Equation 16 with the coefficients in Table 13.

The annual fatal and injury crash frequency for horizontal curves on two-lane highways can be estimated by the following equation:

$$\mu_{2L} = L \times y \times e^{-8.0034} \times F^{0.8225} \times CMF_R \times CMF_{LW} \times CMF_{SW} \times CMF_{SK} \tag{17}$$

with:

$$CMF_R = 1 + 0.5796(0.147V)^4 \frac{(1.47V)^2}{32.2R^2} \tag{18}$$

$$CMF_{LW} = e^{-0.0642(LW-12)} \tag{19}$$

$$CMF_{SW} = e^{-0.0421(SW-8)} \tag{20}$$

$$CMF_{SK} = e^{-0.0032(SK-40)} \tag{21}$$

where:

μ_{2L} = estimated number of crashes per year per mile for curves on two-lane highways.
CMF_R = curve radius crash modification factor.
CMF_{LW} = lane width crash modification factor.
CMF_{SW} = shoulder width crash modification factor.
CMF_{SN} = skid number crash modification factor.
R = curve radius, ft.
LW = lane width, ft.
SW = shoulder width, ft.
SK = skid number.

The annual wet-weather crash frequency for horizontal curves on two-lane highways can be estimated by the following equation:

$$\mu_{2L} = L \times y \times e^{-9.9089} \times F^{0.8462} \times CMF_{LW} \times CMF_{SK} \tag{22}$$

with:

$$CMF_{LW} = e^{-0.0903(LW-12)} \tag{23}$$

$$CMF_{SK} = e^{-0.0189(SK-40)} \tag{24}$$

The annual ROR crash frequency for horizontal curves on two-lane highways can be estimated by the following equation.

$$\mu_{2L} = L \times y \times e^{-8.186} \times F^{0.8018} \times CMF_{HC} \times CMF_{LW} \times CMF_{SW} \times CMF_{SK} \tag{25}$$

with:

$$CMF_{HC} = 1 + 0.8129(0.147V)^4 \frac{(1.47V)^2}{32.2R^2} \tag{26}$$

$$CMF_{LW} = e^{-0.0625(LW-12)} \tag{27}$$

$$CMF_{SW} = e^{-0.0473(SW-8)} \tag{28}$$

$$CMF_{SK} = e^{-0.0047(SK-40)} \tag{29}$$

The annual wet-weather ROR crash frequency for horizontal curves on two-lane highways can be estimated by the following equation:

$$\mu_{2L} = L \times y \times e^{-9.8329} \times F^{0.8152} \times CMF_{LW} \times CMF_{SK} \tag{30}$$

with:

$$CMF_{LW} = e^{-0.0962(LW-12)} \tag{31}$$

$$CMF_{SK} = e^{-0.0233(SK-40)} \tag{32}$$

The effects of traffic volume and the site characteristics described by the preceding CMFs are discussed in the following paragraphs.

Traffic Volume. Figure 20 shows the relationship between the traffic demand variable and crash frequency for two-lane horizontal curves. The estimated values are for a one-mile section of a horizontal curve with a 2,500-ft radius. All other variables are fixed at the base values. The positive value of the associated coefficient (in Table 13) indicates that as the volume increases, all type of crashes increases, almost in a linear fashion. The length of the trend lines in Figure 20 reflects the range of ADT in the data. The trends in Figure 20 indicate that wet-weather crashes represent about 15 percent of all crashes.

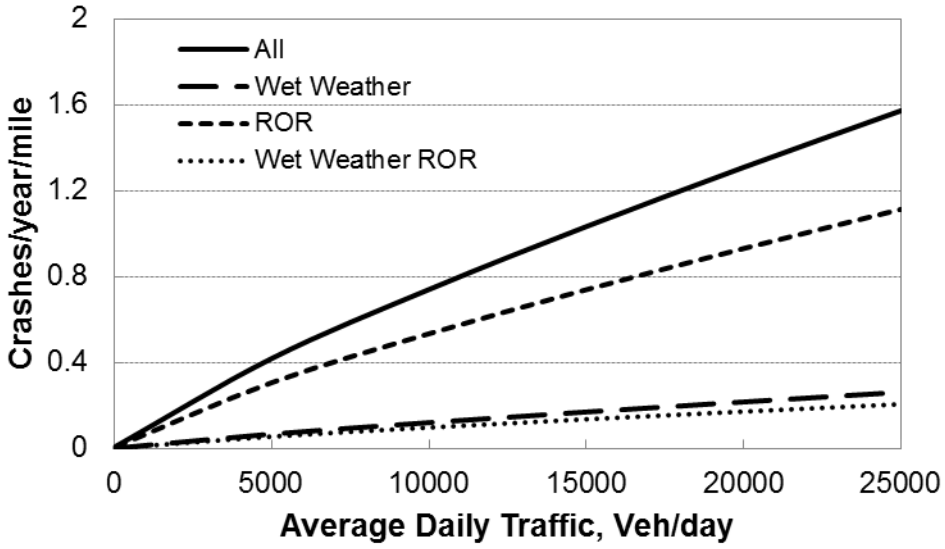

Figure 20. Number of Crashes with Change in the Average Daily Traffic.

Curve Radius. Figure 21 illustrates the CMF for curve radius. This figure shows that the CMF becomes lower as the radius increase, which previous studies have supported. For instance, the CMF that Bonneson and Pratt developed (*4*) is applicable to both two-lane and four-lane horizontal curves, and shows a similar relationship.

Lane Width. Figure 22 illustrates the CMF for lane width. The lane width used in this CMF is an average for all through lanes on the segment. The nominal condition reflects a 12-ft lane width. The CMF is shown in Figure 3 using a dotted trend line, whereas the two other lines are extracted from the work of Bonneson and Pratt (*4*). This figure shows that the number of crashes goes down as the lane width increases. The relationship found in this study is close to the low-volume CMF documented in Bonneson and Pratt (*4*).

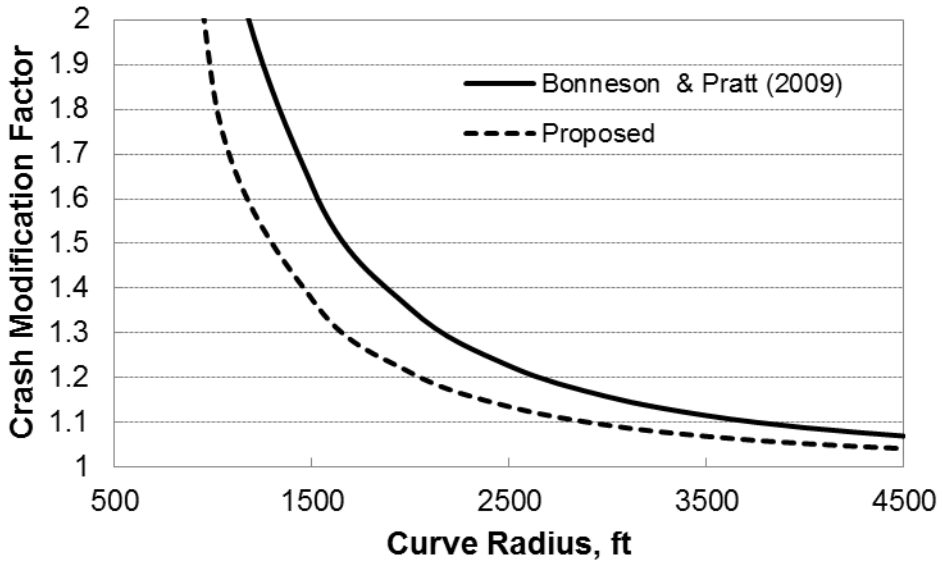

Figure 21. Curve Radius CMF.

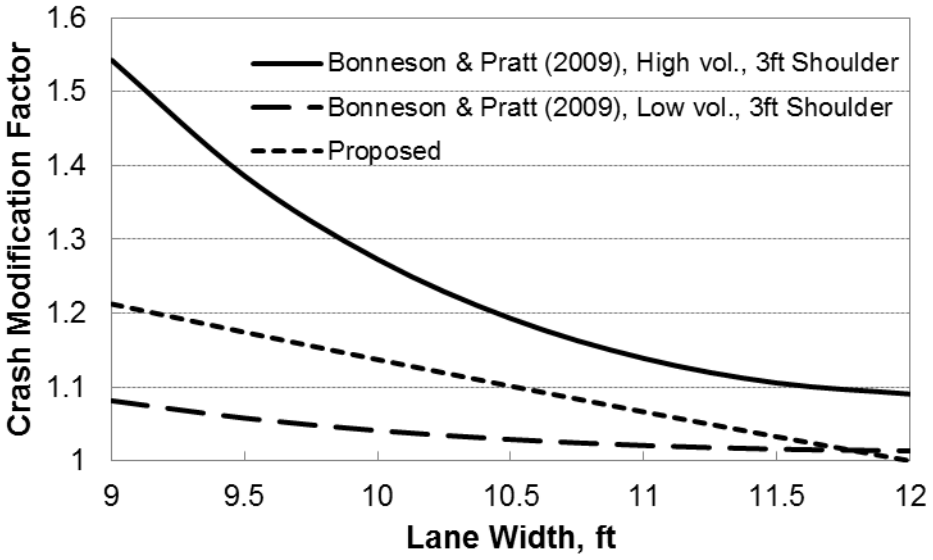

Figure 22. Lane Width CMF.

Outside Shoulder Width. Figure 23 illustrates the CMF for outside shoulder width. As before, the results are compared to the work of Bonneson and Pratt (*4*). Interestingly, although the number of crashes goes down as the shoulder width increases, the number of crashes is not as sensitive to a modification in shoulder width as in the work of Bonneson and Pratt (*4*), since the curve is relatively flat.

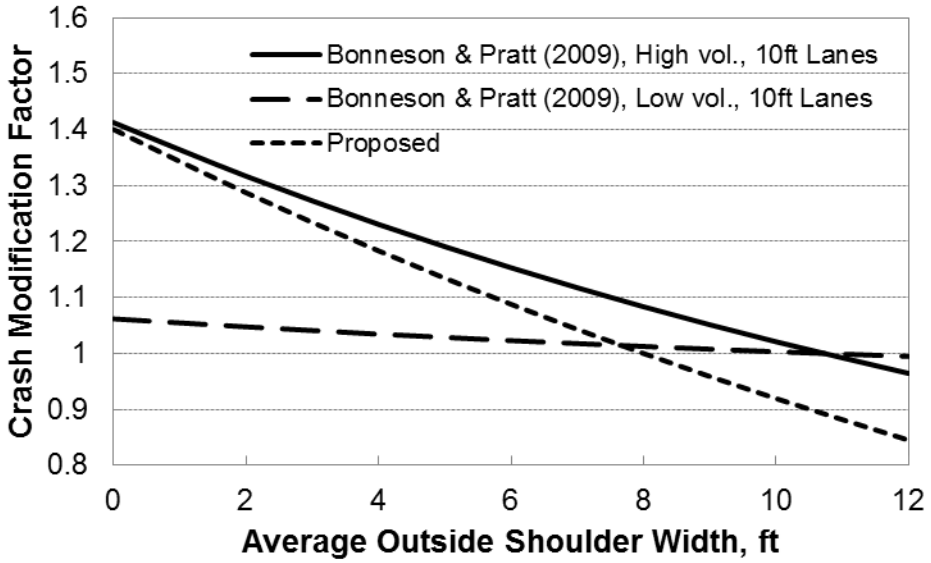

Figure 23. Outside Shoulder Width CMF.

Skid Number. The CMF for skid number on two-lane horizontal curves is shown in Figure 24. The skid number describes the overall skid resistance of the road section (e.g., representative of values obtained from skid tests in the vicinity of the curve, not just in the curve itself, based on the assumption that the same type of pavement is used on the curve as in the general road section). Skid number is based on measurements that the skid trailer made and the score varies from 01 (least skid resistance) to 99 (most skid resistance). A value greater than 70 is rarely found and the nominal condition was set at 40. The positive value of the associated coefficient (in Table 13) indicates that as the skid number increases, the crash frequency decreases.

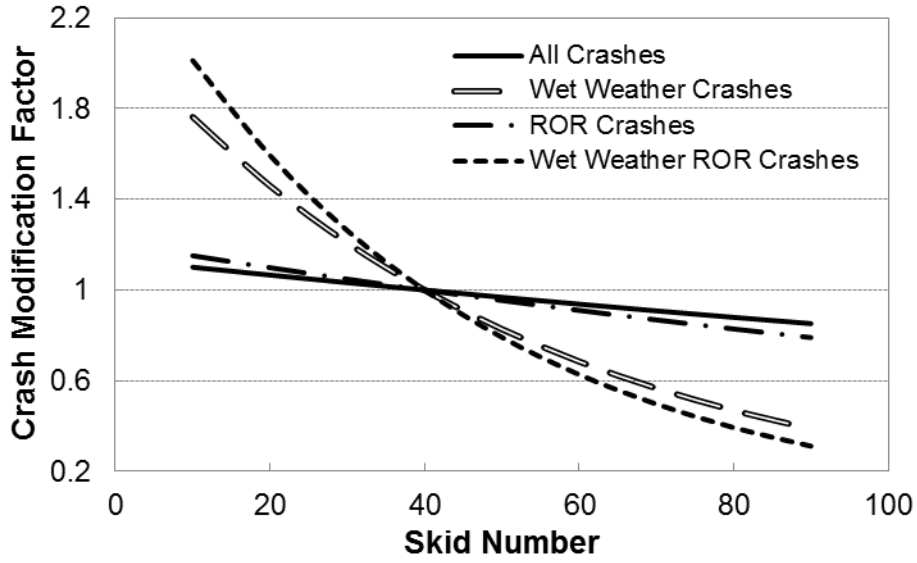

Figure 24. Skid Number CMF.

Four-Lane Horizontal Curves

Table 14 summarizes the parameter estimates associated with the calibrated SPFs for horizontal curves on four-lane undivided highways. In general, the sign and magnitude of the regression coefficients in this table are logical and consistent with previous research findings. An examination of the coefficient values and their implication on the corresponding SPF predictions are documented further below. The list of variables reflects the findings from several preliminary regression analyses where different combinations of variables were examined. The list represents the variables that provided the best fit to the data, while also having coefficient values that are logical and constructs that are theoretically defensible and properly bounded.

Table 14. Parameter Estimation for the Horizontal Curves on Four-Lane Undivided Highways.

Variable	All Crashes		Wet Weather Crashes		Run-off-the-Road Crashes		Wet Weather Run-off-the-Road Crashes	
	Estimate	Std. err	Estimate	Std. err	Estimate	Std. err	Estimate	Std. err
Intercept	−6.6487	0.905	−12.582	2.439	−6.5047	1.132	−12.4655	3.112
LN(ADT)	0.6588	0.091	1.0221	0.236	0.5596	0.112	0.9597	0.297
Curve Radius	1.0077	0.379	3.2688	2.334	2.3278	0.828	5.3898	5.679
Lane Width	−0.0406	0.0396	--	--	−0.0676	0.051		
Skid Number	−0.0077	0.005	−0.0331	0.013	−0.0049	0.006	−0.0254	0.016
Dispersion	1.2430	0.203	0.6559	0.359	1.0298	0.242	0.2797	0.139
AIC	1494		393		1091		316	

The annual crash frequency for horizontal curves on four-lane undivided highways is obtained by combining the Equation 16 with the coefficients in Table 14.

The annual fatal and injury crash frequency for horizontal curves on four-lane undivided highways can be estimated by the following equation:

$$\mu_{4L,U} = L \times y \times e^{-6.6487} \times F^{0.6588} \times CMF_R \times CMF_{LW} \times CMF_{SK} \tag{33}$$

with:

$$CMF_R = 1 + 1.0077(0.147V)^4 \frac{(1.47V)^2}{32.2R^2} \tag{34}$$

$$CMF_{LW} = e^{-0.0406(LW-12)} \tag{35}$$

$$CMF_{SK} = e^{-0.0077(SK-40)} \tag{36}$$

where:

$\mu_{4L,U}$ = estimated number of crashes per year per mile for curves on four-lane undivided highways.

The annual wet-weather crash frequency for horizontal curves on four-lane undivided highways can be estimated by the following equation:

$$\mu_{4L,U} = L \times y \times e^{-12.582} \times F^{1.0221} \times CMF_R \times CMF_{SK} \tag{37}$$

with:

$$CMF_R = 1 + 3.2688(0.147V)^4 \frac{(1.47V)^2}{32.2R^2} \tag{38}$$

$$CMF_{SK} = e^{-0.0331(SK-40)} \tag{39}$$

The annual ROR crash frequency for horizontal curves on four-lane undivided highways can be estimated by the following equation:

$$\mu_{4L,U} = L \times y \times e^{-6.5047} \times F^{0.5596} \times CMF_R \times CMF_{LW} \times CMF_{SK} \tag{40}$$

with:

$$CMF_R = 1 + 2.3278(0.147V)^4 \frac{(1.47V)^2}{32.2R^2} \tag{41}$$

$$CMF_{LW} = e^{-0.0676(LW-12)} \tag{42}$$

$$CMF_{SK} = e^{-0.0049(SK-40)} \tag{43}$$

The annual wet-weather ROR crash frequency for horizontal curves on four-lane undivided highways can be estimated by the following equation:

$$\mu_{4L,U} = L \times y \times e^{-12.4655} \times F^{0.9597} \times CMF_R \times CMF_{SK} \tag{44}$$

with:

$$CMF_R = 1 + 5.3898(0.147V)^4 \frac{(1.47V)^2}{32.2R^2} \tag{45}$$

$$CMF_{SK} = e^{-0.0254(SK-40)} \tag{46}$$

Table 15 summarizes the parameter estimates associated with the calibrated SPFs for horizontal curves on four-lane divided highways. An examination of the coefficient values and their implication on the corresponding SPF predictions are documented below. In general, the sign and magnitude of the regression coefficients in Table 15 are logical and consistent with previous research findings. The list of variables presented in this table reflects the findings from several preliminary regression analyses where different combinations of variables were examined. Similar to the results for undivided curved segments, the list represents the variables that provided the best fit to the data, while also having coefficient values that are logical and constructs that are theoretically defensible and properly bounded.

The annual crash frequency for horizontal curves on four-lane divided highways is obtained by combining the Equation 16 with the coefficients in Table 15.

Table 15. Parameter Estimation for the Horizontal Curves on Four-Lane Divided Highways.

Variable	All Crashes		Wet Weather Crashes		Run-off-the-Road Crashes		Wet Weather Run-off-the-Road Crashes	
	Estimate	Std. err	Estimate	Std. err	Estimate	Std. err	Estimate	Std. err
Intercept	−9.3399	0.562	−9.4156	1.097	−8.4124	0.643	−7.602	1.218
LN(ADT)	0.9437	0.054	0.7758	0.105	0.7985	0.061	0.5601	0.118
Curve Radius	0.8213	0.260	0.8351	0.492	1.0199	0.319	0.7480	0.523
Lane Width	--	--	--	--	−0.1436	0.091	−0.2726	0.217
Inside Shoulder Width	−0.0373	0.019	–0.0296	0.042	−0.0228	0.022	−0.0491	0.048
Average Skid Score	−0.0071	0.003	−0.0319	0.006	−0.0065	0.003	−0.0298	0.007
Dispersion	2.0358	0.221	0.5759	0.092	2.0004	0.297	0.4833	0.093
AIC	3749		1669		3036		1367	

The annual fatal and injury crash frequency for horizontal curves on four-lane divided highways can be estimated by the following equation:

$$\mu_{4L,D} = L \times y \times e^{-9.3399} \times F^{0.9437} \times CMF_R \times CMF_{ISW} \times CMF_{SK} \tag{47}$$

with:

$$CMF_R = 1 + 0.8213(0.147V)^4 \frac{(1.47V)^2}{32.2R^2} \tag{48}$$

$$CMF_{ISW} = e^{-0.0373(ISW-4)} \tag{49}$$

$$CMF_{SK} = e^{-0.0071(SK-40)} \tag{50}$$

where:

$\mu_{4L,D}$ = estimated number of crashes per year per mile for curves on four-lane divided highways.
CMF_{ISW} = inside shoulder width crash modification factor.
ISW = inside shoulder width, ft.

The annual wet-weather crash frequency for horizontal curves on four-lane divided highways can be estimated by the following equation:

$$\mu_{4L,D} = L \times y \times e^{-9.4156} \times F^{0.7758} \times CMF_R \times CMF_{ISW} \times CMF_{SK} \tag{51}$$

with:

$$CMF_R = 1 + 0.8351(0.147V)^4 \frac{(1.47V)^2}{32.2R^2} \quad (52)$$

$$CMF_{ISW} = e^{-0.0296(ISW-4)} \quad (53)$$

$$CMF_{SK} = e^{-0.0319(SK-40)} \quad (54)$$

The annual ROR crash frequency for horizontal curves on four-lane divided highways can be estimated by the following equation:

$$\mu_{4L,D} = L \times y \times e^{-8.4124} \times F^{0.7985} \times CMF_R \times CMF_{LW} \times CMF_{ISW} \times CMF_{SK} \quad (55)$$

with:

$$CMF_R = 1 + 1.0199(0.147V)^4 \frac{(1.47V)^2}{32.2R^2} \quad (56)$$

$$CMF_{LW} = e^{-0.1436(LW-12)} \quad (57)$$

$$CMF_{ISW} = e^{-0.0228(ISW-4)} \quad (58)$$

$$CMF_{SK} = e^{-0.0047(SK-40)} \quad (59)$$

The annual wet-weather ROR crash frequency for horizontal curves on four-lane divided highways can be estimated by the following equation:

$$\mu_{4L,D} = L \times y \times e^{-7.602} \times F^{0.5601} \times CMF_R \times CMF_{LW} \times CMF_{ISW} \times CMF_{SK} \quad (60)$$

with:

$$CMF_R = 1 + 0.7480(0.147V)^4 \frac{(1.47V)^2}{32.2R^2} \quad (61)$$

$$CMF_{LW} = e^{-0.2726(LW-12)} \quad (62)$$

$$CMF_{ISW} = e^{-0.0491(ISW-4)} \quad (63)$$

$$CMF_{SK} = e^{-0.0298(SK-40)} \quad (64)$$

The effects of traffic volume and the site characteristics described by the preceding CMFs are discussed in the following paragraphs.

Traffic Volume. The relationship between the traffic demand variable and crash frequency, as obtained from the calibrated models, is shown in Figure 25 and Figure 26 for undivided and divided four-lane horizontal curves, respectively. The estimated values are for a 1-mile section with other variables fixed at their average value in the calibration data set. The positive value of the associated coefficient (in Table 14 and Table 15) indicates that, as the volume increases, all type of crashes increases for both undivided and divided facilities. The length of the trend lines in Figure 25 and Figure 26 reflects the range of ADT in the data.

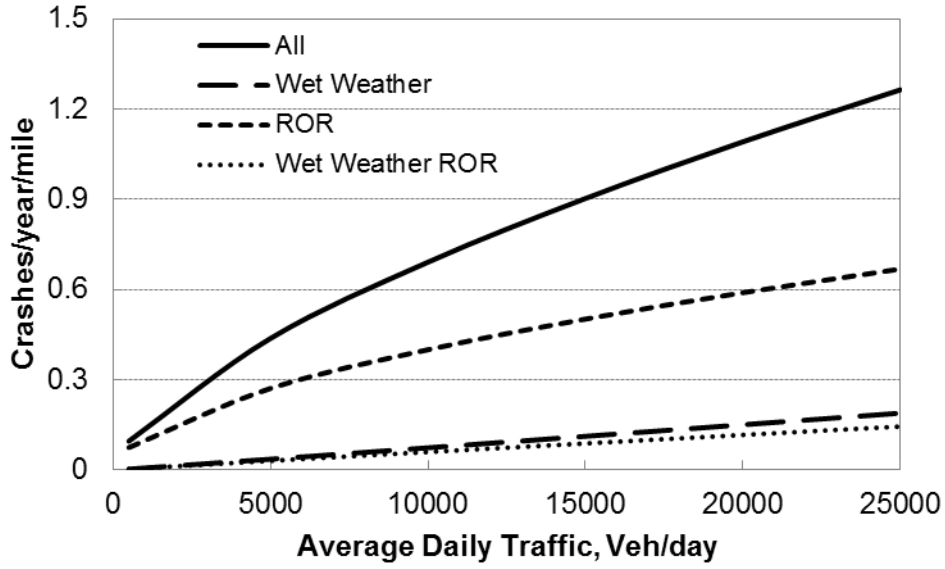

Figure 25. Number of Crashes with Change in the Average Daily Traffic on Undivided Highways.

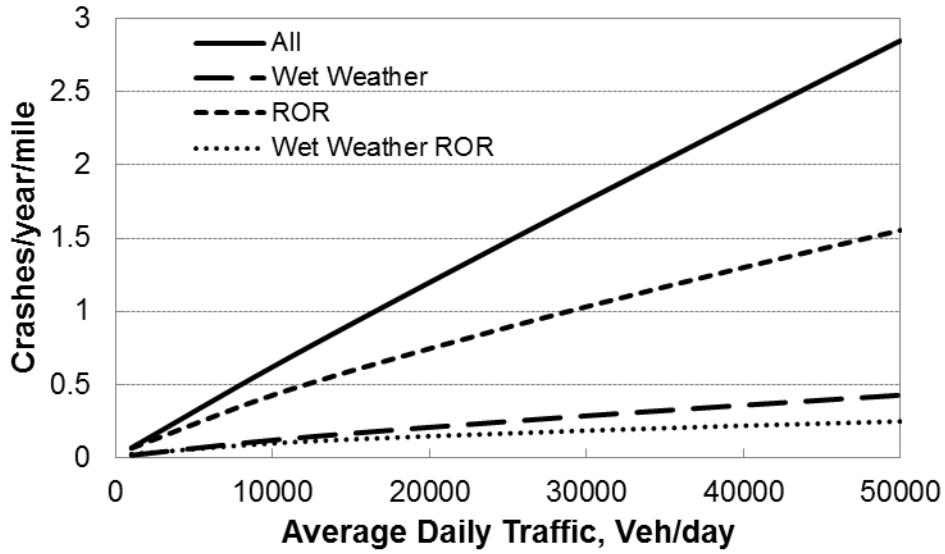

Figure 26. Number of Crashes with Change in the Average Daily Traffic on Divided Highways.

Curve Radius. Figure 27 illustrates the CMF for the curve radius for undivided and divided four-lane highways. This figure shows that the CMFs become lower as the radius increase, as expected. The two CMFs are very similar to the one that Bonneson and Pratt developed(*4*), which can be used for both two- and four-lane highways.

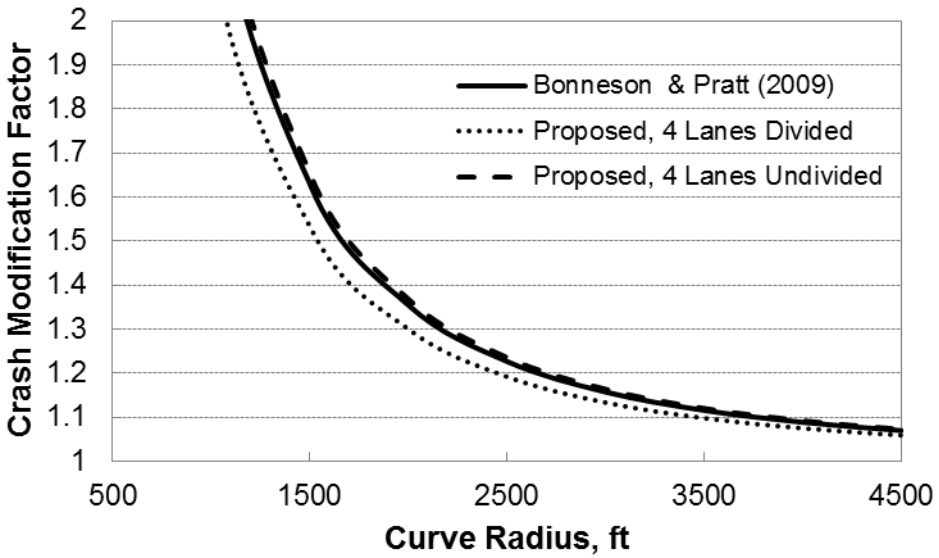

Figure 27. Curve Radius CMF.

Lane Width. Figure 28 illustrates the CMF for the lane width for four-lane undivided highways. It reflects the average for all through lanes on the segment. The nominal condition represents 12-ft lanes. Figure 28 shows that the number of crashes goes down as the lane width increases. The relationship found in this analysis is close to the CMF documented in Bonneson and Pratt (*4*).

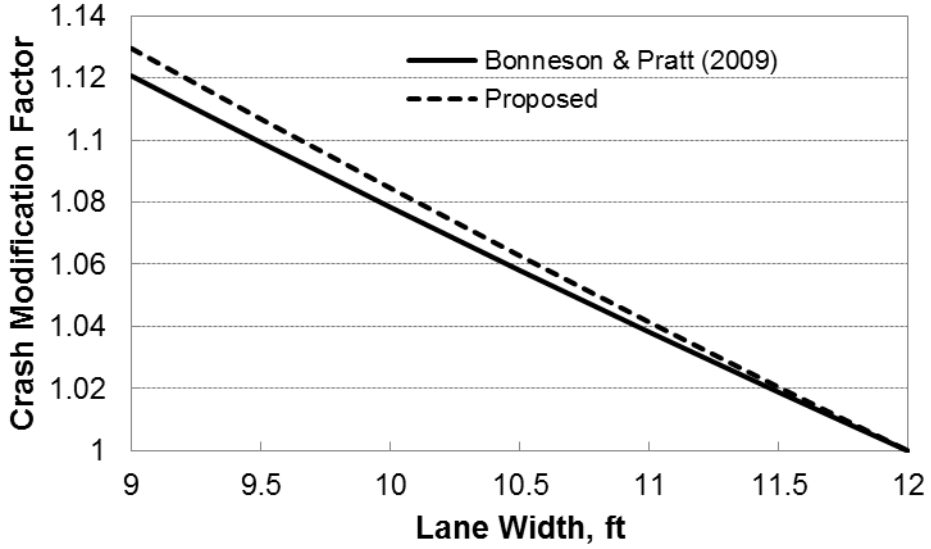

Figure 28. Lane Width CMF for Undivided Highways.

Inside Shoulder Width. Figure 29 shows the CMF inside shoulder width for four-lane divided horizontal curves. The shoulder width represents an average for both directions of travel. The negative value of the associated coefficient (in Table 15) indicates that as the shoulder width increases, all type of crashes decreases. The relationship found in this analysis is close to the CMF documented in Bonneson and Pratt (*4*).

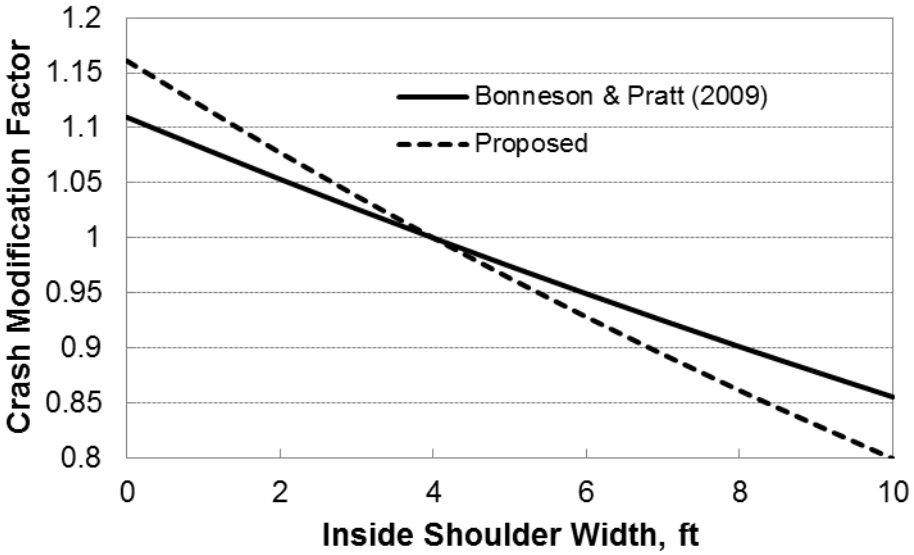

Figure 29. Inside Shoulder Width CMF for Divided Highways.

Skid Number. Figure 30 and Figure 31 show the CMF for the skid number variable for undivided and divided four-lane horizontal curves, respectively. The positive value of the associated coefficient (in Table 14 and Table 15) indicates that as the skid number increases, the crash frequency decreases. The skid number variable is significant in the wet-weather crash prediction model only for both highway types.

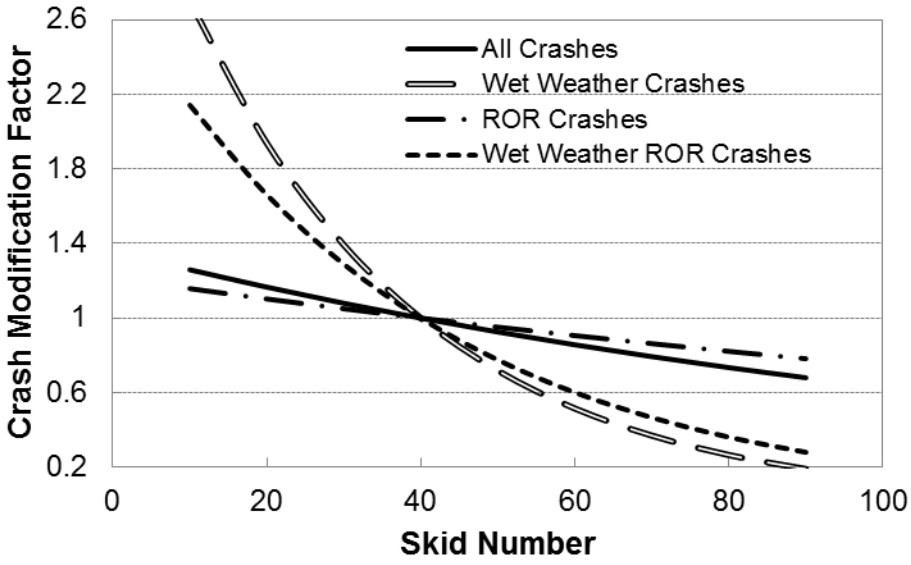

Figure 30. Skid Number CMF for Undivided Highways.

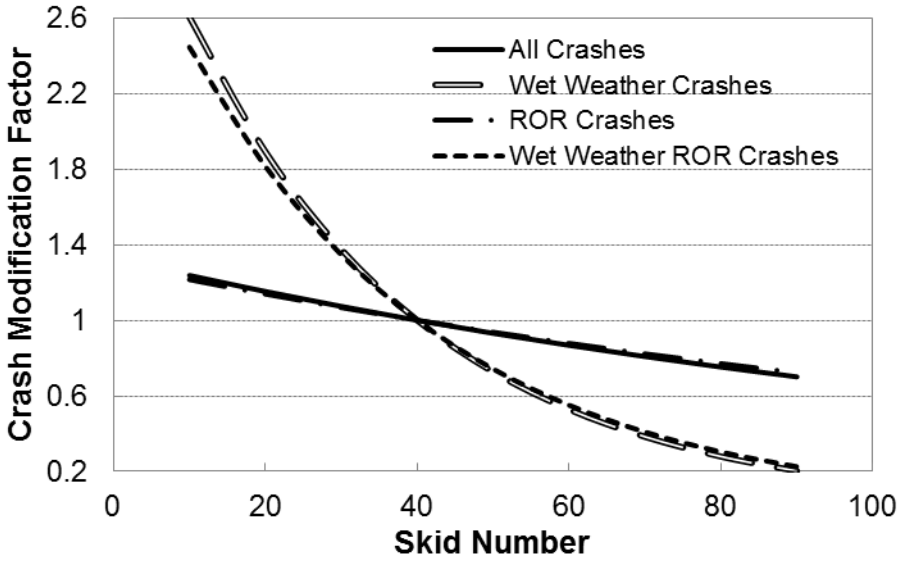

Figure 31. Skid Number CMF for Divided Highways.

Findings

This chapter has presented the results of the statistical analyses conducted on crashes that occurred on horizontal curve segments from 2007 to 2011. The primary objective of this analysis was to develop SPFs to describe the relationship between crash frequency and traffic and geometric variables for horizontal curves in Texas. Curve radius, lane width, and shoulder width have been identified as key geometric variables. The skid number, which describes the skid resistance of a pavement, was found to significantly influence wet-weather-related crashes.

The key points of the statistical analysis results are as follows:

- The regression models showed that curve radius has a significant effect on all crashes and ROR crashes but had little influence on wet-weather crashes on two-lane horizontal curves. However, the curve radius has a significant influence on all crashes on four-lane horizontal curves.
- Wider lane and shoulder widths on horizontal curves have a notable positive impact on safety.
- The skid number, which describes the skid resistance of a pavement, showed that pavement friction influence crashes. Importantly, friction conditions highly influence wet-weather crashes.

REFERENCES

1. Torbic, D., D. Harwood, D. Gilmore, R. Pfefer, T. Neuman, K. Slack, and K. Hardy. *Guidance for Implementation of the AASHTO Strategic Highway Safety Plan. Volume 7: A Guide for Reducing Collisions on Horizontal Curves*. NCHRP Report 500. TRB, National Research Council, Washington, D.C., 2004.
2. *Horizontal Curve Safety*. Federal Highway Administration, http://safety.fhwa.dot.gov/roadway_dept/horicurves/ . Accessed June 5, 2012.
3. McGee, H.W., and F. R. Hanscom. *Low-Cost Treatments for Horizontal Curve Safety*. Report FHWA-SA-07-002, U.S. Department of Transportation, Washington, D.C., 2006.
4. Bonneson, J., and M. Pratt. *Roadway Safety Design Workbook*. Report FHWA/TX-09-0-4703-P2, Texas Transportation Institute, College Station, Texas, 2009.
5. Lord, D., M. Brewer, K. Fitzpatrick, S. Geedipally, and Y. Peng. *Analysis of Roadway Departure Crashes on Two-Lane Rural Roads in Texas*. Report FHWA/TX-11/0-6031-1, Texas Transportation Institute, College Station, Texas, 2011.
6. Miaou, S.P.,and D. Lord, 2003. *Modeling Traffic Crash-Flow Relationships for Intersections: Dispersion Parameter, Functional Form, and Bayes Versus Empirical Bayes Methods*. Transportation Research Record No. 1840, Transportation Research Board, Washington, D.C. pp. 31–40.
7. Hauer, E., 2001. *Overdispersion in Modeling Accidents on Road Sections and in Empirical Bayes Estimation*. *Accident Analysis & Prevention*, Vol. 33, No. 6, pp. 799–808.
8. Heydecker, B.G., and J. Wu, 2001. *Identification of Sites for Road Accident Remedial Work by Bayesian Statistical Methods: An Example of Uncertain Inference. Advances in Engineering Software*, Vol. 32, University College London, Oxford, England, pp. 859–869.
9. Geedipally, S.R., D. Lord, and B.-J. Park, 2009. Analyzing Different Parameterizations of the Varying Dispersion Parameter as a Function of Segment Length. Transportation Research Record 2103, pp. 108–118.
10. *SAS/STAT User's Guide, Version 9.2*. Second edition, SAS Institute, Inc., Cary, North Carolina, 2009.

CHAPTER 4. OPERATIONAL AND PAVEMENT DATA ANALYSIS

INTRODUCTION

This chapter describes data collection activities that were undertaken to provide quantitative information about the influence of horizontal curve geometry, traffic control characteristics, and pavement characteristics on vehicle speeds and travel path behavior. The insights gained from the cross-sectional analysis of speeds and travel path at an assortment of sites were then used to analyze margin of safety trends for curves and develop guidelines.

Chapter 4 is divided into four parts. The first part summarizes background information and identifies knowledge gaps that were addressed by the data collection activities. The second part describes the procedures that were used to collect cross-sectional speed and travel path data on curves with a range of site characteristics. The third part presents a summary of the operational data set, including exploratory analysis results. The fourth part describes models that were calibrated using the operational data set.

BACKGROUND

The objective of a curve safety treatment is to improve the curve's margin of safety, which is defined as follows:

$$M.S. = f_S - f_D \tag{65}$$

where:

$M.S.$ = margin of safety.
f_S = side friction supply (= skid number divided by 100g).
f_D = side friction demand (lateral acceleration divided by g).

Side friction demand is related to vehicle speeds and curve geometry using the "point-mass model" that AASHTO's *A Policy on Geometric Design of Highways and Streets* (*Green Book*) (*1*) described as follows:

$$f_D = \frac{v^2}{gR} - \frac{e}{100} \tag{66}$$

where:

v = vehicle speed, ft/s.
g = gravitational constant (= 32.2 ft/s^2).
R = curve radius, ft.
e = superelevation rate, percent.

Margin of safety can be increased by increasing side friction supply (e.g., by installing a high-friction surface treatment) or by decreasing side friction demand (e.g., by reducing vehicle speeds or increasing the curve radius or superelevation rate). These principles are embodied in

TxDOT's Surface Aggregate Selection Form (Form 2088), which is referenced in the *Pavement Design Guide* (*2*). Form 2088 is listed as a document to be included in a pavement design report when surface treatments are implemented on flexible pavements as part of the Wet Surface Crash Reduction Program (WSCRP).

Bonneson et al. calibrated models to estimate average and 85th-percentile passenger car and truck speeds at the midpoint of a horizontal curve (*3*). These models were calibrated using data from 41 horizontal curve sites in Texas, where a "site" is one direction of travel on a two-lane horizontal curve. The models were formulated as follows:

$$v_C = \sqrt{\frac{15.0R\left(b_0 - b_1 v_T + b_2 {v_T}^2 + e/100\right)}{1 + 32.2Rb_2}} \tag{67}$$

where:

v_C = curve midpoint speed, mph.
v_T = approach tangent speed, mph.
b_i = calibration coefficients.

When Equation 67 is combined with Equation 66, the following model form results:

$$f_D = b_0 - b_1 v_T + b_2\left({v_T}^2 - {v_C}^2\right)I_v \tag{68}$$

where:

I_v = indicator variable (= 1 if $v_T > v_C$, 0 otherwise).

The models can be used with Equation 2 to estimate side friction demand based on *path* radius, superelevation rate, and approach tangent speed. These models were calibrated based on the assumption that most drivers shift toward the inside of their lane while traversing a curve, a trend that Emmerson observed in 1969 (*4*). As a result, the radius of a vehicle's travel path through a curve, on average, tends to be somewhat larger than that of the curve itself, resulting in a slight mitigation in side friction demand.

Other researchers have subsequently observed path-shifting behavior and determined that it is the most common descriptor of curve travel paths (*5*, *6*). However, Spacek observed that other travel path types are also common, such as a consistent swinging inward or drifting outward to the point of encroachment on the centerline or edgeline, or even correcting maneuvers that may be associated with localized side friction demands well above that assumed in the design of the curve (*6*). Figure 32 illustrates the travel plan types that Spacek observed.

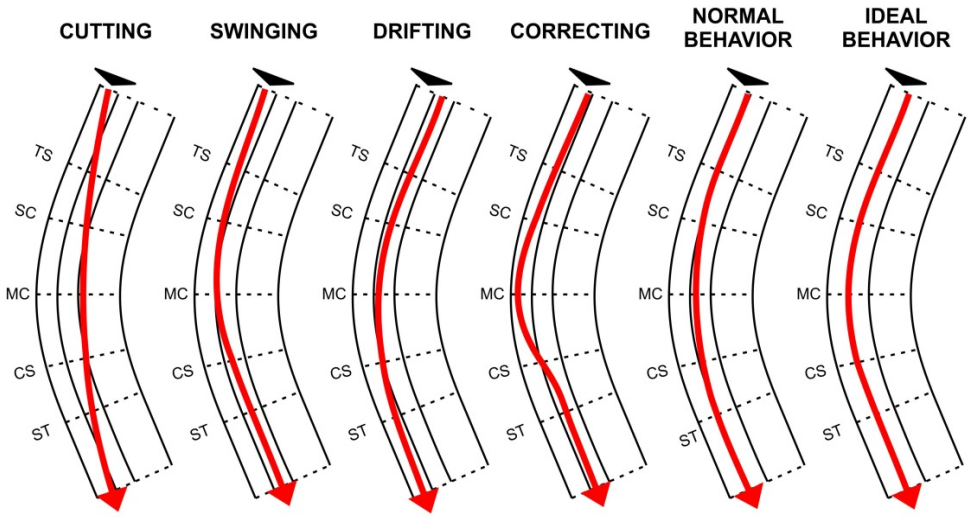

Figure 32. Curve Travel Path Types (*6*).

Spacek further stated that the travel paths labeled as "ideal behavior" and "normal behavior" are most common on curves with the following conditions:

- Radius between 400 and 750 ft.
- Spiral transitions with parameter A ($A = \sqrt{RL_s}$, where L_s = length of spiral transition, ft) between 0.33 and 0.5R.
- Circular arc length equating to at least 5 seconds of travel time.
- Lane width between 11.1 and 11.5 ft.

These findings are based on an investigation of eight two-lane highway curves in Switzerland.

As previously stated, the models that Bonneson et al. developed (*3*) provide estimates of vehicle speeds at the midpoint of the curve. They do not provide estimates of speeds at other points along the curve, though research has shown that drivers continue to reduce speed after entering into a curve and begin to increase speed before exiting a curve (*7*, *8*). That is, speeds tend to be higher at the point of curvature (PC) or point of tangency (PT) than at the midpoint of the curve (MC). Additionally, braking and acceleration both force tires to provide longitudinal forces (braking friction or tractive effort), which reduces the amount of side friction that they can provide (*9*). At the PC and PT, higher speeds combined with braking or acceleration and the lack of fully-developed superelevation may combine to yield higher friction demand and lower margin of safety than would be expected based on constant speed and average conditions for the curve (*10*).

Based on the preceding discussion, the following knowledge gaps are identified:

- Vehicle speeds at the PC and PT. Numerous models have been developed for estimating vehicle speeds at the midpoint of a curve. Relatively few models have been developed for estimating speeds at the PC or PT. The combination of incomplete superelevation

and possible braking or accelerating suggests the need for an investigation of speeds at these points.

- Travel path behavior. Some research has been conducted to determine the relationship between curve geometry and travel path behavior. It is not known if the trends reported in the literature transfer to Texas highways, particularly those with higher speeds.

DATA COLLECTION PLAN

To address the knowledge gaps described in the previous section, a database was assembled and used to develop cross-sectional models of vehicle speeds and travel path. This part of the chapter describes the data collection plan.

Database Attributes

The cross-sectional database includes the following attributes for vehicles traversing horizontal curves:

- Approach tangent speed.
- Curve speed, at the PC, the MC, and the PT.
- Headway (leading and trailing).
- Vehicle classification (car or truck).
- Lane placement (distance from edgeline).

Vehicle speeds and lane placement at the curve PC, MC, and PT represent the dependent variables in the models to be developed. Approach tangent speed was collected because it has been found to be an important predictor of curve speed (*3*). Headways were collected because the models will be calibrated to describe the behavior of free-flowing vehicles. Hence, it is necessary to identify only free-flowing vehicles for inclusion in the model calibration data set.

Additionally, attributes to describe the data collection sites were recorded. These attributes are listed in Table 16, along with the desired ranges for the attributes. A site is defined as one direction of travel on a horizontal curve. Thus, if data are collected in both travel directions on a curve, the curve provides two data collection sites.

Radius, deflection angle, superelevation rate, grade, lane width, and shoulder width will be included in the speed and lane placement models as appropriate. Radius and superelevation rate were collected because they directly affect both vehicle speeds and side friction demand. Deflection angle, lane width, and shoulder width were collected because they are likely to affect lane placement.

Ranges in the site attributes were sought to ensure that the calibrated speed and lane placement models will be transferable to a range of site conditions. In particular, ranges in the attributes of radius, regulatory speed limit, and speed reduction are essential to ensure that both gradual and severe curves are included in the calibration data set.

Table 16. Site Description Data.

Variable	Basis	Range Among Sites
Curve radius	Site	150 to 1500 ft
Deflection angle	Site	5 to 90 degrees
Spiral transition presence	Site	None present
Regulatory speed limit	Site	55 to 70 mph
Speed reduction (regulatory – advisory)	Site	0 to 30 mph
Functional classification	Site	Rural two-lane highway
Superelevation rate	PC, MC, PT	0 to 12 percent
Grade	PC, MC, PT	–4 to +4 percent
Lane width	PC, MC, PT	9 to 14 ft
Shoulder width	PC, MC, PT	0 to 12 ft

The inclusion of only rural two-lane highway curves without spiral transitions represents a limitation of the data collection scope. A query of the TRM database reveals that 64 percent of curves on state-maintained roads in Texas are located on rural two-lane highways and do not have spiral transitions. Inclusion of other area or highway types would require a significant increase in the number of data collection sites needed to calibrate the vehicle speed model. Inclusion of curves with spiral transitions would require a significant increase in the number of sites needed to calibrate the lane placement model.

Data Collection Methods

The data collection sites were chosen using preliminary information available in the TRM database and aerial photography, with the goal of achieving a range in the variables listed in Table 16. A data collection crew was assembled, and preliminary data collection occurred in the office. Then, the crew visited various sites to conduct a field survey and deploy the equipment needed to collect the speed and lane placement data. Finally, they collected pavement friction data using a skid trailer and a specialist technician trained in its use.

Preliminary Data

The researchers queried the TRM database to develop a list of data collection sites. The data extracted from TRM included:

- Degree of curve (which can be used to compute radius).
- Deflection angle.
- Regulatory speed limit.
- ADT.
- Lane width.
- Shoulder width.

When possible, the Street View imagery available in Google Earth was used to verify the regulatory speed data obtained from TRM. The Street View imagery was also used to obtain the curve advisory speed and determine the presence of supplemental traffic control devices like

delineator posts, Chevrons, and the Large Arrow sign, and special treatments like wide edgelines and rumble strips.

Site Survey

The site survey task involved hand-measuring lane width, shoulder width, superelevation rate (or cross slope), and grade. These measurements were taken at four locations (approach tangent, PC, MC, and PT). The crew took width measurements using a tape measure, and superelevation and grade measurements with a smart level. They also took photos to document the street-level appearance of the site and the placement of the speed-trap sensors.

Speed and Lane Placement Data

Vehicle speeds and lane placement were collected using traffic classifiers and sensors. These data were collected at three locations within the curve (PC, MC, and PT). To collect lane placement data, it is necessary to deploy three sensors in the Z configuration shown in Figure 33. Chrysler et al. (*11*) described the procedure for computing lane placement from the Z configuration data. Vehicle speeds were also collected on the approach tangent to each site. Collection of speeds requires the use of two sensors. Figure 34 illustrates the locations of these sensors at an example site.

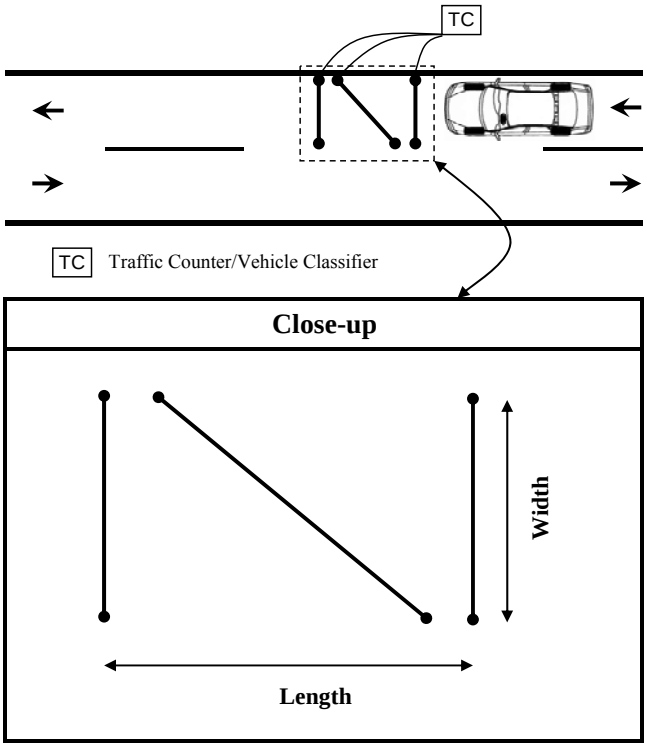

Figure 33. Z Configuration for Lane Placement Measurement.

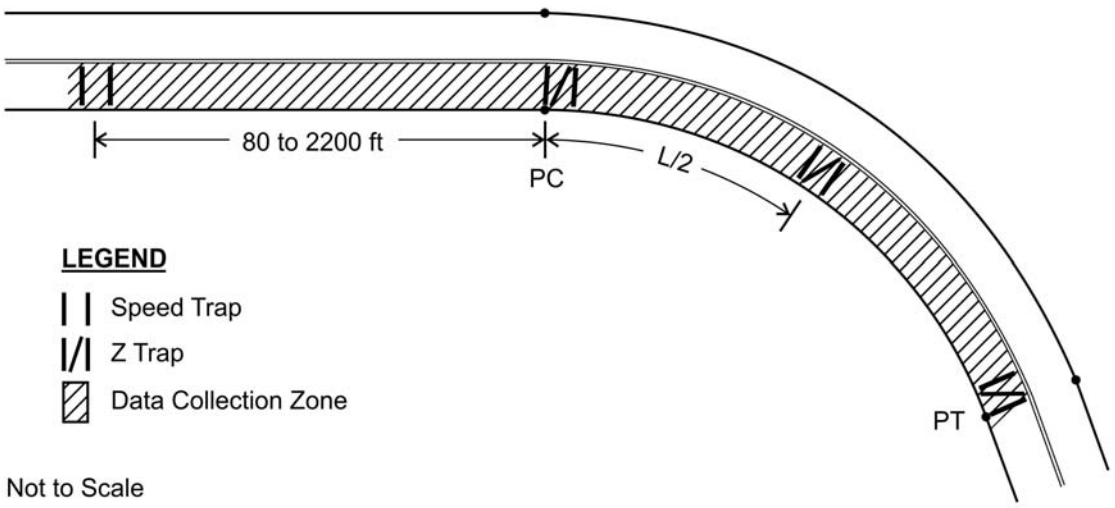

Figure 34. Sensor Locations at a Data Collection Site.

Ideally, the Z-configuration traps were located at the PC, the MC, and the PT. However, site conditions sometimes required the locations of the traps to be adjusted (e.g., if there was a driveway located near the ideal trap location). Adjustments were made based on the travel time through the curve at the posted advisory speed (or regulatory speed limit if there is no posted advisory speed). The Z-configuration trap locations were adjusted no more than the distance traveled at the posted advisory speed in two seconds. Additionally, the PC and PT traps were located no more than 15 percent of the curve's total length toward the MC, and the MC trap was located within the zone that represents 45–55 percent of the curve's length.

The approach tangent trap was located such that the free-flow speeds of vehicles can be observed. Locations were identified where drivers have likely not yet started to decelerate because of the curve, using the following equation:

$$D_{\min} = 1.47 t_{pr}\left(v_{SL} + 5\right) + 1.47^2 \frac{\left(v_{SL} + 5\right)^2 - \left(v_{ADV} + 5\right)^2}{2d_r} \tag{69}$$

where:

D_{min} = minimum distance from curve PC to approach tangent speed trap, ft.
t_{pr} = 85th-percentile perception-reaction time (use 1.0 s), s.
v_{SL} = regulatory speed limit, mph.
v_{ADV} = posted advisory speed, mph.
d_r = deceleration rate (use 3.3 ft/s^2), ft/s^2.

The regulatory speed limit and advisory speed are increased by 5 mph to reflect a conservative estimate of the 85th-percentile approach tangent and curve midpoint speeds.

Pavement Data

Pavement friction data were collected using TTI's skid trailer, which helped determine the skid number of the pavement at the PC, the MC, and the PT of each curve. The data collection crew took four measurements at each of these locations, which were marked on the pavement when the sensors and classifiers were retrieved so that the trailer technician would be able to identify the locations. The skid tests were conducted at the curve advisory speed, or at the regulatory speed limit if there was no posted advisory speed.

Site Selection and Screening

A query of the TRM database was conducted to identify curves with characteristics that fit within the ranges described in Table 16 (with the exception of superelevation rate, which is not included in the TRM database). To minimize travel time during data collection activities, the query was limited to the TxDOT districts of Bryan and portions of Waco, Yoakum, Lufkin, Tyler, and Dallas. This query yielded 461 candidate curves for further screening.

The candidate curves were screened using aerial and street-level photography available in Google Earth and Google Street View. The screening process was conducted to:

- Check for paved driveways or crossroad approaches on the curve or within the approach tangent area.
- Verify that the curve is isolated from other curves (such that free-flow vehicle speeds could be measured on the approach tangent).
- See if the curve is located sufficiently close to a town that vehicle speeds would likely not reflect free-flow conditions. The list of candidate curves was reduced to 43 curves for preliminary site visits.

During the curve screening process, the street-level photography was used to obtain information about traffic control characteristics of the curves. These characteristics included regulatory speed limit, advisory speed, and the presence of delineators or Chevrons.

Preliminary site visits were conducted for 28 curves. During these visits, a researcher drove through the curves in both directions to assess the curve and its general surroundings. Particular attention was given to vertical curvature, grade, and side slope, which are most easily observed in the field. Curves with limited sight distance, obscured traffic control devices, or significantly distressed pavement were excluded from further consideration. The traffic control device data collected during the aerial and street-level photography review were checked and updated when needed, and the curves were photo-documented. Additionally, it was determined which of the curve travel directions more closely matched site selection criteria.

DATA SUMMARY

This part of the chapter presents the results of the data collection efforts, including a description of the sites and an exploratory analysis of the operational data set.

Data Collection Site Characteristics

A total of 15 curves were ultimately used for speed and lane placement data collection. Table 17 shows the distribution of these curves by regulatory speed limit and posted advisory speed. The curves are denoted by their identification numbers in the TRM database.

Table 17. Data Collection Site Distribution by Speed Limit.

		Regulatory Speed Limit, mph			
		55	**60**	**65**	**70**
Advisory Speed, mph	**30**			50754	
	35	22186	4160		
	40			9964	
	45		11652	3347, 3359	
	50	6618		1114	2794, 43414
	55	11848 [1]			2776, 32199, 40767

Notes:
1–Curve 11848 did not have a posted advisory speed.

The five leftmost columns of Table 18 provide descriptions of the approximate data collection site locations, including the TxDOT district and nearest city, and the travel direction that was used for data collection. To obtain a larger cross section of site characteristics with the available resources, only one travel direction was used on each curve. The travel direction indicates the direction that vehicles turned while traversing the data collection site.

Table 18. Site Location and Traffic Control Characteristics.

District	Nearest City	Curve Number	Travel Direction	Highway	ADT, veh/d (2007)	Delineation Treatments
Bryan	Normangee	1114	R	FM 3	1950	None
	Hearne	2776	R	FM 50	2100	None
	Mooring	2794	L	FM 50	1800	None
	Deanville	3347	L	FM 60	1150	Chevrons
	Birch	3359	R	FM 60	1400	Chevrons
	Donie	4160	L	FM 80	1900	None
	Carlos	9964	L	FM 244	1850	Chevrons
	Cooks Point	32199	L	FM 1362	1100	None
	Caldwell	40767	R	FM 2000	1200	Delineators
	Bryan	43414	R	FM 2223	2500	Chevrons
	Anderson	50754	R	FM 3090	650	Chevrons
Dallas	Crandall	6618	R	FM 148	3200	Chevrons
	India	22186	R	FM 780	1300	None
Tyler	Palestine	11652	R	FM 315	1400	Chevrons
	Montalba	11848	L	FM 321	1150	Profiled centerline

The two rightmost columns of Table 18 provide the sites' average daily traffic volumes extracted from the TRM database, and descriptions of delineation devices that were present at the sites. Eight of the 15 sites had either delineator posts or Chevrons, and one site had a profiled centerline marking, which was present along the entire section of highway where the curve was located.

Table 19 provides the site geometric characteristics. The deflection angle values in the third column were extracted from aerial photographs and the TRM database. The radius in the second column of the table was computed from the deflection angle and the curve lengths that were measured during the site surveys. Lane and shoulder widths were also measured at all four speed trap locations during the site survey, and are included in the eight rightmost columns of Table 19. The speed trap locations are denoted TN, PC, MC, and PT for approach tangent, point of curvature, midpoint of curve, and point of tangency, respectively.

Table 20 summarizes the cross slope and superelevation rate measurements that were recorded during the site surveys. On the approach tangent, the "typical" cross slope of 2 percent is defined as positive for curves deflecting to the right and negative for curves deflecting to the left. Within the curve, superelevation is defined as positive if its direction contributes to an increase in side friction supply (i.e., slopes downward to the right for right-deflecting curves or to the left for left-deflecting curves).

The skid number measurements that were recorded using the skid trailer are summarized in the right portion of Table 20. To obtain these numbers, four test runs were conducted at each speed trap location, and the skid numbers measured during each test run were averaged.

Table 19. Site Geometric Characteristics.

Curve Number	Radius, ft	Deflection Angle, deg.	Lane Width, ft (by speed trap location)				Shoulder Width, ft (by speed trap location)			
			TN	PC	MC	PT	TN	PC	MC	PT
1114	1159	44	9.6	9.8	9.9	10.5	1.0	2.1	2.4	3.2
2776	1204	59	10.0	10.0	10.2	10.3	3.8	3.0	3.4	2.8
2794	1210	41	10.2	10.1	9.1	10.5	2.9	3.4	3.8	3.0
3347	847	51	9.7	9.7	9.2	10.1	1.7	2.3	2.8	2.0
3359	1003	72	9.8	9.9	10.4	9.9	2.0	1.7	2.0	1.9
4160	674	75	10.2	11.1	10.8	10.0	2.8	2.2	4.3	4.3
9964	1012	90	10.0	10.0	10.4	10.5	1.0	1.0	1.5	1.5
32199	816	40	11.3	11.7	10.6	10.7	3.7	4.3	4.5	2.9
40767	1055	34	10.2	10.1	10.0	10.3	1.1	1.1	1.3	1.5
43414	1617	45	9.8	9.9	9.9	9.8	1.3	3.0	0.9	1.8
50754	402	90	8.9	9.1	9.8	9.5	1.0	0.3	0.3	1.0
6618	1524	47	10.0	9.9	10.0	10.6	4.0	3.9	4.0	2.7
22186	1539	48	9.9	9.9	10.2	9.7	0.8	1.5	0.7	0.6
11652	974	46	10.7	10.2	10.2	11.1	3.3	3.3	3.0	3.3
11848	436	86	10.0	9.9	10.3	9.7	1.1	1.4	3.3	1.5

Table 21 contains the grade measurements that were recorded during the site surveys. The measurements were taken on the centerline of the highway, and the signs (positive or negative) are defined based on the travel direction of the vehicles being observed.

Table 20. Site Pavement Characteristics.

Curve Number	Cross Slope at Approach Tangent Trap, %	Superelevation Rate, % (by speed trap location)			Skid Number (by speed trap location)		
		PC	MC	PT	PC	MC	PT
1114	2.6	6.8	8.7	7.3	32.4	37.4	41.8
2776	2.8	4.7	6.0	5.7	22.7	29.9	32.7
2794	−2.9	0.9	6.7	4.2	42.0	30.7	28.4
3347	−0.2	6.5	7.8	2.6	61.5	61.6	53.3
3359	2.9	5.0	11.4	5.3	65.7	64.6	66.1
4160	1.9	6.1	9.2	4.7	44.9	35.8	54.3
9964	1.2	2.8	8.2	3.5	50.7	58.8	59.9
32199	−1.6	1.4	5.8	−2.6	60.3	58.7	28.0
40767	4.1	5.5	8.4	3.2	21.3	15.4	16.8
43414	2.5	6.1	5.6	2.8	59.9	57.8	57.4
50754	3.5	6.6	10.2	5.1	43.9	23.2	48.5
6618	−2.2	−0.7	5.0	−1.1	20.1	15.6	49.5
22186	1.2	3.9	3.7	5.6	58.2	58.6	67.4
11652	1.1	4.5	5.4	4.6	57.3	58.2	59.2
11848	−3.0	3.8	7.2	4.4	31.7	23.1	33.1

Table 21. Site Vertical Grade Measurements.

Curve Number	Grade, % (by speed trap location)			
	TN	PC	MC	PT
1114	0.5	−0.2	−0.8	−2.0
2776	−0.6	0.5	−0.2	−0.4
2794	−0.3	−0.8	0.1	−0.3
3347	1.4	0.6	−1.2	0.3
3359	−0.1	3.2	2.3	1.6
4160	−0.7	−1.0	−2.9	−2.6
9964	−0.5	−0.5	−0.1	–0.9
32199	0.1	−1.5	3.0	−3.9
40767	−3.0	3.8	0.6	0.3
43414	2.1	1.4	0.2	0.6
50754	−0.8	−0.9	−1.1	−0.5
6618	2.2	0.3	0.9	1.8
22186	1.4	0.3	3.1	−2.4
11652	0.3	−2.5	−1.7	−1.9
11848	−1.7	−1.7	−4.1	−0.7

Speed Data Exploratory Analysis

Traffic classifiers and sensors were deployed at each data collection site for at least 18 hours, and often for two full days, to maximize the number of vehicles that could be observed with the available resources while obtaining a notable cross section of the key site characteristics. In total, about 22,000 vehicles were observed. However, many vehicles had to be discarded from the data set because:

- They were not observed at all four speed trap locations.
- Their length measurements, axle counts, or vehicle classification numbers differed between locations.
- They could not be defined as "free-flow."

Additionally, vehicles that were observed during weekend days or during periods of rain were excluded from the data set.

Vehicles were defined as "free-flow" based on the following criteria:

- At the approach tangent speed trap, the vehicle's leading and trailing headways equaled or exceeded 7 seconds.
- At the PC speed trap, the vehicle's leading and trailing headways equaled or exceeded 5 seconds.
- At the MC and PT speed traps, the vehicle's leading and trailing headways equaled or exceeded 3 seconds.

It was rationalized that vehicles could be considered "free-flow" with shorter headways as they entered and traversed the curve. This is because a curve represents a constrained environment where drivers' speeds are influenced more by the horizontal alignment of the highway than by interactions with leading and trailing vehicles.

After screening, the refined speed data set included 6,106 vehicles. The distribution of these vehicles based on the commonly-used "Classification Scheme F" is provided in Table 22. Classification Scheme F is described in Appendix A of TxDOT's *Traffic Recorder Instruction Manual* (*12*).

Table 22. Vehicle Count by Vehicle Classification.

Vehicle Class Description	Classification Number	Count
Motorcycle	1	14
Passenger car	2	2832
2-axle, 4-tire single unit; pickup; van	3	2193
Bus	4	35
2-axle, 6-tire single unit	5	791
3-axle single unit	6	30
3-4 axles, single trailer	8	70
5 axles, single trailer	9	140
6 or more axles, single trailer	10	1
	Total:	6106

Table 23 provides vehicle counts by site and summary statistics of the observed vehicle speeds. These speeds are presented for the PC, MC, and PT speed traps as well as for the approach tangent (TN) speed trap. The regulatory speed limit and posted advisory speed for each site are also included in the table.

Several trends can be noted in Table 23. First, compliance with the regulatory speed limit at the approach tangent speed trap is higher when the regulatory speed limit is higher. This trend, which is illustrated in Figure 35, is consistent with the trend that Bonneson et al. observed (*3*).

Table 23. Vehicle Speed Statistics by Site.

Curve Number	Vehicle Count	Posted Speed Limit, mph [1]		Average Speed, mph (by speed trap location)				85th-Percentile Speed, mph (by speed trap location)			
		Reg.	Adv.	TN	PC	MC	PT	TN	PC	MC	PT
1114	489	65	50	61.7	58.9	58.5	60.2	69.0	66.0	65.0	67.0
2776	118	70	55	61.1	57.9	57.6	58.9	69.0	65.0	64.0	66.0
2794	16	70	50	70.1	62.3	59.4	60.4	78.0	75.0	67.0	67.0
3347	45	65	45	60.7	53.8	51.0	54.4	69.0	60.0	57.0	61.0
3359	1097	65	45	62.2	56.3	54.8	56.2	69.0	63.0	61.0	63.0
4160	522	60	35	59.9	51.6	49.1	53.9	67.0	58.0	55.0	59.0
9964	821	65	40	56.6	55.2	50.7	52.2	69.0	62.0	57.0	58.0
32199	131	70	55	60.2	58.0	57.5	56.9	69.0	66.0	67.0	65.0
40767	414	70	55	61.0	62.9	60.0	61.3	68.0	70.0	67.0	68.0
43414	521	70	50	61.8	56.5	55.0	56.3	69.0	63.0	61.0	63.0
50754	20	65	30	56.2	41.7	38.0	42.0	66.0	52.5	43.0	47.5
6618	803	55	50	57.2	54.1	54.8	56.1	63.0	60.0	60.0	62.0
22186	182	55	35	51.0	43.0	40.4	43.8	58.0	47.0	44.0	48.0
11652	262	60	45	63.2	57.0	53.6	55.7	69.0	63.0	59.0	61.0
11848	665	55	None	61.2	60.3	59.6	59.0	67.0	66.0	65.0	64.0

Notes:
1–Reg. = regulatory speed limit; Adv. = curve advisory speed

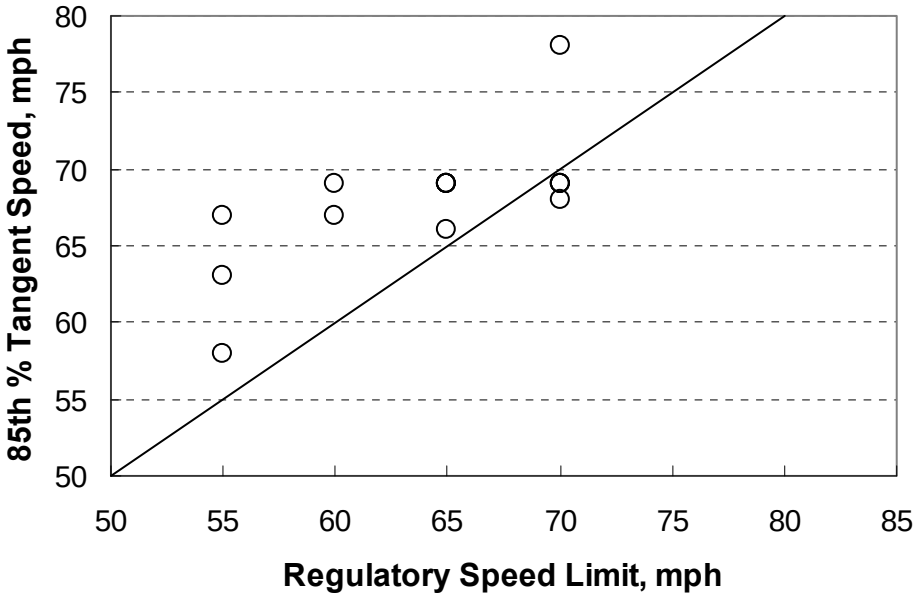

Figure 35. Comparison of Regulatory Speed Limit and 85th-Percentile Tangent Speed.

Second, the average speed observed at the mid-curve speed trap is always higher than the advisory speed, to varying degrees (see Figure 36). This trend, too, is consistent with the trend that Bonneson et al. reported (*3*).

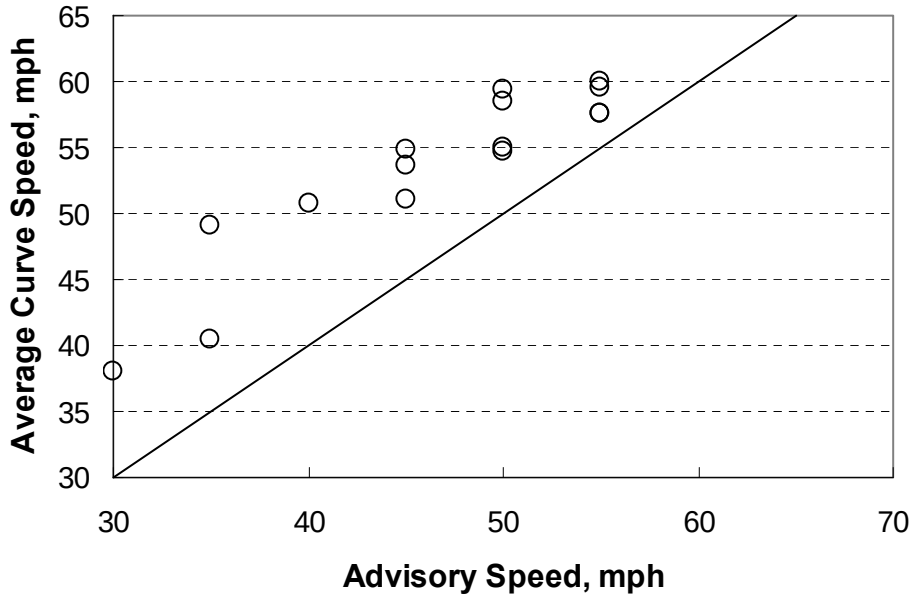

Figure 36. Comparison of Advisory Speed and Average Mid-Curve Speed.

Third, it can be seen that at almost all sites, vehicle speeds (both average and 85th-percentile) were higher at the PC trap than at the MC trap. This trend is consistent with

trends reported in the literature (*8*, *13*), and shows that most drivers have not fully decelerated to their chosen curve speed when they enter the curve. Further, it can be seen that vehicle speeds are almost always higher at the PT trap than at the MC trap, showing that drivers begin to increase their speed once they have passed through the midpoint of the curve.

The researchers conducted a more thorough examination of curve speed change trends by computing the speed change of each vehicle as it progresses through the site, and then computing descriptive statistics on the distribution of speed-change values. Misaghi and Hassan (*14*) suggested this approach as being more representative of actual speed changes at the curve, compared with simply subtracting the pertinent speed statistics (e.g., average or 85th-percentile) at successive traps. Table 24 provides the distribution of average and 15th-percentile speed change values observed at the sites. Note that negative numbers in this table indicate a reduction in speed, and that the 15th percentile is correctly interpreted as the amount of speed reduction that is exceeded by only 15 percent of vehicles.

As shown in Table 24, many drivers continue to decelerate after they enter the curve, and at 11 of the 15 sites, the amount of deceleration equaled or exceeded 3 mph for at least 15 percent of drivers. The occurrence of deceleration at the beginning portion of the curve—where superelevation is not yet fully developed (see Table 20)—suggests that this portion of the curve is likely to be of particular interest in the conduct of a margin of safety analysis.

Table 24. Vehicle Speed Change Statistics by Site.

Curve Number	Vehicle Count	Average Speed Change, mph (by speed trap locations)			15th-Percentile Speed Change, mph (by speed trap locations)		
		TN - PC	PC - MC	MC - PT	TN - PC	PC - MC	MC - PT
1114	489	−2.8	−0.4	1.7	−5.0	−2.0	0.0
2776	118	−3.3	−0.2	1.3	−8.0	−2.0	−1.0
2794	16	−7.8	−2.9	1.0	−18.0	5.0	−3.0
3347	45	−6.9	−2.8	3.4	−13.0	−6.0	1.0
3359	1097	−5.9	−1.5	1.4	−10.0	−4.0	0.0
4160	522	−8.2	−2.5	4.8	−13.0	−5.0	2.0
9964	821	−1.4	−4.5	1.5	−11.0	−6.0	0.0
32199	131	−2.3	−0.4	−0.6	−4.0	−3.0	−2.0
40767	414	1.9	−2.8	1.3	−1.0	−4.0	0.0
43414	521	−5.3	−1.5	1.3	−10.0	−8.0	−4.0
50754	20	−14.5	−3.7	4.0	−28.5	−11.5	1.5
6618	803	−3.1	0.7	1.3	−5.0	−2.0	0.0
22186	182	−8.0	−2.6	3.4	−13.0	−2.0	1.0
11652	262	−6.3	−3.4	2.2	−10.0	−6.0	0.0
11848	665	−0.9	−0.7	−0.6	−2.0	−3.0	−2.0

Lane Placement Data Exploratory Analysis

For each vehicle in the operational data set, the lane placement at each of the three in-curve speed traps (PC, MC, and PT) was computed using the raw-data timestamps, the known proportions of the Z-configuration sensor deployment, and trap dimensions that were measured in the field. A small number of vehicles were excluded because lane placement data could not be obtained at all three in-curve traps. A total of 5,968 vehicles were included in the lane placement data set.

Summary statistics for the observed lane placement values are provided in Table 25. "Lane placement" is defined as the lateral location of the vehicle's front-right tire away from the marked edgeline. A negative value would indicate that the front-right tire was on the shoulder.

Once the lane placements at each in-curve trap were computed, the travel paths for each vehicle were defined based on the amount of lateral shift observed between subsequent traps. The rules used for defining travel paths were developed based on the travel path descriptions that Spacek provided (*6*) are summarized in Table 26.

The distribution of the travel path types across the lane placement data set is provided in Figure 37. As shown, the travel path types defined as ideal or normal are uncommon, together representing just 11 percent of the total data set. Conversely, drifting and swinging travel paths together represent over half of the data set. About 24 percent of the travel paths did not fit into any of the defined path types.

Table 25. Lane Placement Statistics by Site.

Curve Number	Vehicle Count	Average Lane Placement, ft (by speed trap locations)			Standard Deviation of Lane Placement, ft (by speed trap locations)		
		PC	MC	PT	PC	MC	PT
1114	484	1.49	1.47	2.13	0.77	1.14	1.18
2776	116	1.95	1.36	2.73	0.97	1.13	1.25
2794	14	1.70	2.36	3.22	1.46	1.65	1.81
3347	44	2.06	3.61	3.21	0.77	1.18	1.31
3359	1080	2.39	2.16	2.45	0.87	0.97	0.84
4160	476	1.82	0.47	2.96	0.94	1.39	1.46
9964	804	3.36	3.11	3.34	1.03	1.07	1.06
32199	125	1.71	3.51	3.73	1.12	1.18	0.98
40767	401	2.51	1.19	2.34	0.88	0.84	0.95
43414	516	1.65	1.00	2.44	0.95	1.19	1.33
50754	5	3.73	0.28	3.52	1.31	0.81	1.26
6618	802	2.52	2.27	2.63	0.93	1.10	1.17
22186	182	2.22	2.67	3.01	1.13	0.94	1.21
11652	259	2.14	1.64	2.19	0.74	0.98	0.86
11848	660	2.91	2.25	2.05	0.72	0.80	0.69

Table 26. Characterization of Travel Paths.

Travel Path Type	Shift from PC to MC	Shift from MC to PT
I (ideal)	Absolute value of shift ≤ 3 inches	
N (normal)	> 3 inches toward curve center and lane placement at MC does not exceed lane width minus 7 ft	> 3 inches away from curve center and lane placement at MC does not exceed lane width minus 7 ft
K (correcting)	> 3 inches away from curve center	> 3 inches toward curve center
C (cutting)	> 3 inches toward curve center and lane placement at MC exceeds lane width minus 7 ft	> 3 inches away from curve center and lane placement at MC exceeds lane width minus 7 ft
D (drifting)	> 3 inches away from curve center (L deflection) > 3 inches toward curve center (R deflection)	
S (swinging)	> 3 inches toward curve center (L deflection) > 3 inches away from curve center (R deflection)	
O (other)	All other combinations	

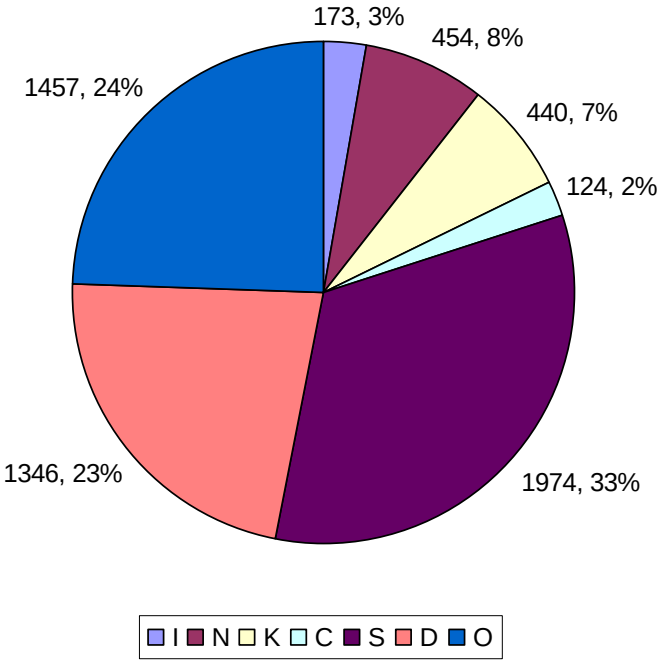

Figure 37. Distribution of Travel Path Types.

CROSS-SECTIONAL MODEL DEVELOPMENT

This part of the chapter describes the calibration of several models using the operational data set. The objective of the model development process was to formulate a framework that could be used to conduct a margin of safety analysis of a curve and assess the potential need and effectiveness of a high-friction surface treatment.

Speed Models

Two speed models were calibrated. The first model predicts 85th-percentile tangent speed as a function of regulatory speed limit and curve radius, and is described by Equation 70. Bonneson et al. calibrated a similar model (*3*).

$$v_{t,85} = b_0 \sqrt{v_{sl}} \left(1 - e^{\frac{b_1 (R+100)}{5730}} \right) \quad (70)$$

The model was calibrated using the NLMIXED procedure in the Statistical Analysis Software (SAS) program (*15*). Table 27 provides the results of the model calibration. A comparison of measured and predicted values is provided in Figure 38. As shown, the model predicts 85th-percentile tangent speed without bias.

Table 27. Tangent Speed Model Calibration Results.

Model Statistics				
R^2	0.59			
Observations	15 sites (6106 vehicles)			
Range of Model Variables				
Variable	Variable Name	Units	Minimum	Maximum
v_{sl}	Regulatory speed limit	mph	55	70
R	Radius of curve	ft	402	1617
Calibrated Coefficient Values				
Coefficient	Coefficient Definition	Value	Std. dev	*t*-value
b_0	Intercept	8.59	0.11	78.09
b_1	Effect of Radius	−30.47	5.71	−5.33

With the calibration coefficients substituted into Equation 70, this model is described as:

$$v_{t,85} = 8.59 \sqrt{v_{sl}} \left(1 - e^{\frac{-30.47 (R+100)}{5730}} \right) \quad (71)$$

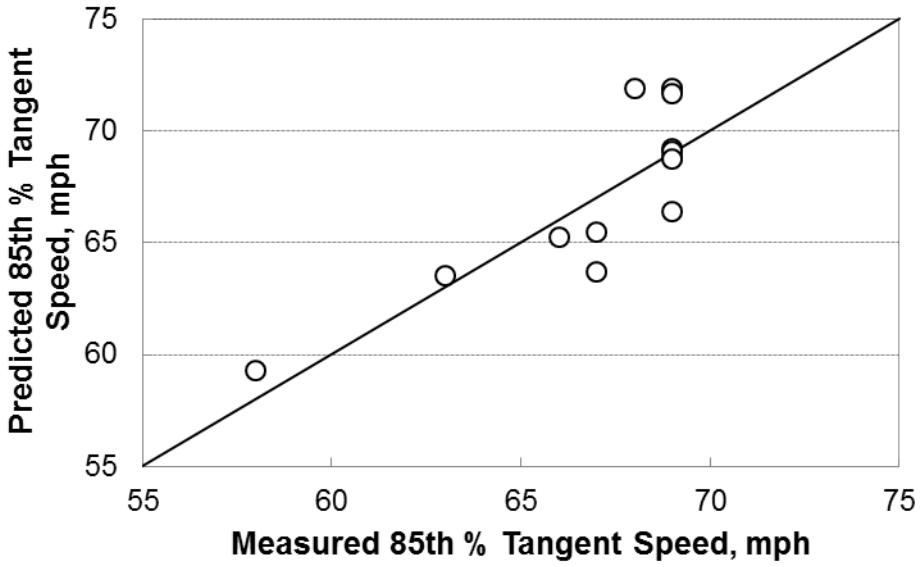

Figure 38. Comparison of Measured and Predicted Tangent Speeds.

Figure 39 shows a comparison of Equation 71 and the model that Bonneson et al developed. The models are shown to provide almost identical predicted values.

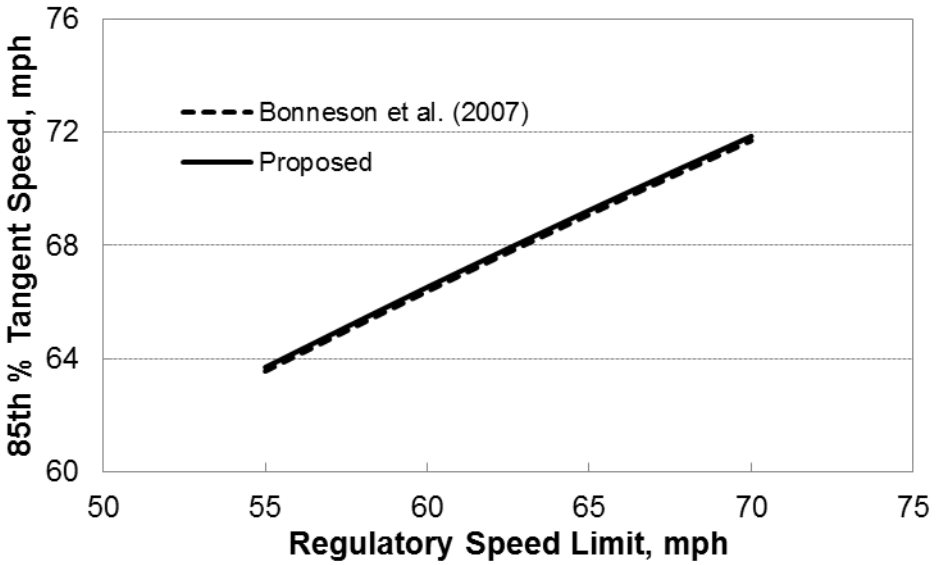

Figure 39. Comparison of Tangent Speed Models.

The second speed model predicts 85th-percentile curve speed at the MC as a function of 85th-percentile tangent speed, curve radius, deflection angle, and superelevation rate, and is described by Equation 72. Bonneson et al. calibrated a similar model (*3*).

$$v_{c,85} = \sqrt{\frac{15.0R_p(b_0 - b_1(1.47v_{t,85}) + 0.001b_2(1.47v_{t,85})^2 + e/100)}{1 + 0.00322R_p b_2}} \leq v_{t,85} \quad (72)$$

with:

$$R_p = \frac{3.0}{1 - \cos\frac{\Delta}{2}} \quad (73)$$

The model was calibrated using the NLMIXED procedure in the SAS program. Table 28 provides the results of the model calibration. A comparison of measured and predicted values is provided in Figure 40. As shown, the model predicts 85th-percentile curve speed without bias.

With the calibration coefficients substituted into Equation 72, this model is described as:

$$v_{c,85} = \sqrt{\frac{15.0R_p(0.2202 - 0.00142v_{t,85} + 0.000041{v_{t,85}}^2 + e/100)}{1 + 0.000061R_p}} \leq v_{t,85} \quad (74)$$

Table 28. Curve Speed Model Calibration Results.

Model Statistics				
R^2	0.94			
Observations	15 sites (6106 vehicles)			
Range of Model Variables				
Variable	Variable Name	Units	Minimum	Maximum
$v_{t,85}$	85th-percentile tangent speed	mph	58	78
$v_{c,85}$	85th-percentile curve speed	mph	43	67
R	Radius of curve	ft	402	1617
Δ	Curve deflection angle	degrees	34	90
e	Superelevation rate	%	3.7	11.4
Calibrated Coefficient Values				
Coefficient	Coefficient Definition	Value	Std. dev	t-value
b_0	Intercept	0.2202	0.1295	1.7
b_1	Effect of tangent speed	0.00097	0.0013	0.8
b_2	Effect of speed reduction	0.0189	0.0056	3.4

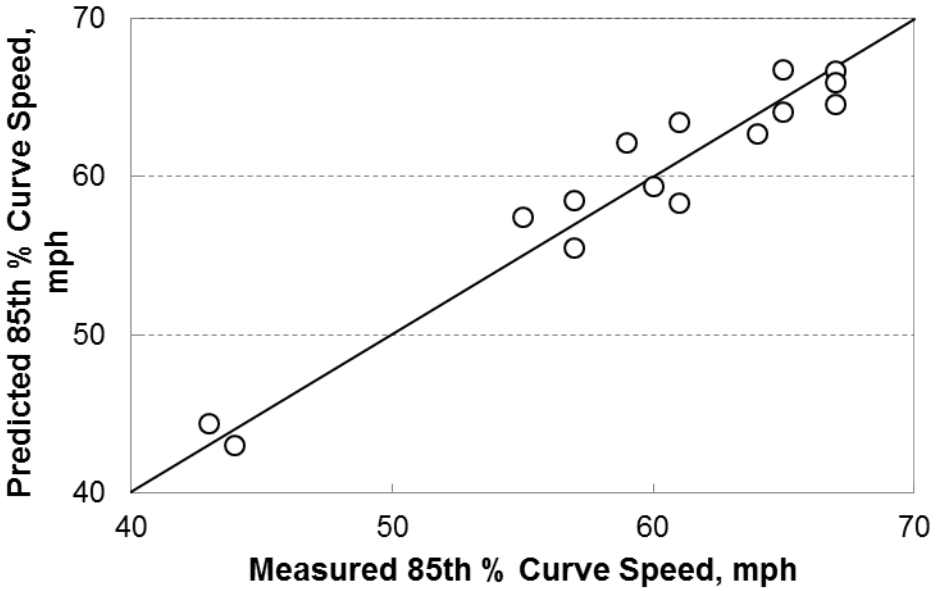

Figure 40. Comparison of Measured and Predicted Curve Speeds.

Figure 41 shows a comparison of Equation 74 and the model that Bonneson et al developed. The models are shown to provide similar predicted values. The differences observed are likely a consequence of the different vehicle mixes used in the calibration of the models. Bonneson et al. developed the plotted model to predict passenger car speeds, while Equation 74 was developed to predict speeds based on the overall vehicle mix, which was described in Table 22. The inclusion of some trucks in the calibration data set results in lower speeds being predicted, particularly for the lower range of curve radii.

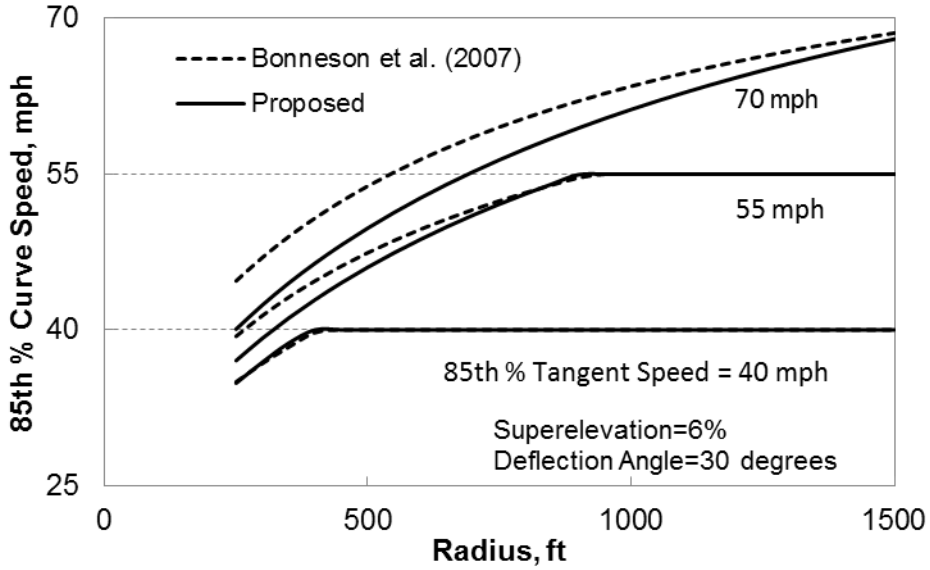

Figure 41. Comparison of Curve Speed Models.

In addition to the input variables that are included in Equation 74, variables describing other site characteristics were tested for significance. These site characteristics included:

- Skid number.
- Presence of delineation devices (e.g., delineators or Chevrons).
- Grade.
- Lane width.
- Shoulder width.
- Advisory speed.

None of these variables were found to be statistically significant, so they were excluded from the model.

Speed Differential Models

Equations 71 and 74 can be used to predict the 85th-percentile vehicle speed at both the approach tangent and the curve MC. However, to conduct a margin of safety analysis of the entire length of the curve, knowledge of vehicle speeds at the PC and PT is also needed. Hence, speed differential models were calibrated to obtain predicted values of vehicle speeds at these points as a function of tangent speed, MC curve speed, and site characteristics.

The models were formulated based on the approach that Misaghi and Hassan described (*14*). Specifically, the dependent variable for the speed differential models is the 85th-percentile speed differential from PC to MC and from MC to PT (defined as the PC speed minus the MC speed, and the PT speed minus the MC speed; and labeled as $\Delta_{85}v_{PC\text{-}MC}$ and $\Delta_{85}v_{MC\text{-}PT}$; respectively). Misaghi and Hassan stated that:

- An analysis of the distribution of speed differentials, as computed for each vehicle in the data set, gives a more accurate an unbiased representation of the actual speed changes that occur between successive roadway elements.
- A simple subtraction of the 85th-percentile speeds observed at the two successive elements (i.e., $\Delta v_{85,PC}$ - $\Delta v_{85,MC}$ and $\Delta v_{85,MC}$ - $\Delta v_{85,PT}$, respectively) underestimates the speed changes that actually occur.

This trend was verified in an examination of the calibration data set and is illustrated in Figure 42 for speed changes between the approach tangent trap and the MC trap.

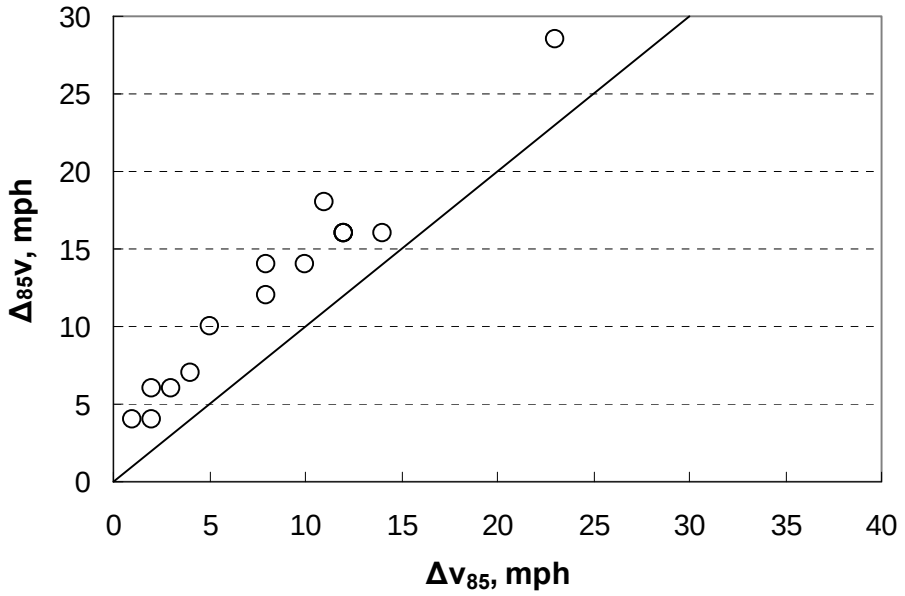

Figure 42. Comparison of Speed Differential Calculations.

The model for PC-MC speed differentials was formulated as follows:

$$\Delta_{85}v_{PC-MC} = b_0 + b_1\sqrt{\frac{v_{t,85}}{v_{c,85}}} + b_2\frac{5730}{R} \tag{75}$$

The model was calibrated using the NLMIXED procedure in the SAS program. Table 29 provides the results of the model calibration. A comparison of measured and predicted values is provided in Figure 43. As shown, the model predicts 85th-percentile PC-MC speed differential without bias.

Table 29. PC-MC Speed Differential Model Calibration Results.

Model Statistics				
R^2	0.77			
Observations	15 sites (6106 vehicles)			
Range of Model Variables				
Variable	Variable Name	Units	Minimum	Maximum
$v_{t,85}$	85th-percentile tangent speed	mph	58	78
$v_{c,85}$	85th-percentile curve speed	mph	43	67
R	Radius of curve	ft	402	1617
$\Delta_{85}v_{PC\text{-}MC}$	Speed differential (PC to MC)	mph	2.0	11.5
Calibrated Coefficient Values				
Coefficient	Coefficient Definition	Value	Std. dev	*t*-value
b_0	Intercept	−54.886	12.199	−4.5
b_1	Effect of speed change	58.768	12.637	4.7
b_2	Effect of radius	−0.521	0.241	−2.2

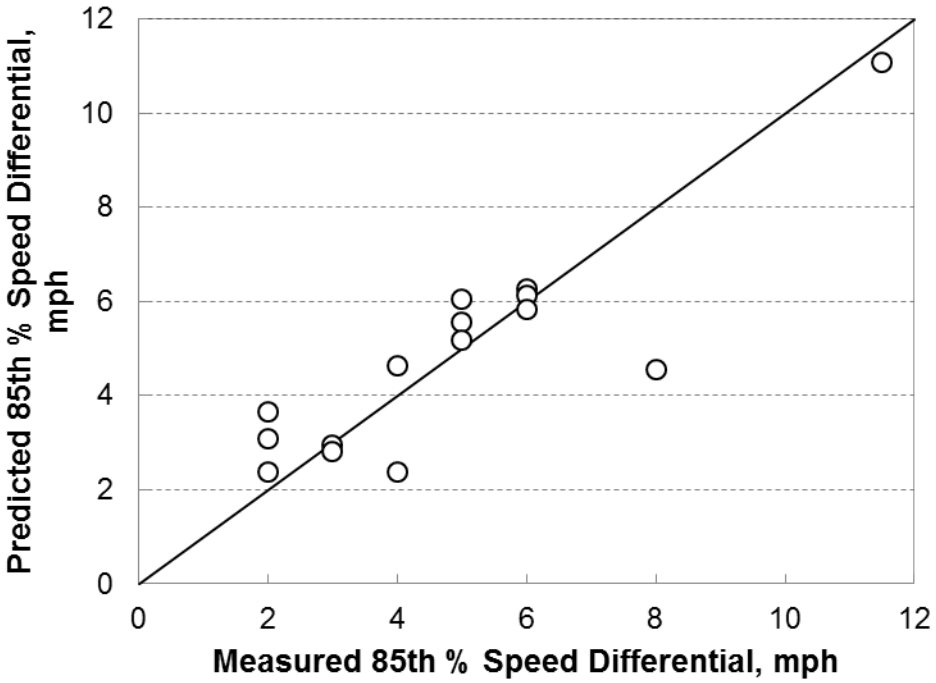

Figure 43. Comparison of Measured and Predicted PC-MC Speed Differentials.

With the calibration coefficients substituted into Equation 75, this model is described as:

$$\Delta_{85} v_{PC-MC} = -54.886 + 58.768\sqrt{\frac{v_{t,85}}{v_{c,85}}} - 0.521\frac{5730}{R} \quad (76)$$

Figure 44 show the trends that Equation 76 predicted. As the three lines illustrated, for a given MC speed and curve radius, the speed differential increases if the tangent speed increases, indicating that a greater amount of deceleration occurs within the curve if drivers approach the curve at higher speeds. This trend is consistent with the observation that Bonneson et al. made (*3*) that when approach tangent speeds are higher, drivers are more reluctant to reduce speed and hence will accept a larger side friction demand within the curve.

In addition to the input variables that are included in Equation 76, variables describing other site characteristics were tested for significance. These site characteristics included:

- Skid number.
- Presence of delineation devices (e.g., delineators or Chevrons).
- Grade.
- Lane width.
- Shoulder width.
- Advisory speed.

None of these variables were found to be statistically significant, so they were excluded from the model.

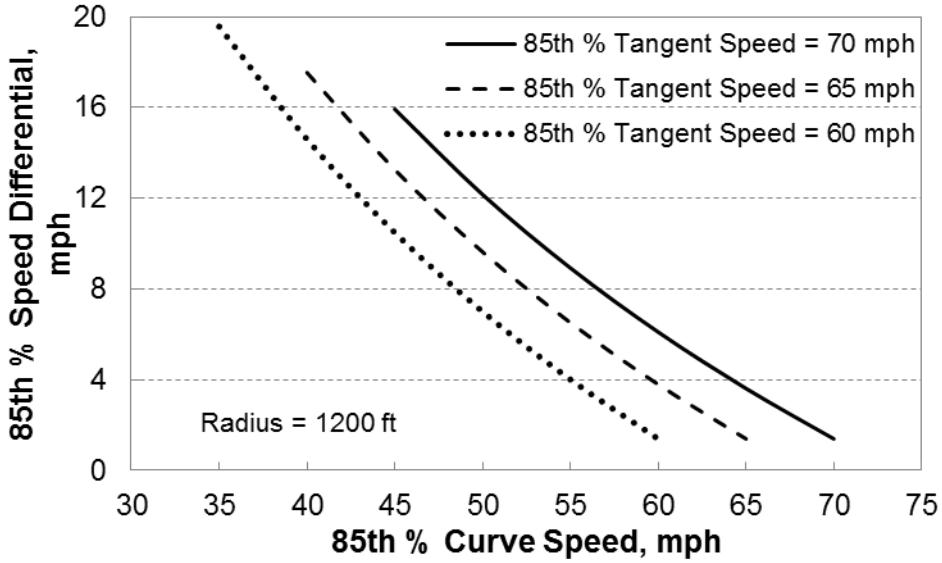

Figure 44. PC-MC Speed Differential Prediction Trends.

The model for MC-PT speed differentials was formulated as follows:

$$\Delta_{85} v_{MC-PT} = b_0 + b_1 \sqrt{\frac{v_{t,85}}{v_{c,85}}} + b_2 \left(\frac{G_{MC} + G_{PT}}{2} \right) \tag{77}$$

The model was calibrated using the NLMIXED procedure in the SAS program. Table 30 provides the results of the model calibration. A comparison of measured and predicted values is provided in Figure 45. As shown, the model predicts 85th-percentile MC-PT speed differential without bias.

Table 30. MC-PT Speed Differential Model Calibration Results.

Model Statistics				
R^2	0.62			
Observations	15 sites (6106 vehicles)			
Range of Model Variables				
Variable	Variable Name	Units	Minimum	Maximum
$v_{t,85}$	85th-percentile tangent speed	mph	58	78
$v_{c,85}$	85th-percentile curve speed	mph	43	67
G_{MC}	Grade at MC	%	−4.1	3.1
G_{PT}	Grade at PT	%	−3.9	1.8
$\Delta_{85} v_{MC-PT}$	Speed differential (MC to PT)	mph	2.0	11.5
Calibrated Coefficient Values				
Coefficient	Coefficient Definition	Value	Std. dev	*t*-value
b_0	Intercept	−12.399	8.032	−1.5
b_1	Effect of speed change	15.197	7.547	2.0
b_2	Effect of radius	−0.803	0.358	−2.2

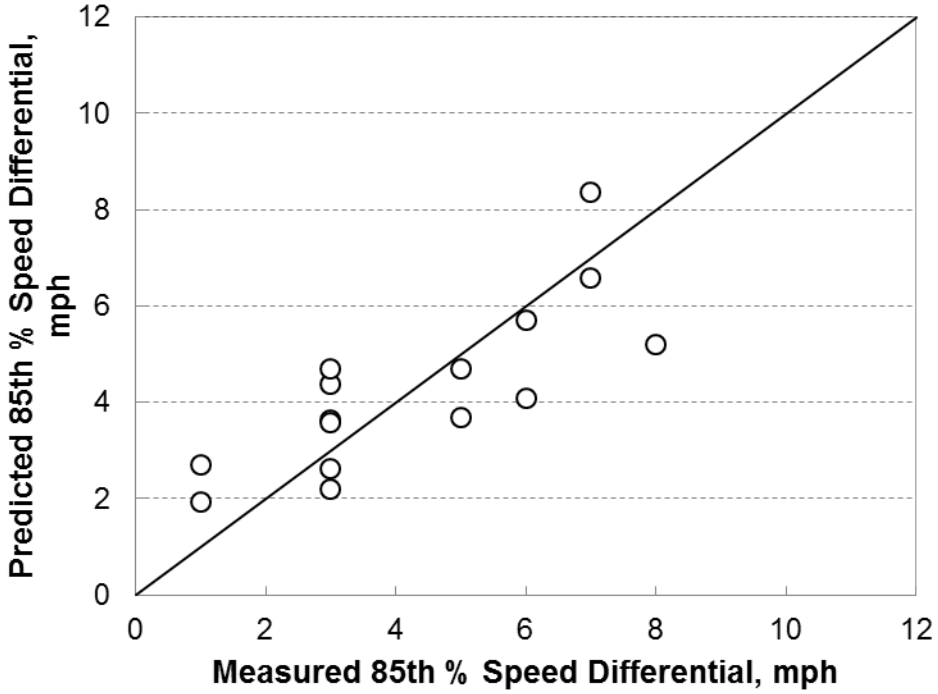

Figure 45. Comparison of Measured and Predicted MC-PT Speed Differentials.

With the calibration coefficients substituted into Equation 77, this model is described as:

$$\Delta_{85}v_{MC-PT} = -12.399 + 15.197\sqrt{\frac{v_{t,85}}{v_{c,85}}} - 0.803\left(\frac{G_{MC} + G_{PT}}{2}\right) \quad (78)$$

Figure 46 shows the trends that Equation 78 predicted. As the three lines illustrated, for a given MC speed and curve radius, the speed differential increases if the tangent speed increases, indicating that a greater amount of acceleration occurs within the curve if drivers approach the curve at higher speeds.

In addition to the input variables that are included in Equation 78 variables describing other site characteristics were tested for significance. These site characteristics included:

- Skid number.
- Presence of delineation devices (e.g., delineators or Chevrons).
- Curve radius.
- Lane width.
- Shoulder width.
- Advisory speed.

None of these variables were found to be statistically significant, so they were excluded from the model.

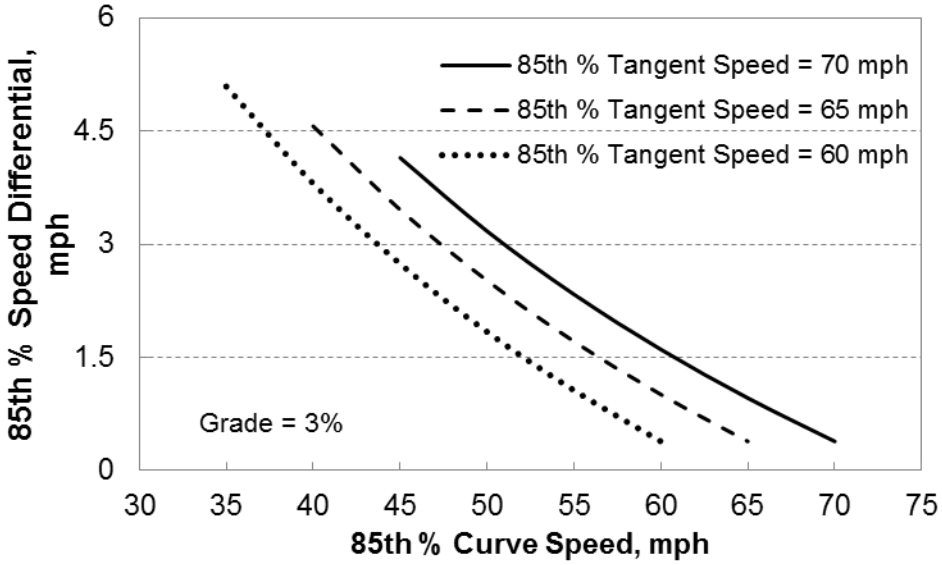

Figure 46. MC-PT Speed Differential Prediction Trends.

Travel Path Distribution Models

Models were developed to predict the distribution of travel path types as a function of curve characteristics. The development of the models, and discussion of the calibrated models' trends, are discussed in the following subsections.

Model Development

The multinomial logit (MNL) model form was used to predict the probability of vehicle path types on a given horizontal curve. Since the path types cannot be arranged in a logical "severity" order, an ordered probability model is not the preferred model form. Given the characteristics of the data, the MNL is the most suitable model form for estimating the probabilities. Each path type likelihood function was considered to have a deterministic component and an error/random component. While the deterministic part is assumed to contain variables that can be measured, the random part corresponds to the unaccounted factors that impact the vehicle path.

The model forms given in Equations 1–3 were used for the deterministic component of the vehicle paths during the regression analysis. The vehicle path types are separated into three categories. The first category consists of desirable path types, namely normal (N) and ideal (I) paths. The cutting (C), swinging (S), and drifting (D) paths are considered to be undesirable, though less severe, are included in the second category. These paths represent situations where drivers may have misjudged the severity of the curve, but not to the extent that they see the need to make a course correction. The third category consists of highly-undesirable correcting (K) path types, where the chance of a crash is higher due to the occurrence of a high side friction demand during the correction.

The following paragraphs describe the final form of the models and present the analysis results. The final model forms reflect findings from several preliminary analyses where alternative model forms were examined. The forms that are described represent those that provided the best fit to the data, while also having coefficient values that are logical and constructs that are theoretically defensible and properly bounded.

The probability for each vehicle path type category is given by the following equations:

$$P_{N+I} = \frac{e^{V_{N+I}}}{1 + e^{V_{N+I}} + e^{V_{C+S+D}}} \tag{79}$$

$$P_{C+S+D} = \frac{e^{V_{C+S+D}}}{1 + e^{V_{N+I}} + e^{V_{C+S+D}}} \tag{80}$$

$$P_K = 1 - (P_{N+I} + P_{C+S+D}) \tag{81}$$

with:

$$V_{N+I} = ASC_{N+I} + b_{SK,N+I}\frac{SK}{100} + b_{LW,N+I}LW + b_{\Delta,N+I}\Delta + b_{\delta V,N+I}\delta V \tag{82}$$

$$V_{C+S+D} = ASC_{C+S+D} + b_{SK,C+S+D}\frac{SK}{100} + b_{LW,C+S+D}LW + b_{\Delta,C+S+D}\Delta + b_{\delta V,C+S+D}\delta V \tag{83}$$

where:

P_{N+I} = probability of the occurrence of vehicle path type N or I.
P_{C+S+D} = probability of the occurrence of vehicle path type C, S, or D.
P_K = probability of the occurrence of vehicle path type K.
V_{N+I} = systematic component of path type likelihood for vehicle path type N or I.
V_{C+S+D} = systematic component of path type likelihood for vehicle path type C, S, or D.
δV = speed difference (85^{th}-percentile curve speed - posted advisory speed), mph.
ASC_j = alternative specific constant for path type j.
$b_{k,j}$ = calibration coefficient for variable k and path type j.

The database assembled for calibration included vehicle path type as the dependent variable. Geometric design features, traffic control features, and pavement characteristics were included as independent variables. Table 31 presents a brief summary of the variables used for model development. The variables listed were those found to have an important influence on the travel path distribution. The calibration data set included only vehicles exhibiting paths that could be categorized as normal, ideal, cutting, swinging, drifting, or correcting (see Table 26 for travel path characteristics). Vehicles with travel paths categorized as "other" were excluded. As a result, the calibration data set included 4511 vehicles.

Table 32 summarizes the estimation results of the travel path distribution models. The *t*-values indicate a test of the hypothesis that the coefficient value is equal to 0.0. Those *t*-values with an absolute value that is larger than 2.0 indicate that the hypothesis can be rejected with the probability of error in this conclusion being less than 0.05. For those few variables where the absolute value of the *t*-value is smaller than 2.0, it was decided that the variable was

important to the model and its trend was found to be intuitive (even if the specific value was not known with a great deal of certainty as applied to this database).

Table 31. Range of Travel Path Distribution Model Variables.

Variable	Variable Name	Range (Min./Max.)	Mean	Frequency
SK	Skid number	18/65	46	4511
LW	Average lane width, ft	9.5/11.0	10.3	4511
Δ	Deflection angle, degrees	34/90	59	4511
δV	Speed difference, mph	−31/30	7.7	4511
Travel path types	Normal and ideal	Not applicable		627 (14%)
	Cutting, swinging, and drifting	Not applicable		3444 (76%)
	Correcting	Not applicable		440 (10%)

Table 32. Parameter Estimation for the Travel Path Distribution Models.

Model Statistics					
AIC	6349				
Observations	4511 (vehicle paths)				
Calibrated Coefficient Values					
Coefficient	Coefficient Definition	N+I paths		C+S+D paths	
		Value	t-value	Value	t-value
ASC	Alternative specific constant	−2.486	−1.4	−0.699	−0.5
b_{SK}	Effect of skid number	2.079	5.0	1.284	3.8
b_{LW}	Effect of lane width	0.147	0.8	0.169	1.1
b_{Δ}	Effect of deflection angle	0.007	2.1	0.006	2.1
$b_{\delta V}$	Effect of speed differential	--	--	0.017	2.2

The coefficients in Table 32 were combined with Equations 82 and 83 to obtain the systematic component of each travel path type. The form of each model is:

$$V_{N+I} = -2.486 + 2.079 + \frac{SK}{100} + 0.147LW + 0.007\Delta \quad (84)$$

$$V_{C+S+D} = -0.699 + 1.284\frac{SK}{100} + 0.169LW + 0.006\Delta + 0.017\delta V \quad (85)$$

The probability of each vehicle path type category is obtained by combining Equations 79–81 with Equations 84 and 85.

Discussion

Skid Number. The relationship between skid number and travel path distribution is shown in Figure 47. The positive value of the associated coefficient (in Table 32) indicates that as the skid number increases, the likelihood of path types N and I increases. At the same time, the likelihood of path type K decreases with the increase in skid number. There is no major change in other path types with skid number. The trends in Figure 47 indicate that the K path type probability changes from 14.7 percent with a skid number of 10 to 5.3 percent with a skid number of 90. The percentage of normal and ideal path types almost doubles with the change in skid number from 10 to 90.

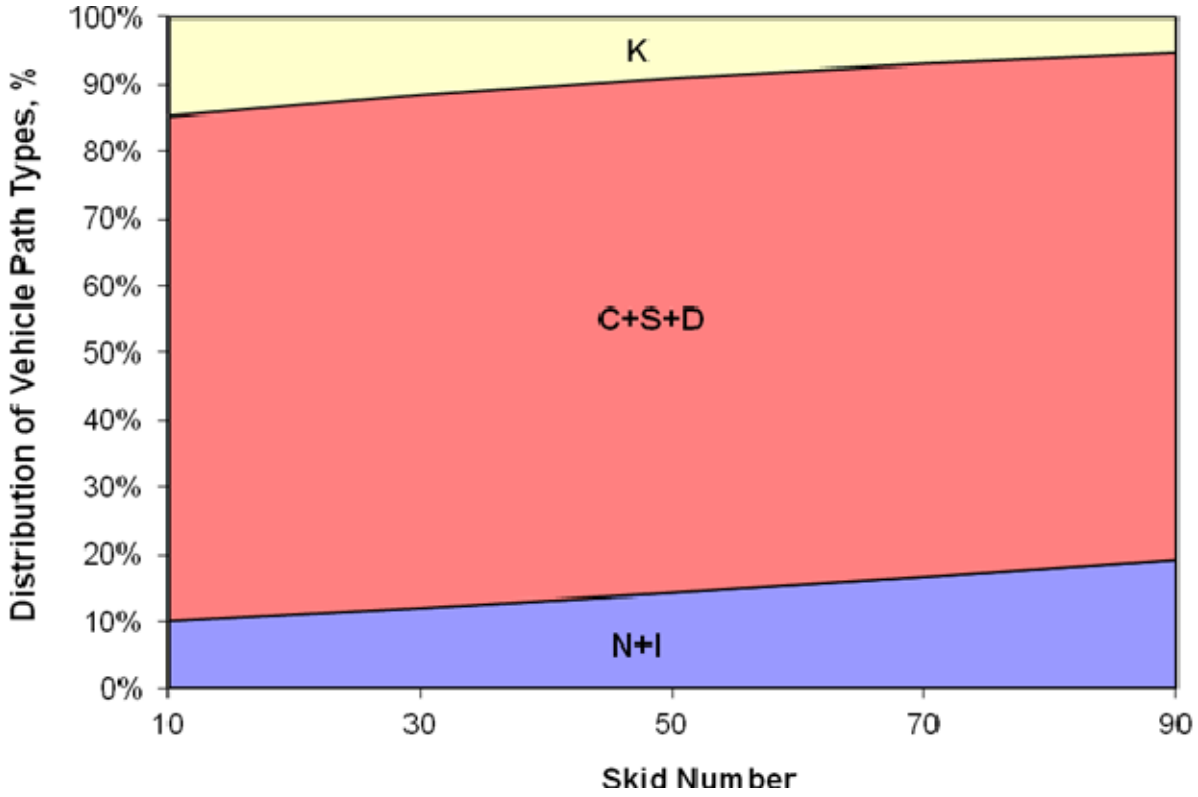

Figure 47. Travel Path Distribution with Change in Skid Number.

Lane Width. The relationship between lane width and travel path distribution is shown in Figure 48. The positive value of the associated coefficient (in Table 32) indicates that as lane width increases, the likelihood of path types C, S and D increases when compared to path type K. This also means that the likelihood of path type K decreases with the increase in lane width. This variable is not statistically significant in influencing the N and I path types. With a change in lane width from 9 ft to 13 ft, the probability of path type K changes from 11.4 percent to 6.2 percent.

Generally, path type K occurs when drivers realize that they are about to depart their lane and feel compelled to correct their path to stay in the lane. With a wider lane, such corrections are less frequent because the lane can accommodate a larger magnitude of cutting, swinging, or drifting (i.e., travel path types C, S, and D) before drivers encroach on the edgeline or the centerline.

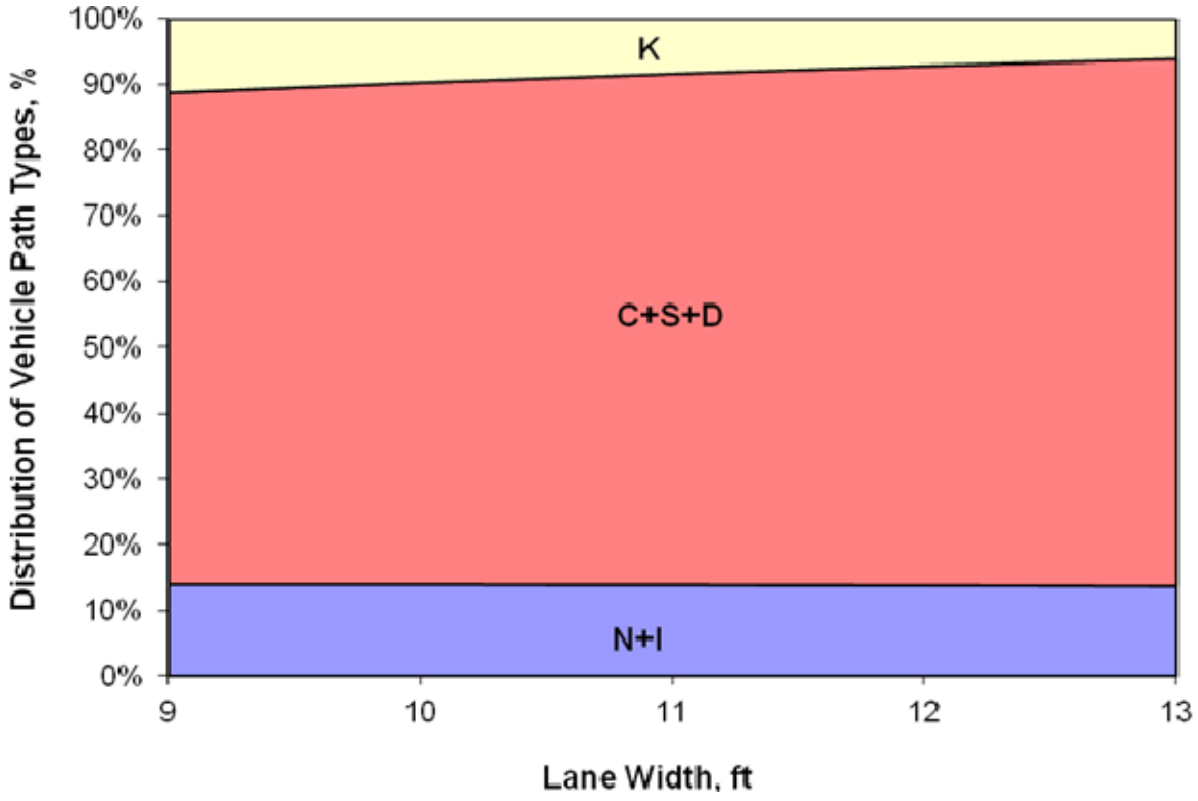

Figure 48. Travel Path Distribution with Change in Lane Width.

Deflection Angle. The relationship between deflection angle and travel path distribution is shown in Figure 49. The positive value of the associated coefficient (in Table 32) indicates that as the deflection angle increases, the likelihood of path types N, I, C, S, and D increases. At the same time, as the deflection angle increases, the likelihood of path type K decreases. The trends in Figure 49 indicate that the change in different path types is marginal with the change in the curve deflection angle. Compared with the rest of the variables in the models, deflection angle has a relatively subtle effect on travel path distribution.

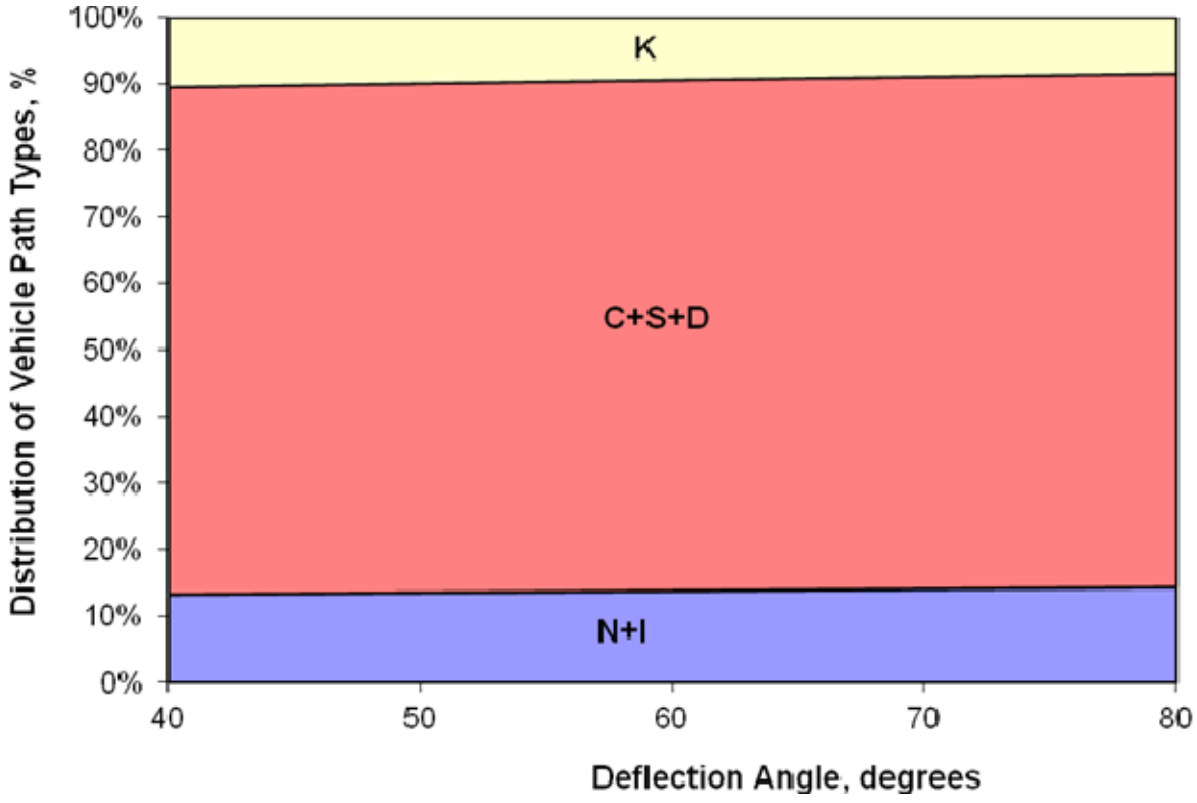

Figure 49. Travel Path Distribution with Change in Deflection Angle.

Speed Difference. The relationship between the speed difference variable (i.e., 85th-percentile curve speed - posted advisory speed) and travel path distribution is shown in Figure 50. The positive value of the associated coefficient (in Table 32) indicates that as speed difference increases, the likelihood of travel path types C, S, and D increases. This also means that the likelihood of path types K decreases with the increase in speed difference. This variable is not significant in influencing the N, and I path types. As the sum of proportion of all the travel path types must be equal to one, increase in path types C, S, and D will automatically lead to a decrease in the proportions for path types N, and I.

The increase in travel path types C, S, and D for higher speed differentials may reflect the level of care exhibited by the range of drivers. That is, drivers who accept higher speeds (and higher side friction demands) in curves may also be more willing to encroach on the edgeline or the centerline. The trend may also reflect traffic conditions. That is, drivers who accept higher speeds through curves are able to do so because they did not encounter slower vehicles in their lane or opposing vehicles in the opposite direction of travel. Hence, they do not perceive the need to correct if they begin to encroach on the opposing travel lane.

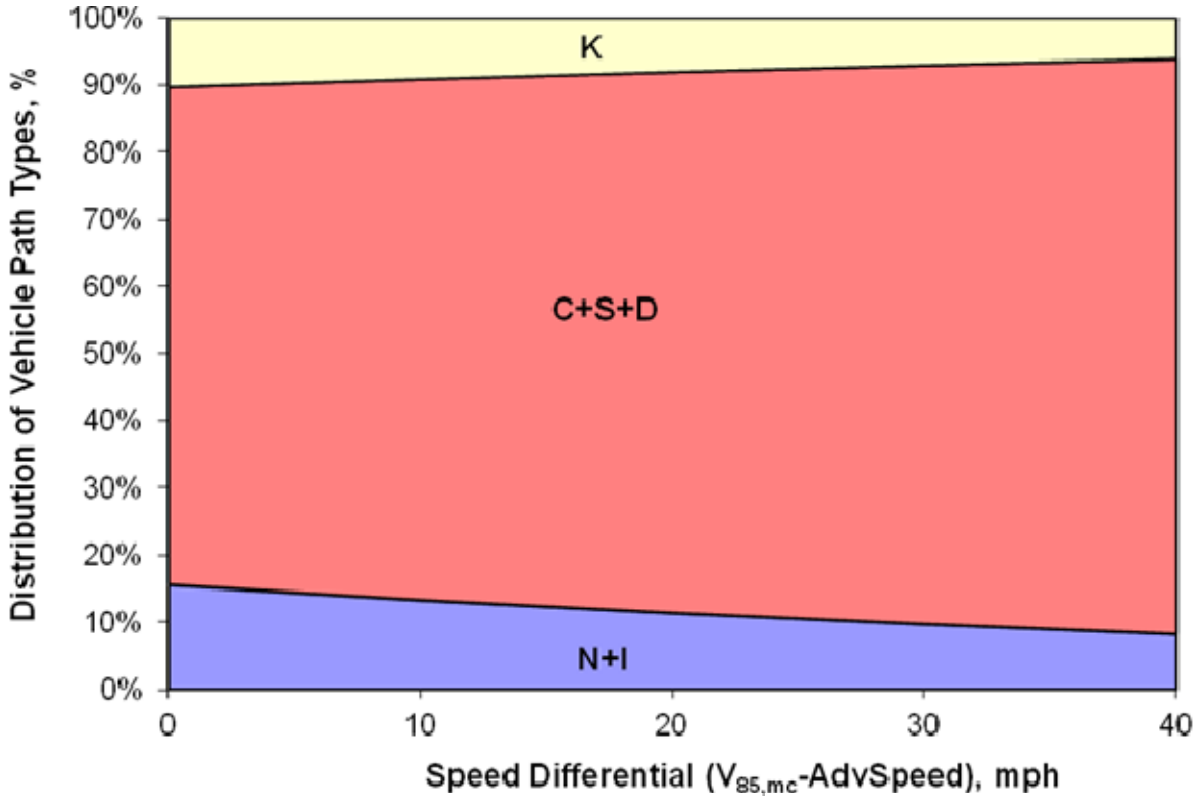

Figure 50. Travel Path Distribution with Change in Speed Difference.

REFERENCES

1. *A Policy on Geometric Design of Highways and Streets*. 5th Edition. American Association of State Highway and Transportation Officials, Washington, D.C., 2004.
2. *Pavement Design Guide.* Texas Department of Transportation, Austin, Texas, 2008.
3. Bonneson, J., M. Pratt, J. Miles, and P. Carlson. *Development of Guidelines for Establishing Effective Curve Advisory Speeds*. Report FHWA/TX-07/0-5439-1, Texas Transportation Institute, College Station, Texas, 2007.
4. Emmerson, J. Speeds of Cars on Sharp Horizontal Curves. In *Traffic Engineering & Control*, Vol. 11, No. 3, July 1969, pp. 135–137.
5. Yu, L., and N. Jiangfeng. Effect of Highway Horizontal Alignment on Driver Decision Behavior on Trajectory Path. International Conference on Transportation Engineering, ASCE, 2011.
6. Spacek, P. Track Behavior in Curve Areas: Attempt at Typology. In *Journal of Transportation Engineering*, Vol. 131, No. 9, September 2005, pp. 669–676.
7. Koorey, G., S. Page, P. Stewart, J. Gu, A. Ellis, R. Henderson, and P. Cenek. *Curve Advisory Speeds in New Zealand.* Transfund New Zealand Research Report No. 226. Transfund New Zealand, Wellington, New Zealand, 2002.

8. Fitzpatrick, K., L. Elefteriadou, D.W. Harwood, J.M. Collins, J. McFadden, I.B. Anderson, R.A. Krammes, N. Irizarry, K.D. Parma, K.M. Bauer, and K. Passetti. *Speed Prediction for Two-Lane Rural Highways.* FHWA-RD-99-171. Federal Highway Administration, U.S. Department of Transportation, Washington, D.C., 2000.
9. Bonneson, J. *Superelevation Distribution Methods and Transition Designs*. NCHRP Report 439. TRB, National Research Council, Washington, D.C., 2000.
10. Glennon, J. *State of the Art Related to Safety Criteria for Highway Curve Design.* Research Report 134-4. Texas Transportation Institute, College Station, Texas, 1969.
11. Chrysler, S., J. Re, K. Knapp, D. Funkhouser, and B. Kuhn. *Driver Response to Delineation Treatments on Horizontal Curves on Two-Lane Roads*. Report FHWA/TX-09/0-5772-1, Texas Transportation Institute, College Station, Texas, 2009.
12. *Traffic Recorder Instruction Manual.* Texas Department of Transportation, Austin, Texas, 2012.
13. Hassan, Y. Traffic and Speed Characteristics on Two-Lane Highways: Field Study. In *Canadian Journal of Civil Engineering*, Vol. 30, No. 6, 2003, pp. 1042–1054.
14. Misaghi, P., and Y. Hassan. Modeling Operating Speed and Speed Differential on Two-Lane Rural Roads. In *Journal of Transportation Engineering*, Vol. 131, No. 6, June 2005, pp. 408–417.
15. *SAS/STAT User's Guide, Version 9.2*. Second edition, SAS Institute, Inc., Cary, North Carolina, 2009.

CHAPTER 5. GUIDELINE DEVELOPMENT AND APPLICATION

INTRODUCTION

The safety performance of a horizontal curve is influenced by a variety of factors, including curve geometry, pavement friction, and vehicle speed, the latter of which is influenced by the former. Though drivers generally reduce to a safe speed by the time they arrive at the middle of a curve, they often misjudge the sharpness of the curve before entering it, and are compelled to decelerate or make correcting maneuvers while in the curve. Excessive deceleration or braking on a curve can lead to a sliding failure of the tire-pavement interface and result in a crash.

A margin of safety analysis represents a good method for evaluating curve safety as a function of geometry and pavement friction. Margin of safety is defined as the side friction supply minus the side friction demand. Because vehicle speeds and the superelevation rate change along the length of a curve, it is necessary to evaluate the margin of safety along the entire length of the curve. This type of analysis requires estimation of vehicle speed at key points along the curve length, such as the PC, the MC, and the PT. Furthermore, consideration must be given to the occurrence and frequency of correcting maneuvers, which are associated with side friction demands well in excess of demands incurred by vehicles tracking the curve with geometric exactness.

The researchers developed guidance material to help practitioners assess the potential safety benefit of curve pavement improvements. This material is in the form of a spreadsheet program called the Texas Curve Margin of Safety (TCMS) worksheet. TCMS is designed to compute the benefits of increasing pavement friction through the provision of a high-friction surface treatment, or increasing superelevation rate. The computation methodology and the application of the TCMS program are described in the next two sections of this chapter.

CALCULATION FRAMEWORK

This section describes the calculation framework used by the TCMS program. Specifically, the methods used to compute margin of safety, travel path distribution, crash prediction, and curve severity are detailed in the following subsections.

Margin of Safety Analysis

A detailed margin of safety analysis requires knowledge of the side friction supply and the side friction demand. These quantities are influenced by curve geometry, pavement characteristics, and vehicle speeds.

Side Friction Demand

The point-mass model or the simplified curve formula that was described in Chapter 2 (see Equation 6) describes the side friction demand that an individual vehicle incurred. A modified form of this equation has been developed to incorporate the effect of grade on side friction demand (*1*). This equation is described as follows:

$$f_D = \frac{v^2}{gR_p}\cos\left(\frac{e}{100}\right) - \sin\left(\frac{e}{100}\right)\cos G \tag{86}$$

where:

G = vertical grade (ft/ft).

To compute the side friction demand for an individual vehicle, the speed v and the radius R_p in Equation 86 must be chosen to represent the speed and path radius of the vehicle. Equation 74 can be used to compute the 85th-percentile speed at the MC, and Equations 76 and 78 can be used to compute the 85th-percentile vehicle speeds at the PC and the PT. To compute the side friction demand at the three points of the curve (PC, MC, and PT), the vehicle speeds at each point must be matched with the superelevation rate and grade at the same point.

To determine the path radius R_p for use with Equation 86, it is necessary to identify the travel path characteristics of the vehicle. The lane placement models described in Chapter 4 can be used to determine the percentage of vehicles exhibiting the travel path types that were illustrated in Figure 32. For the purpose of estimating side friction demand, the following two travel path types that Spacek described (*2*) are used:

- Travel path type I ("ideal"): The driver traverses the curve with "geometric exactness", which has historically been the implicit assumption in curve design practice (*3*).
- Travel path type K ("correcting"): The driver makes a correcting maneuver in the curve, during which he experiences a side friction demand in excess of that experienced during the traversal of an ideal travel path. The steering fluctuation factor of 1.15 suggested by Bonneson (*4*) is used to estimate the path radius for this travel path.

By evaluating travel path types I and K at three points within the curve (PC, MC, and PT), six estimates of side friction demand are obtained.

Side Friction Supply

The side friction supply available to vehicles depends on characteristics of the pavement and the tire. Pavement friction is described in terms of skid number, which varies based on speed. TxDOT measures and archives skid data at a test speed of 50 mph (*5*). To convert skid number measurements to different speeds, Olson et al. (*6*) used the following equations:

$$SK_v = SK_{50} e^{P(v-50)} \tag{87}$$

with:

$$P = -0.0016 D_m^{-0.47} \tag{88}$$

where:

SK_v = skid number at speed v.
SK_{50} = skid number at 50 mph.
P = normalized skid gradient, mph^{-1}.
D_m = mean pavement texture depth measured by the sandpatch method, in.

Olson et al. suggested a D_m value of 0.015 in. to represent a "poor" road surface. Using this value with Equation 88, the normalized skid gradient is computed as −0.32 skid numbers per mile per hour. In other words, the skid number decreases by 0.32 with each 1-mph increase in vehicle speed.

Skid number is measured using a locked-wheel trailer, and it represents the coefficient of friction observed with a smooth, locked tire on a wet surface. To compute the amount of rolling friction available for a typical passenger car, Olson et al. offered the following equation:

$$f_{s,max} = 0.2 + 1.12 SK_v \tag{89}$$

where:

$f_{s,max}$ = maximum side friction supply.

The $f_{s,max}$ value from Equation 89 represents the maximum amount of side friction that could be obtained from the tire-pavement interface, in the case where the vehicle is coasting through the curve. If the driver is braking or accelerating while traversing the curve, the tire-pavement interface is forced to provide some braking friction or tractive effort, and the available side friction supply is reduced. The actual available (or downward-adjusted) side friction supply is computed using the friction ellipse equation that Bonneson described (*4*):

$$f_s = f_{s,\max} \sqrt{1 - \frac{f_{x,D}}{f_{s,\max}}} \tag{90}$$

where:

f_s = available side friction supply.
$f_{x,D}$ = tractive or braking friction demand factor.

The tractive or braking friction demand factor $f_{x,D}$ is equivalent to the acceleration or deceleration rate describing the vehicle's speed change as it traverses the curve.

The average deceleration rate between PC and MC is computed as follows:

$$d_{PC-MC} = \frac{1.47\Delta_{85} v_{PC-MC}}{t_{PC-MC} g} \tag{91}$$

with:

$$t_{PC-MC} = \frac{0.5L}{1.47 \frac{v_{PC,85} + v_{MC,85}}{2}} \tag{92}$$

where:

$d_{PC\text{-}MC}$ = average deceleration rate between PC and MC, ft/s^2.
$t_{PC\text{-}MC}$ = travel time from PC to MC, ft.

Similarly, the average acceleration rate between MC and PT is computed as follows:

$$a_{MC-PT} = \frac{1.47\Delta_{85} v_{MC-PT}}{t_{MC-PT} g} \tag{93}$$

with:

$$t_{MC-PT} = \frac{0.5L}{1.47 \frac{v_{MC,85} + v_{PT,85}}{2}} \tag{94}$$

where:

$a_{MC\text{-}PT}$ = average acceleration rate between MC and PT, ft/s^2.
$t_{MC\text{-}PT}$ = travel time from MC to PT, ft.

The average deceleration and acceleration rates $d_{PC\text{-}MC}$ and $a_{MC\text{-}PT}$ obtained from Equations 91 and 93 are used in the place of $f_{x,D}$ in Equation 90.

Acceptable Margin of Safety Level

The margin of safety is computed as the side friction demand subtracted from the side friction supply. Glennon (*3*) suggested that the margin of safety should be at least 0.08–0.12 along the entire length of the curve.

Travel Path Distribution

The calculations of probabilities of the different travel path types are conducted using the travel path models. These models include skid number as a variable influencing the distribution of travel paths. The skid number used to calibrate these models was the average skid number along the length of the curve, measured at the curve advisory speed or the regulatory speed limit if no advisory speed is posted. In the input data cells, the TCMS program accepts skid number

measured at a test speed of 50 mph, and then converts these skid numbers to the skid numbers that would apply to the advisory speed using Equation 87.

The skid test speed is entered into one of the calibration factor cells on the third page of the worksheet and can be adjusted if needed. Additionally, if the analyst is evaluating the effectiveness of a high-friction surface treatment, and the skid number of the treatment is known only at the advisory speed, the analyst can enter skid number values into the input data cells and adjust them on a trial-and-error basis until the computed skid number values at the advisory speed (which are provided in one of the output data boxes) match the value measured at the advisory speed.

Crash Prediction

The predicted crash counts provided on the right side of the first page of the worksheet are obtained using the crash prediction models that were documented in Chapter 3. For the length and traffic volume observed at a typical rural two-lane highway curve, the predicted crash count is small. Additionally, the way the worksheet is formulated, the only CMF that would change based on the input data is the skid number CMF. Hence, the worksheet provides estimates of the predicted change in crash count (in percent) based on the change in skid number CMF that would result from the specified changes to skid number. The skid number used for the computation of this CMF is the skid number measured at 50 mph.

The analyst may apply an empirical Bayes adjustment to the predicted crash count if desired. The TCMS program uses the empirical Bayes methodology that Bonneson et al. described (*7*).

Curve Severity

The TCMS provides a calculation of the curve's severity category and the recommended advisory speed using the methodology that Bonneson et al. described (*8*). The advisory speed value can be checked against the speed posted on the curve if desired.

DESCRIPTION OF TEXAS CURVE MARGIN OF SAFETY PROGRAM

The Texas Curve Margin of Safety (TCMS) program is an Excel®-based spreadsheet program. It was developed to automate the calculations required to facilitate a margin of safety analysis of a curve. TCMS also incorporates the crash prediction models that were described in Chapter 3. The organization of the program is described in the next section, followed by discussion of the required input data and explanation of the output data.

Organization

The TCMS program is organized so the entire worksheet can be printed on four pages. The first page contains input data entry cells, output cells, and some additional calculations of quantities like the probabilities of travel path types, vehicle speeds, and speed differentials. The second page provides three charts to illustrate margin of safety trends and vehicle speeds throughout the curve. The third page contains calibration cells where the model coefficients and other key constants can be adjusted. The third and fourth pages contain intermediate calculations that are used to produce the output calculations on the first and second pages.

Figure 51 provides a screen shot of a portion of the first page of TCMS. The cells are color-coded so the analyst can easily identify data entry cells and output data cells. The main set of data entry cells is blue. With the exception of the "general information" data entry cells (describing quantities like district, highway, and curve location), the blue cells must be filled. Several additional data entry cells are orange. The orange cells differ from the blue cells in that the program requires the quantities that are entered into the orange cells, but can estimate the quantities if the analyst leaves the cells blank. The key output data cells are colored rose. The cells containing calibration factors on the third page of the program are yellow.

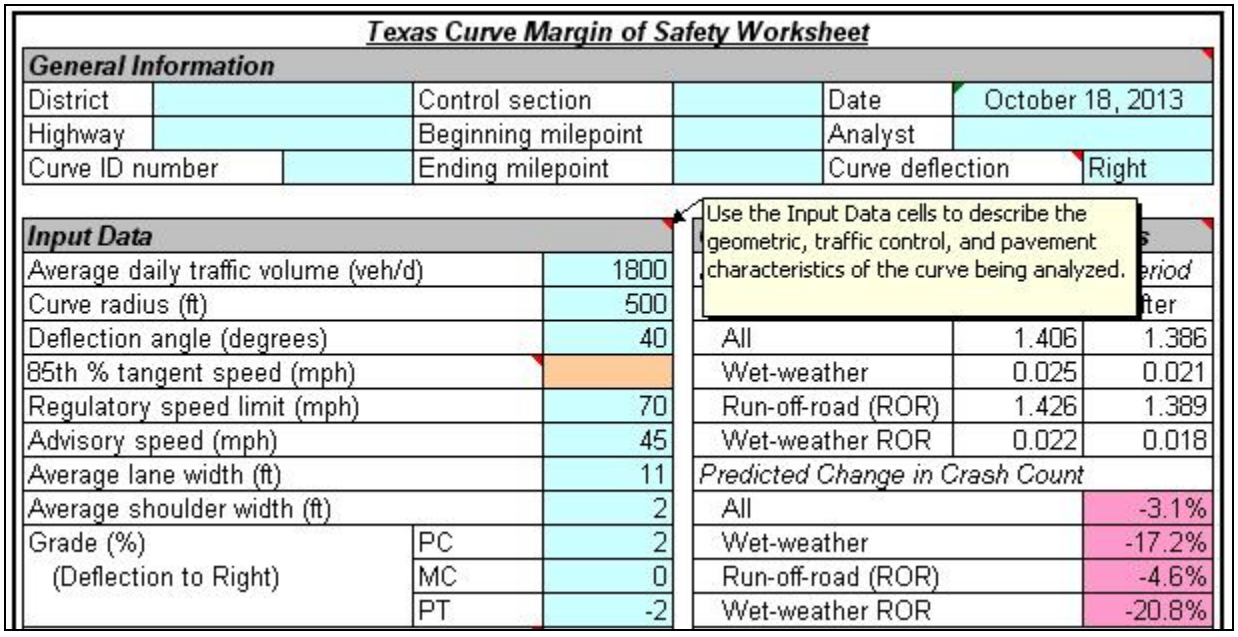

Figure 51. TCMS Screenshot.

Some of the cells, data boxes, or graphs in TCMS have comment boxes that provide additional clarification about the needed input data or interpretation of the output data. Red triangles indicate the presence of these comments. The comments can be viewed by placing the cursor on top of the red triangles. In Figure 51, a comment is shown for the Input Data box.

The input and output data cells are organized into logical groups. For example, the quantitative input data cells are contained within one box, and additional output data boxes are

provided for margin of safety analysis calculations, crash prediction model calibrations, curve speed calculations, and several other sets of calculations.

Most of the output data cells are white. These cells do not represent key output quantities but are made visible because their contents may be of interest. The output data cells are protected so the analyst cannot inadvertently alter an equation and obtain erroneous calculations from the program.

The input data cells are configured with data validation features to prevent illogical values from being entered. For example, regulatory speed limit and advisory speed must be multiples of 5 mph, and the skid numbers must be between 0 and 100.

Input Data

Cells containing general information are located on the upper portion of the TCMS worksheet (see Figure 51). These cells can be used to document the location of the curve, as well as the date, the analyst's name, and the direction of curve deflection (left or right) corresponding to the grade data that are entered into the Input Data box. Of these quantities, only the curve deflection direction affects the calculations performed by the program.

Figure 52 shows the box containing the input data cells. The following data are needed:

- Average daily traffic volume (veh/d).
- Curve radius (ft). Enter the geometric radius of the curve.
- Deflection angle (degrees). Enter the total deflection angle for the curve.
- 85^{th}-percentile tangent speed (mph). Enter the field-measured 85^{th}-percentile tangent speed, if available. This speed should be measured at a location sufficiently far upstream of the curve that the curve geometry does not affect vehicle speeds. If this quantity is not entered, the program will estimate the 85^{th}-percentile tangent speed using the model that Equation 74 described.
- Regulatory speed limit (mph). Enter the regulatory speed limit. This quantity is used to estimate the 85^{th}-percentile tangent speed if a field-measured value is not available.
- Advisory speed (mph). Enter the curve advisory speed, or the regulatory speed limit if no advisory speed is posted.
- Average lane width (ft). Enter the average lane width that exists along the length of the curve.
- Average shoulder width (ft). Enter the average shoulder width that exists along the length of the curve.
- Grade (%). Enter the roadway grade, as measured at the centerline of the roadway in the direction of travel, for the PC, the MC, and the PT. The entered grade numbers should be measured in the direction of travel corresponding with the curve deflection direction that was entered in the General Information box.
- Analysis period (yr). Enter the number of years included in the analysis period. This quantity defines the time period for the calculation of predicted crash counts.

- Reported crash count in analysis period. If empirical Bayes adjustment to the predicted crash counts is desired, enter the number of crashes observed during the analysis period. Separate cells are provided for four different categories of crashes—all crashes, wet-weather crashes, run-off-road crashes, and wet-weather run-off-road crashes. Leave these cells blank if empirical Bayes adjustment is not desired.
- Superelevation rate (%). Enter the superelevation rate observed at the MC, and optionally the value observed at the PC and PT. A positive superelevation rate value corresponds to a cross slope that decreases side friction demand. If values are not provided for the PC and the PT, the program estimates the superelevation rate at these points using the default proportion of 0.5, which can be adjusted in the calibration factor cells if desired. A proportion of 0.5 means that the superelevation rate at the PC and the PT is equal to 0.5 times the value observed at the MC. Cells are provided for the "before" and "after" cases so the effects of changing the superelevation rate can be computed. Cells are also provided for the two travel directions so differences in superelevation rate between the two directions can be accommodated.
- Skid number at test speed: Enter the skid numbers observed at the PC, MC, and PT. The test speed is 50 mph by default and can be adjusted in the calibration factor cells if desired. Cells are provided for the "before" and "after" cases so the effects of changing the skid number (e.g., by adding a high-friction surface treatment) can be computed.

Input Data			
Average daily traffic volume (veh/d)			1800
Curve radius (ft)			500
Deflection angle (degrees)			40
85th % tangent speed (mph)			
Regulatory speed limit (mph)			70
Advisory speed (mph)			45
Average lane width (ft)			11
Average shoulder width (ft)			2
Grade (%) (Deflection to Right)		PC	2
		MC	0
		PT	-2
Analysis period (yr)			10
Reported crash count in analysis period	All		10
	Wet-weather		3
	Run-off-road (ROR)		9
	Wet-weather ROR		2
Superelevation rate (%)		Before	After
Deflection to Left	PC	4.5	6.5
	MC	6	8
	PT	4.5	6.5
Deflection to Right	PC	6.5	8.5
	MC	8	10
	PT	6.5	8.5
Skid number at test speed		Before	After
Deflection to Left	PC	30	40
	MC	30	40
	PT	30	40
Deflection to Right	PC	30	40
	MC	30	40
	PT	30	40

Figure 52. Input Data Cells.

In the example described by the input data in Figure 52, a safety improvement project is being considered for a curve with a 500-ft radius and a 40-degree deflection angle. The proposed project will involve increasing the superelevation rate by 2 percent along the entire length of the curve and installing a new pavement surface with a skid number of 40 to replace the existing surface that has a skid number of 30.

Output Data

Calculation results are provided on the first and second pages of the TCMS worksheet. These results include margin of safety analysis, crash prediction model calculations, speed profile, travel path distribution, and curve severity. Details are provided in the following subsections.

Margin of Safety Analysis

Figure 53 shows the table containing the margin of safety analysis results. Results are provided in the rose-colored cells for the two directions of travel and for the "before" and "after" cases. The "change" values in the white cells provide the change in margin of safety between the two cases. These calculations can be made for the ideal or correcting travel path types, as indicated in the blue cell.

Margin of Safety Analysis Calculations				
Correcting		Before	After	Change
Deflection	PC	0.000	0.077	+0.077
to	MC	0.172	0.288	+0.115
Left	PT	0.126	0.235	+0.108
Deflection	PC	0.000	0.098	+0.098
to	MC	0.164	0.278	+0.114
Right	PT	0.086	0.192	+0.106

Figure 53. Margin of Safety Analysis Calculations–Tabular Form.

In the example shown, the existing configuration (described by the "before" case) has a margin of safety of 0.000 for correcting travel path type in both travel directions at the PC. This result indicates that there is no margin of safety if a driver makes a correcting maneuver at the PC. The margin of safety at the PT is also borderline acceptable for the "before" case, based on the suggested minimum of 0.08–0.12. In the "after" case, the entire curve has a margin of safety of at least approximately 0.08, while the PC still has the lowest margin of safety of any point along the curve.

The margin of safety analysis results are shown in graphical form on the second page of the TCMS worksheet. Two graphs are provided—one for ideal travel paths and one for correcting travel paths (see Figure 54). The blue bars illustrate the "before" cases and the pink lines illustrate the "after" cases. The direction of the hatch lines correspond to the direction of travel (curve deflecting to the left or the right). In all cases, the pink bars are taller than the blue bars, indicating an improvement in margin of safety following the installation of the safety treatment.

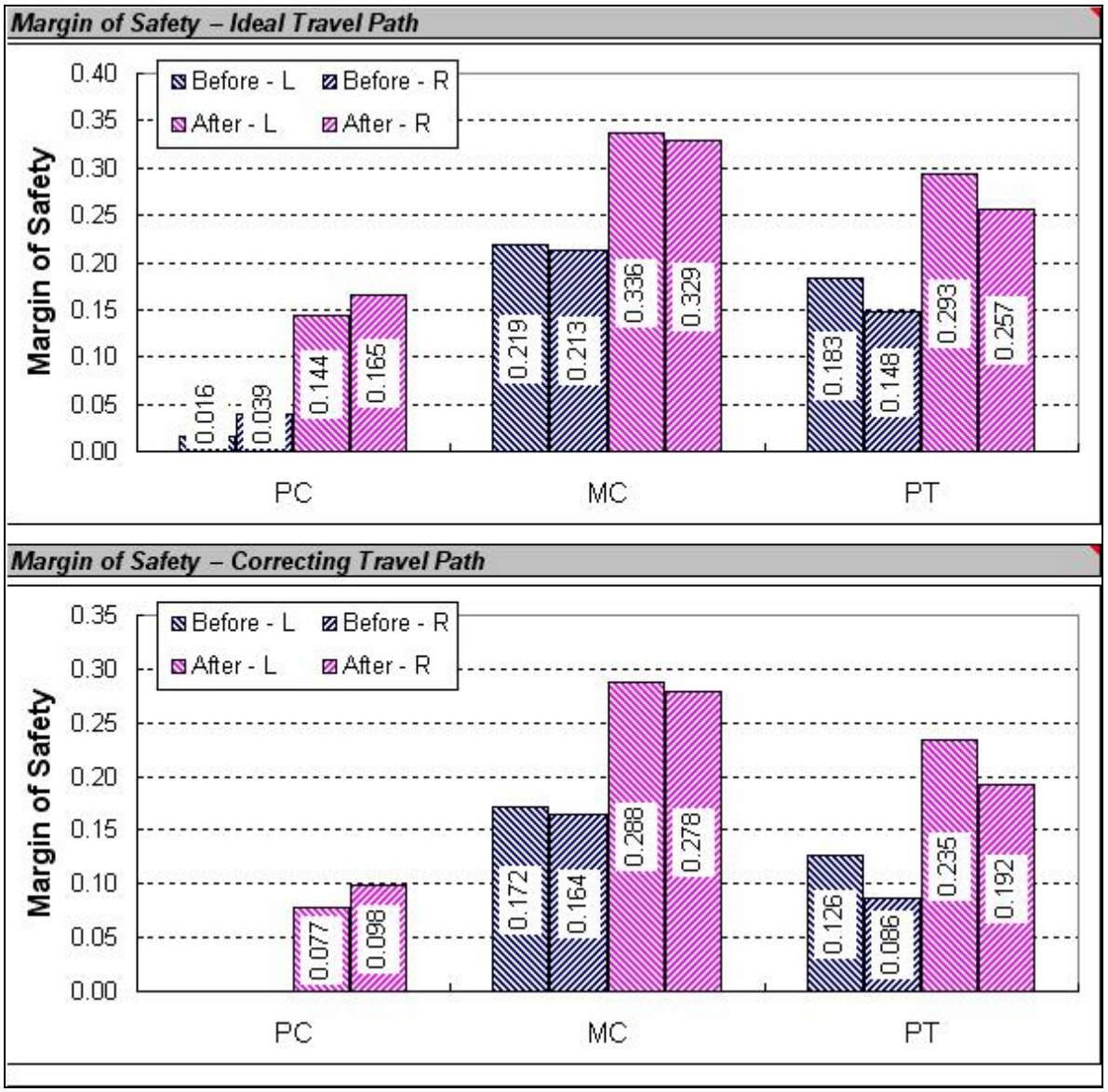

Figure 54. Margin of Safety Analysis Calculations–Graphical Form.

Crash Prediction Model Calculations

The crash prediction model calculations are provided on the right side of the first page of the TCMS worksheet. Figure 55 shows a portion of these calculations. Crash counts are provided for the four crash categories (all crashes, wet-weather crashes, run-off-road crashes, and wet-weather run-off-road crashes), along with the CMFs associated with the four models. The rose-colored cells show the change in skid number CMF and resulting change in predicted crash count due to the installation of the friction surface treatment.

Crash Prediction Model Calculations		
Predicted Crash Counts in Analysis Period		
	Before	After
All	1.406	1.386
Wet-weather	0.025	0.021
Run-off-road (ROR)	1.426	1.389
Wet-weather ROR	0.022	0.018
Predicted Change in Crash Count		
All		-3.1%
Wet-weather		-17.2%
Run-off-road (ROR)		-4.6%
Wet-weather ROR		-20.8%
Overall Crash Modification Factors (CMFs)		
Curve radius	9.432	
Lane width	1.066	
Shoulder width	1.287	
Skid number	1.033	1.000
Combined	13.368	12.947

Figure 55. Crash Prediction Model Calculations.

Speed Profile

Because curve geometry affects vehicle speeds through the curve, the predicted vehicle speed must be considered in both the "before" and "after" cases. In the input data shown in Figure 52, an increase in superelevation rate is described as part of the proposed safety improvement project. For a given vehicle speed, an increase in superelevation rate would generally increase the margin of safety by decreasing the side friction demand (see Equation 86). However, increasing superelevation rate also tends to increase vehicle speeds (see Equation 74), and the increase in speed may offset the expected benefit. This tradeoff is reflected in the margin of safety calculations that were shown in Figure 53 and Figure 54. The speed profile for the 85th-percentile vehicle is also illustrated in Figure 56 so the analyst can see how the proposed changes to the curve affect vehicle speeds.

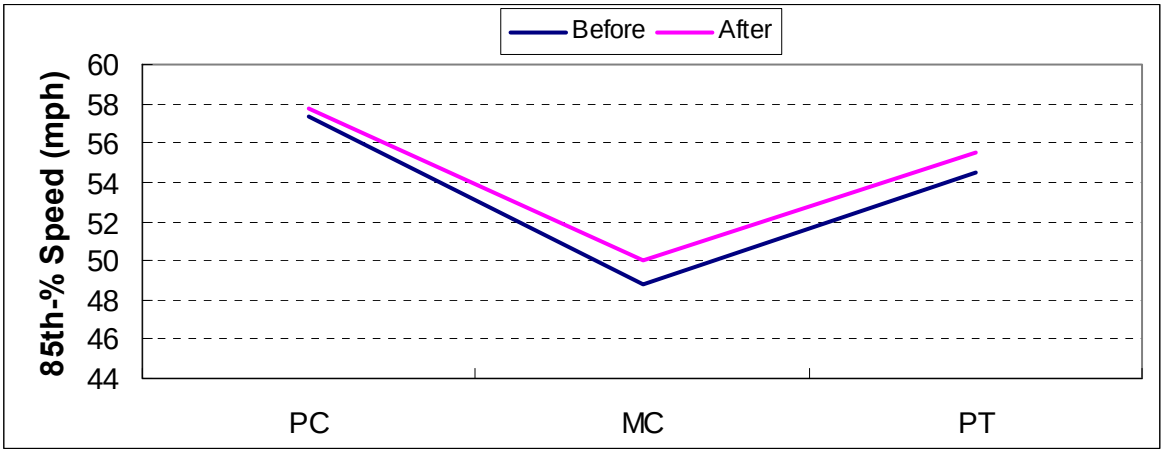

Figure 56. Speed Profile.

A comparison of Figure 54 and Figure 56 reveals the reason for the different margins of safety that are expected at the PC and the PT. Though the curve geometry is identical at these points (see the input data in Figure 52), vehicle speeds are higher at the PC than at the PT.

Travel Path Distribution

The distribution of travel path types is illustrated in Figure 57. In the example shown, the occurrence of correcting maneuvers is rare in both the "before" and the "after" cases—about 12 percent and 10 percent of vehicles, respectively. Conversely, many vehicles cut, swing, or drift through the curve in both cases.

Travel Path Distribution Calculations		
Path type	Probability	
	Before	After
Normal or Ideal	0.125	0.135
Cut, Swing, or Drift	0.758	0.765
Correcting	0.117	0.100

Figure 57. Travel Path Distribution.

When the results in Figure 54 and Figure 57 are compared, note that a small percentage of drivers will execute a correcting maneuver and experience the lower margin of safety that was plotted with the lower graph included in Figure 54. Furthermore, the occurrence of a correcting maneuver at some point along the curve does not necessarily imply that the course correction will occur at the PC where the smallest margin of safety was observed. However, it is a desirable practice to account for the possibility of a course correction at any point along the curve.

Curve Severity

Figure 58 shows the curve severity calculations. The curve severity category was illustrated with the contour plot in Figure 6 and can be used with Table 3 to assess the need for traffic control devices like delineator posts or Chevrons. Additionally, curves with a severity category of E are very likely to benefit from pavement improvement treatments like the addition of a high-friction surface treatment or an increase in superelevation rate. The recommended advisory speed is also provided if the analyst wishes to compare this value to the actual advisory speed that is posted in the field.

Curve Severity Calculations	
Curve severity category	E
Rec'd advisory speed (mph)	45

Figure 58. Curve Severity Calculations.

REFERENCES

1. Dunlap, D., P. Fancher, R. Scott, C. MacAdam, and L. Segel. *Influence of Combined Highway Grade and Horizontal Alignment on Skidding*. NCHRP Report 184. TRB, National Research Council, Washington, D.C., 1978.
2. Spacek, P. Track Behavior in Curve Areas: Attempt at Typology. In *Journal of Transportation Engineering*, Vol. 131, No. 9, September 2005, pp. 669–676.
3. Glennon, J., and G. Weaver. *The Relationship of Vehicle Paths to Highway Curve Design.* Research Report 134-5. Texas Transportation Institute, College Station, Texas, 1971.
4. Bonneson, J. *Superelevation Distribution Methods and Transition Designs*. NCHRP Report 439. TRB, National Research Council, Washington, D.C., 2000.
5. *Pavement Design Guide*. Texas Department of Transportation, Austin, Texas, 2008.
6. Olson, P., D. Cleveland, P. Fancher, L. Kostyniuk, and L. Schneider. *Parameters Affecting Stopping Sight Distance*. NCHRP Report 270. TRB, National Research Council, Washington, D.C., 1984.
7. Bonneson, J., and K. Zimmerman. *Procedure for Using Accident Modification Factors in the Highway Design Process*. Report FHWA/TX-07-0-4703-P5, Texas Transportation Institute, College Station, Texas, 2007.
8. Bonneson, J., M. Pratt, J. Miles, and P. Carlson. *Development of Guidelines for Establishing Effective Curve Advisory Speeds*. Report FHWA/TX-07/0-5439-1, Texas Transportation Institute, College Station, Texas, 2007.